AD NUMBER

AD249378

NEW LIMITATION CHANGE

TO

Approved for public release, distribution unlimited

FROM

Distribution authorized to U.S. Gov't. agencies and their contractors; Administrative/Operational Use; AUG 1960. Other requests shall be referred to Air Force Cambridge Research Labs., Hanscom AFB, MA.

AUTHORITY

Air Force Cambridge Research Lab ltr dtd 3 Nov 1971

AFCRL-TN-60-1107

TECHNICAL REPORT 70 CONTRACT AF 19(604)-3458

A STUDY OF CORONA DISCHARGE NOISE IN AIRCRAFT ANTENNAS

By: *A. Vassiliadis*

Prepared for:

AIR FORCE CAMBRIDGE RESEARCH LABORATORIES
AIR FORCE RESEARCH DIVISION AIR RESEARCH AND DEVELOPMENT COMMAND
LAURENCE G. HANSCOM FIELD BEDFORD, MASSACHUSETTS

STANFORD RESEARCH INSTITUTE
MENLO PARK, CALIFORNIA

SRI

829 form

August 1960

Technical Report 70

A STUDY OF CORONA DISCHARGE NOISE IN AIRCRAFT ANTENNAS

By: A. Vassiliadis

SRI Project 2494

Prepared for:

AIR FORCE CAMBRIDGE RESEARCH LABORATORIES
AIR FORCE RESEARCH DIVISION AIR RESEARCH AND DEVELOPMENT COMMAND
LAURENCE G. HANSCOM FIELD BEDFORD, MASSACHUSETTS

Contract AF 19(604)-3458

Approved:

C L Tanner for
R. L. TANNER, MANAGER ELECTROMAGNETICS LABORATORY

D. R. Scheuch
D. R. SCHEUCH, ASSISTANT DIRECTOR OF ENGINEERING RESEARCH

Copy No. 37

ABSTRACT

One of the more serious problems in aircraft communications is the radio noise interference which is caused by corona discharges on the aircraft. Although corona discharge noise has been known for a long time and attempts to eliminate the interference date back to 1937, very little is known concerning the exact nature of the noise pulses at the antenna terminals. Thus, the basic reason for this study is to investigate the characteristics of this noise.

When an aircraft flies through clouds, it develops a high negative charge due to the triboelectric effect of the impact of the ice particles in the cloud. Eventually, the electric field at the extremities, such as the wing tips, becomes sufficiently high for negative point corona discharges to occur. The discharge, which consists of numerous high-energy pulses of current, causes electromagnetic interference which couples to an aircraft antenna. The character of the noise pulses at the antenna depends not only on the original characteristics of the corona but also on the aircraft structure and aircraft resonances which influence the frequency spectrum of the pulses.

The method used to determine the noise pulse characteristics may be divided into two parts. The first part is the study and measurement of the corona discharge pulse shapes and statistics. The second, involves an evaluation of the electromagnetic coupling to a particular antenna. Techniques developed at SRI made it possible to measure the power spectrum of the noise source and the magnitude of the coupling function from the various vulnerable spots on the aircraft to a particular antenna location. Using these measurements and the antenna input impedance, rational function approximations are obtained for the coupling functions. These functions are interpreted as network transfer functions where the corona pulse as determined from measurements is the input while the output is the noise pulse at the antenna terminals. The characteristics of the noise are calculated for a particular aircraft and antenna, *e.g.*, a Boeing 707 tail-cap antenna.

In view of the interest in interference noise reduction, a large portion of this study is devoted to the analysis and comparison of the two major methods. The first method, which attacks the problem at the source, makes use of decoupled dischargers so as to discharge the aircraft as noiselessly as possible. The second method, that of blanking, is the primary electronic interference reduction method and it has received considerable attention. It is shown that under relatively heavy charging conditions the decoupled discharge method assuming 50 db of decoupling is superior to a blanker operating under ideal conditions.

CONTENTS

CONTENTS

ILLUSTRATIONS

ILLUSTRATIONS

TABLE

A STUDY OF CORONA DISCHARGE NOISE IN AIRCRAFT ANTENNAS

I. INTRODUCTION

A. HISTORY

Since the early thirties when navigation and communication equipment first was installed in commercial aircraft, radio interference known as "precipitation static" has been a problem. This interference, observed when an aircraft flies through clouds or precipitation, was generally attributed to charged particles striking the antenna as had been proposed by Curtis[1]* in 1914. Indeed, early attempts at eliminating precipitation static by Hucke[2] and Morgan[3] were based on this concept, and perhaps the most important improvement was the development of the shielded loop antenna.[3]

An extensive program, including flight tests, was undertaken in 1936 to obtain better interference reduction. This investigation[2] produced the important knowledge that the noise was due to corona discharges occurring at the antenna and at other extremities of the airplane. As a result of this study the trailing wire dischargers were proposed in order to discharge the aircraft. The mechanism involved in charging the aircraft to corona threshold was still not correctly explained.

Thus, although several improvements had been made, precipitation static was still a serious problem in 1943. Consequently, a joint Army-Navy precipitation static project was initiated. As a result of these investigations the phenomena involved in precipitation static were understood much better. The mechanism whereby the aircraft acquires its charge was shown to be primarily triboelectric charging.[4,5] Several methods of reducing radio interference were proposed. Among these, the most important was the use of wick dischargers[5] which became standard equipment on aircraft. Other devices were the dielectric coated wire antenna,[5] and the block and squirter discharger.[6]

* References are listed at end of report

Based on Langmuir's thorough investigation[4] of triboelectric charging using different materials, an attempt was made to eliminate or substantially reduce the charging rate by properly selecting a coating material for the aircraft.[5] This method was unsuccessful.

Since that time several other schemes have been proposed. An example is the use of a biased discharger in which a discharge is forced to occur between a sharp point and a cylinder.[7] Finally, systems have been proposed using flame dischargers, electron gun discharge tubes, and direct thermionic emitters.[8]

Whereas the above proposed methods of eliminating precipitation static were aimed at discharging the aircraft by using a noiseless discharger, another line of attack was proposed as a result of the Army-Navy project. This method involves reducing the noise through electronic means, as by the receiver blanking system.[9] Since then, considerable effort has been directed along these lines, but the usefulness of a blanking system as a means of eliminating noise has not yet been demonstrated.

It was not until 1953 that Tanner[10] analyzed the fundamental electromagnetic coupling mechanism which is involved between the corona discharge and the antenna terminals. In the light of this work, the success of methods which had been used was easily explained. More important, application of the coupling theorem in the laboratory has paved the way to a full understanding of precipitation static and will eventually lead to the development of a noiseless discharger.

B. FORMS OF PRECIPITATION STATIC

As mentioned in the previous section, when an aircraft is flying through precipitation it develops a charge due to the triboelectric phenomenon. When an individual ice particle strikes the aircraft in flight, it acquires a positive charge, leaving an equal but negative charge on the aircraft. The charge separation that results when two dissimilar materials are brought in contact and rubbed is caused by the same mechanism.

The cumulative effect of the ice particles continuously striking the aircraft and depositing charge causes the aircraft's potential to rise to hundreds of thousands of volts in relatively high charging conditions. As the aircraft gains charge, the fields at the sharp

extremities quickly rise to levels high enough for negative point corona discharges to occur. This type of discharge was first investigated by Trichel[11] in 1938. Since then, many others have studied these negative point corona pulses, and among the best measurements are those obtained by Tanner.[10]

Corona discharges can also result from the presence of high external crossfields which often arise due to oppositely charged clouds between which the aircraft is flying. This type of corona most frequently occurs in conjunction with relatively high triboelectric charging so that the two causes are usually not distinguished.

Corona discharge noise has become serious in high speed jet aircraft because the wick dischargers, which are only moderately successful even in propeller aircraft, cannot be used due to aerodynamic problems. Furthermore, the problem is aggravated in jet aircraft because of the higher charging rates which occur at higher speeds. Finally, the jet engines themselves can charge the aircraft to such high potentials that corona discharges occur in clear air. This is observed at low altitudes and it is particularly disturbing at take-offs and during landing maneuvers.

Another form of precipitation static is due to streamering[12] and is most serious in antennas under plastic surfaces—e.g., canopy antennas. When ice particles strike a plastic surface triboelectric charging causes the plastic to accumulate a charge. Since the charge cannot leak off, electric fields ultimately become high enough to cause streamering. Streamering is a discharge over the surface of the plastic between the metal adjacent to the plastic and portions of the plastic surface on which charge is accumulating. The short time structure and high energy of the streamer pulses results in the production of RF components which couple into nearby antennas. A study of streamering noise on canopy antennas was made by Nanevicz.[13]

Finally, noise can arise due to the impact of individual particles which acquire a charge in the antenna field region and move away. This form of precipitation static has been found to be insignificant compared to the others, however.[12]

C. SCOPE OF THIS STUDY

Although radio interference in aircraft due to corona discharges was the first type of precipitation static to be observed, it still remains by far the most serious. Therefore, this study will restrict itself only to noise due to corona discharges.

Techniques developed at SRI, have made it possible to measure the magnitude of the coupling function from the various vulnerable points on the aircraft to a particular antenna location. Using these measurements, together with the antenna input impedance and corona pulse characteristics, it has been possible to calculate adequately the noise at the chosen antenna terminals.

Characteristics of the noise for a Boeing 707 aircraft's tail-cap antenna are computed. The noise pulse shapes and spectrum are calculated.

Finally, in view of the interest in electronic interference reduction, the method of blanking is investigated and the ideal signal to noise ratio calculated. This is compared to the noise reduction which may be attained by using decoupled dischargers.

II COUPLING THEOREM AND ITS APPLICATION

A. STATEMENT OF THEOREM

The characteristics of the noise appearing at the antenna terminals of an aircraft due to corona discharges will depend on the electromagnetic coupling between the discharge and the antenna. In the calculation of electromagnetic coupling between structures, or between a structure and a current, the reciprocity theorem is found to be extremely useful. Several forms of the reciprocity theorem may be found in the literature. Best suited for our purpose, however, is the theorem cited below. This form of the generalized reciprocity theorem was developed by Tanner[10] in his study of corona discharges.

Consider a conducting body of arbitrary shape, Fig. 1, which in our application represents the aircraft. Let region T_1 represent a part of the body that has been removed, thus forming the antenna terminals. If a voltage, V_1, is applied between these terminals, then an electric field, $\mathbf{E}_1$, will result in all space, region T_2 included. On the other hand, if the antenna terminals are shorted and a discharge, of current density, $\mathbf{J}_2$, is made to occur in region T_2, then a current, I_2, will flow through the shorted antenna terminals.

The theorem then states that

$$I_2 = \frac{1}{V_1} \int_{T_2} \mathbf{E}_1 \cdot \mathbf{J}_2 \, dv \qquad (1)$$

The Fourier-transformed form of Maxwell's equations is used in the derivation of Eq. (1),[10] so that all quantities are frequency dependent while $\mathbf{E}_1$ and $\mathbf{J}_2$ are also functions of the space coordinates.

It is possible to use Eq. (1) as an integral equation to find $\mathbf{J}_2$ if I_2 and $\mathbf{E}_1/V_1$ are known. Alternatively, Eq. (1) may be used to compute the short-circuit current, I_2, in the antenna terminals if $\mathbf{E}_1/V_1$ and $\mathbf{J}_2$ are known. It is this latter interpretation of the theorem that is useful in the calculation of the characteristics of noise at the antenna terminals and in the eventual estimate of receiver response.

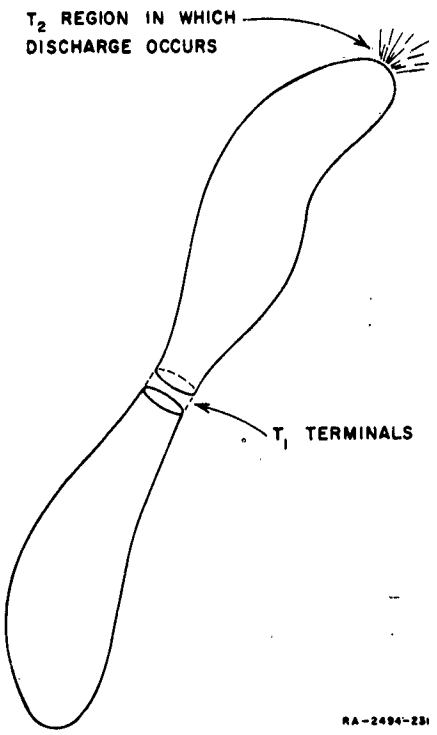

FIG. 1

ILLUSTRATING THE COUPLING FROM A DISCHARGE ON A CONDUCTING BODY

B. APPLICATION

A direct application of this theorem to actual calculation of short circuit current requires a knowledge of the field $\mathbf{E}_1$ in the region of the discharge as well as the space-time structure of the discharge current density $\mathbf{J}_2$. For the case of an aircraft, the boundary value problem to be solved in order to obtain $\mathbf{E}_1$ is impossible. Furthermore, the discharge-current space-time structure is not well known. Thus it becomes apparent that the direct calculation of short circuit current in an aircraft antenna would be of formidable complexity. By the use of laboratory techniques, however, together with the conceptual understanding derived from the theorem, the short-circuit current in a given aircraft antenna can be adequately estimated.

The development which follows illustrates the application of the theorem to the corona discharge coupling problem. The method used is essentially to separate the frequency dependence of the current into two

parts, one due to the aircraft structure and the other due to the discharge. The advantage of this separation is that the two functions can be determined by separate sets of laboratory measurements.

The shor circuit current, Eq. (1), may be written in explicit form as:

$$I_2(\omega) = \frac{1}{V_1(\omega)} \int_{T_2} \mathbf{E}_1(\mathbf{x},\omega) \cdot \mathbf{J}_2(\mathbf{x},\omega) d\mathbf{x}^3 \qquad (2)$$

where

$$\mathbf{x} = x, y, z.$$
$$d\mathbf{x}^3 = dxdydz.$$

For the application to corona discharges on an aircraft, we are interested in finding the short-circuit current at a specific antenna for corona discharges occurring at various locations. These locations are primarily the trailing edges and tips of the wings, elevators, and the rudder.

Let us now suppose that we select a point ξ on the aircraft structure at a point on a trailing edge where corona discharges are likely to occur. Then in a region about this location of the trailing edge, the electric field may be written in the normalized form given below:

$$\mathbf{E}_1(\mathbf{x},\omega) = E(\xi,\omega) \frac{\mathbf{E}_1(\mathbf{x})}{E_1(\xi_0)}$$

This relation will hold in a region which is small compared with a wavelength. For this reason the reference point ξ_0 need not be in the discharge region proper but may be on the wing surface or several inches away from the trailing edge. Substituting this expression in Eq. (2) we obtain:

$$I_2(\omega) = \frac{E(\xi,\omega)}{V_1(\omega)} \frac{1}{E_1(\xi_0)} \int_{T_2} \mathbf{E}_1(\mathbf{x}) \cdot J_2(\mathbf{x},\omega) d\mathbf{x}^3 \qquad (3)$$

$$= \psi(\xi,\omega) D(\omega) \qquad (4)$$

where

$$\psi(\xi,\omega) = \frac{E(\xi,\omega)}{V_1(\omega)} \qquad (5)$$

$$D(\omega) = \frac{1}{E_1(\xi_0)} \int_{T_2} \mathbf{E}_1(\mathbf{x}) \cdot \mathbf{J}_2(\mathbf{x},\omega) d\mathbf{x}^3 \qquad (6)$$

The short-circuit current as expressed in Eq. (4) is a product of two functions. The function $\psi(\xi,\omega)$ depends on the location of the discharge on the aircraft, the location and characteristics of the antenna, the aircraft size, shape, etc. Thus this function may be considered as a coupling function or transfer function. On the other hand, $D(\omega)$ is an expression of the noise source characteristics and depends purely on the local geometry of the discharge and on the discharge current characteristics.

Thus the frequency variations which appear in $\psi(\xi,\omega)$ are due to aircraft and antenna resonances while the frequency variation of $D(\omega)$ is due entirely to the character of the corona discharge and the local geometry. These two functions are evaluated by two separate laboratory experiments which will be briefly described in the following two sections.

III CORONA DISCHARGES

A. GENERAL CONSIDERATIONS

Our main concern in this section will be to obtain an expression for $P(\omega)$. This will be done by laboratory measurements on the corona discharges from a straight edge, which for example might represent the trailing edge of a wing. Before discussing the experimental techniques used in determining the corona characteristics, a brief description of the corona discharge is appropriate.

The actual physical process involved in negative point corona discharges is not completely understood. Qualitative arguments have been proposed, however, which explain the phenomenon. Consider, for example, the situation where a fine hemispherically capped wire is situated near a plane or sphere. As the potential of the plate is increased in the positive direction with respect to the point, a potential will be reached where "onset" of corona will be observed. Above this potential a very steady stream of pulses is observed, whereas at onset the pulses tend to be erratic. An individual pulse is initiated by the formation of a free electron very near the point where a very high field exists.

At threshold, this field is sufficiently high for the electron to have a high probability of gaining ionization energy between collisions, enabling it to produce additional electrons. These, in turn, produce more electrons by collision. In this manner an electron avalanche occurs. As the electrons move away from the point, they move more slowly because the field is decreasing rapidly with distance. The slow moving electrons are readily captured by oxygen molecules to form O_2^- ions.

The positive and negative ions which have been produced, due to their low mobility, accumulate to form separate space charge clouds. The cloud of positive ions is nearer the point than is the negative ion cloud. Its presence augments the field between it and the point, while the field farther out, between the positive and negative clouds, is decreased. This increase of the field near the point will improve the probability that an electron in this region will gain ionization potential between collisions.

Thus, the conditions for the formation of additional avalanches improve, and it is estimated that a large number of avalanches contribute to the build-up of the pulse. From the rapid rate of build-up of the pulses, it is believed that primary electrons for the additional avalanches are supplied by photo emission from the point.

At the same time the pulse is building up, the reduced field further out from the point facilitates the capture of electrons and reduces the distance at which formation of the O_2^- ions can occur. Thus, as the discharge proceeds, the cloud of negative ions becomes larger and crowds closer toward the point. The positive ions, meanwhile, are drawn into the point and disappear. The field near the point is thereby ultimately reduced to a value for which ionization by collision is no longer possible and the pulse is shocked off. The entire sequence of events occupies approximately 0.2 μsecs at atmospheric pressure.

Although each corona pulse is seen to consist of a complicated sequence of physical processes, the over-all influence of the disturbance on nearby structures may be determined by laboratory measurements. Tanner,[10] for example, conducted an extensive and careful study of the corona pulses from thin hemispherically capped cylinders for which the effects of tip radius, pressure, and magnitude of fields were carefully observed.

In calculations for the corona noise in aircraft, however, it becomes necessary to study the discharge obtained from a thin edge. This represents the trailing edges of the aircraft wings and tail surfaces from which the corona discharges take place.

B. DISCHARGE FROM EDGES

The corona discharges which can be obtained from an edge, such as the trailing edge of a wing, for example, might be expected to have similarities to the corona pulses obtained from a point. At the same time, differences in the geometry of the discharge region lead one to expect different corona pulse characteristics. Thus, for an edge, the field falls off more gradually than from a hemispherically topped wire. The discharge should therefore extend farther from the edge due to the fact that the electrons will travel farther out before attachment to the O_2 molecules becomes very probable.

1. Experimental Technique

In order to obtain laboratory measurements of the function $D(\omega)$ defined in Eq. (6), it is necessary to duplicate the local geometry of the aircraft at the locations where discharges take place. The locations of most interest are the trailing edges and tips of the wings, of elevators, and of the rudder. The field about the trailing edge of these airfoils will be approximately hyperbolic at a point away from the tip. Thus, to simulate the field structure, an elliptical metal electrode was assembled. A replica of the trailing edge of the wing could be lowered into this structure with the edge placed at the focus of the elliptical electrode. The fields about a trailing edge are thus reproduced with good accuracy.

A high voltage applied between the model of the trailing edge and the elliptic electrode will then cause corona discharges from the edge. Figure 2 illustrates corona discharges from a trailing edge in the geometry described above.

The dimensions of this electrode system are small compared to the smallest wavelength of interest, so that any frequency variation in the measurements will be due to the corona discharges. This geometry will therefore be satisfactory for a determination of $D(\omega)$ experimentally. If corona discharges are induced, by applying a high positive voltage to the elliptical electrode, then the short-circuit current at the measuring terminals will be

$$\left| I_e(\omega) \right| = \frac{1}{V_e} \left| \int \mathbf{E}(\mathbf{x}) \cdot \mathbf{J}(\mathbf{x},\omega) d\mathbf{x}^3 \right| \tag{7}$$

Since the fields are reproduced with good accuracy, the above integral will be the same as the one appearing in Eq. (6), so that combining Eqs. (6) and (7) we find:

$$\left| D(\omega) \right| = \frac{V_e}{E_1(\xi_0)} \left| I_e(\omega) \right| = \frac{1}{\psi_e(\xi_0)} \left| I_e(\omega) \right| \tag{8}$$

where $\psi_e(\xi_0)$ is the coupling factor for this geometry at an arbitrary point ξ_0. This reference point must correspond to the reference point which is used in the measurement of the aircraft coupling functions $\psi(\xi,\omega)$.


RP-2095-7

The set-up which is used is shown in Fig. 3. The current which flows through the 51 Ω resistor across the terminals is assumed equal to the short-circuit current. This is a good approximation in the frequency range where measurements are taken, since the capacitive reactance parallel with this resistance is very large in comparison. Direct measurement of the current is not taken; instead, use is made of the attenuator in order to make the reading of the meter when the receiver is connected to the discharge electrodes, equal to that obtained when the noise diode is connected. Thus, with the receiver fixed at a 2-Mc center frequency, the DC discharge current was varied and measurements of $|I_e(\omega)|_{f=2\text{Mc}}$ were obtained. These readings are plotted *vs* discharge current in Fig. 4.

The frequency variation of $|I_e(\omega)|$ was obtained using an exactly similar set-up, with the exception of the coupling geometry. A much smaller electrode system was constructed so that it could be placed under a bell jar. In this way, variation of corona spectral characteristics with altitude was obtained. The frequency spectra of the corona discharge from an edge of 20-mil aluminum are shown in Fig. 5. The data were taken for a total discharge current of 100 microamperes, and normalized so that the 2-Mc reading at sea level corresponds to unity. The coupling factor for this geometry, $\psi_e(\xi_0)$ in Eq. (8), may be obtained by laboratory measurement, or it can be estimated theoretically.

The experimental method makes use of an extremely useful technique developed by Nanevicz.[13] The method employs a probe which consists of two small platinum spheres very close to each other. By applying a potential difference between the spheres by the use of high resistance distributed leads, a discharge is made to occur. After the probe is placed near a structure, the short-circuit current which is measured at the terminals will be proportional to the average reciprocal field in the region of the discharge in the absence of the probe. Thus, in our geometry, the probe is placed at a distance ξ_0 from the edge where the field is not changing very rapidly. Then, the probe is placed in a standard parallel-plate geometry (see Fig. 3). From the ratio of the two short-circuit currents and the coupling factor for the parallel plate geometry, which is known, $\psi_e(\xi_0)$ is determined.

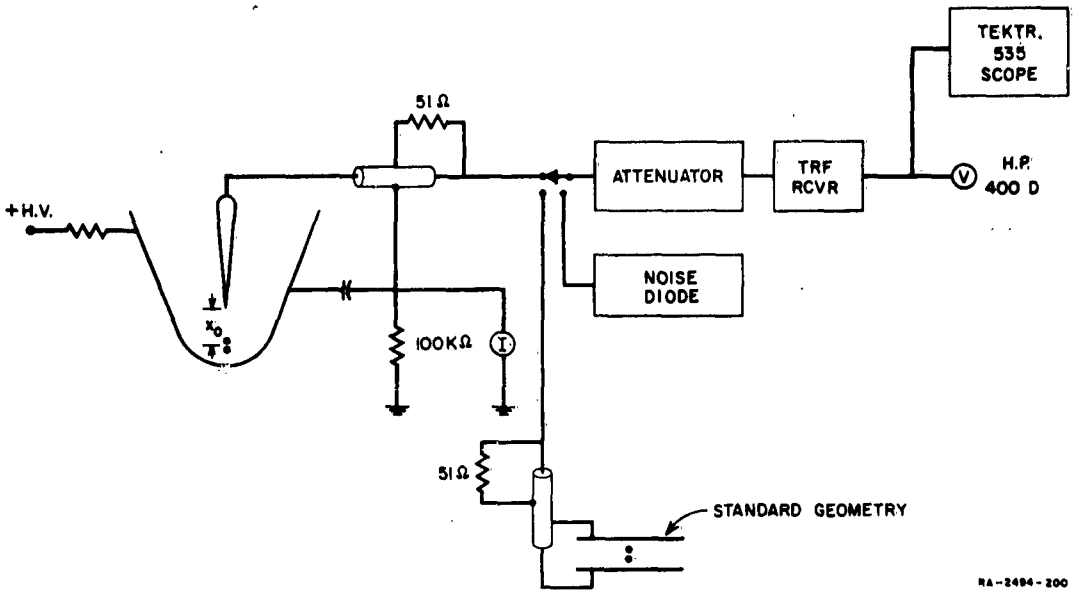

FIG. 3

TRAILING-EDGE NOISE MEASURING SET-UP

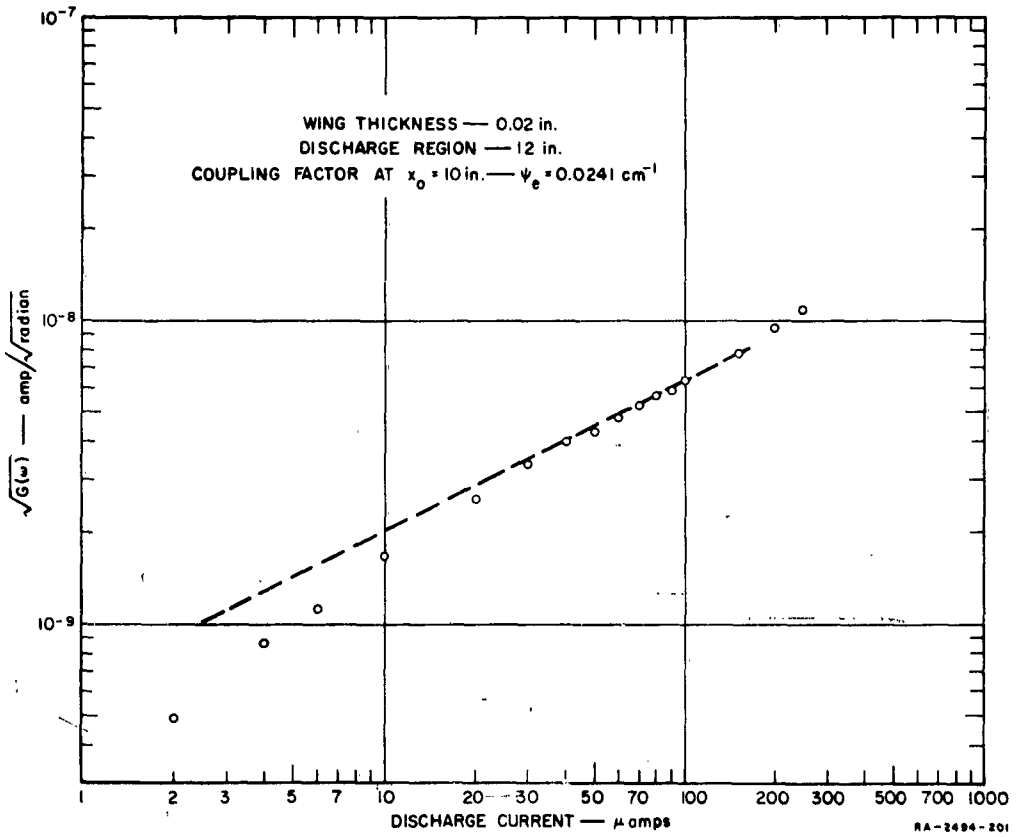

FIG. 4

NOISE AMPLITUDE FROM TRAILING EDGE

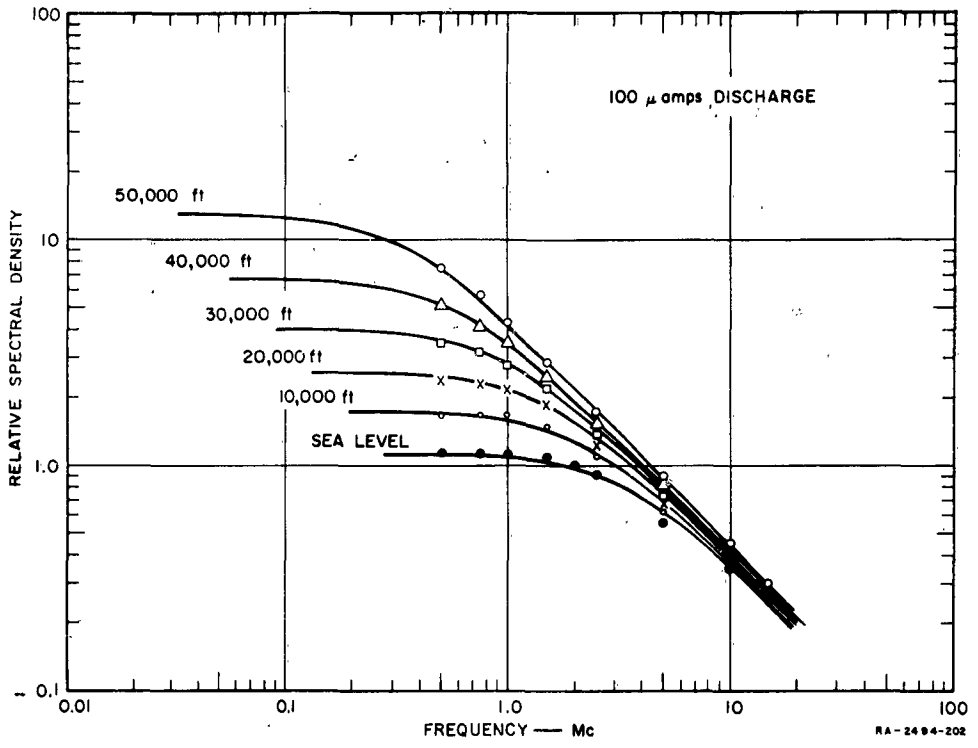

FIG. 5

NORMALIZED NOISE SPECTRUM FROM TRAILING EDGE

The coupling factor for this geometry could be computed theoretically by solving for the field about a semi-infinite sheet. When this was done, good agreement was obtained with the laboratory measurements.

For a detailed description of the measurements and techniques described very briefly above, see the comprehensive study by Tanner and Nanevicz.[14]

2. Results

From Fig. 4 it is observed that as the discharge current increases the noise current soon approaches a half-power relationship to the discharge current. This implies that the corona pulse amplitude is not affected much by the static field and that the corona pulses are random in time.

Consider a signal of ν identical random pulses per second. As shown in Appendix A, the power spectrum is proportional to ν.

Thus

$$\sqrt{G(\omega)} = \sqrt{\frac{\nu}{\pi}}\, A\left|F(\omega)\right| \qquad (9)$$

where $G(\omega)$ is the power spectrum, $F(\omega)$ is the Fourier transform of an individual unit pulse and A is the amplitude of the pulse. Now if A remains constant, since ν is then proportional to the discharge current, the noise current will vary as the half power of the discharge current.

As demonstrated by Tanner,[10] the rise time of the pulse from a point is extremely short, wwhile the decay is approximately exponential with time. Replacing the actual pulse by a simple exponential does not alter the frequency spectrum until well above 30 Mc. This exponential model of the pulses is corroborated by the experimental spectra shown in Fig. 5. These approximate very closely the spectra of a pulse whose shape is given by Eq. (10). For the corona from an edge the rise time should be of the same order of magnitude. Thus let us represent a noise pulse due to corona by a simple exponential of the form

$$f(t) = ae^{-\beta t} \qquad \text{for } t > 0 \qquad (10)$$

The pulses which occur physically will vary in amplitude and slightly in decay time due to the small local differences in geometry, space charge, etc. However, assuming the variation in β is small, the power spectrum for ν random pulses per second is found to be

$$G(\omega) = \frac{\nu}{\pi}\,\frac{A^2}{\omega^2 + \alpha^2} \qquad (11)$$

where $A^2 = \overline{a}^2$ = average amplitude and $\alpha = \overline{\beta}$ = average time constant. Thus the predicted spectrum for $D(\omega)$ is of the form:

$$\left|D(\omega)\right| = \sqrt{G(\omega)} = \sqrt{\frac{\nu}{\pi}}\,\frac{A}{\sqrt{\omega^2 + \alpha^2}} \qquad (12)$$

Curves of this form are plotted in Fig. 5 so as to fit the experimental data points as well as possible. From these curves we obtain α and the value of the spectrum at zero frequency $C = \sqrt{\nu/\pi}(A/\alpha)$. The time constant

$\tau = 1/\alpha$ and C are plotted *vs.* pressure in Fig. 6. The plot clearly indicates that the length of the pulse varies inversely with pressure. The fact that the asymptote C also varies inversely with pressure indicates that the amplitude and the number of pulses per second must vary in such a way as to make $A\sqrt{\nu}$ a constant.

By the use of a counter the value of ν was obtained at sea level and at a pressure equivalent to 50,000 feet. These are shown in Fig. 7, along with the calculated average amplitude of the pulses using C, ν, and α obtained previously. Thus, by interpolation, we can obtain the amplitude, the time constant, and the number of pulses per second for any altitude. Figures 5, 6, and 7 were obtained on the basis of 100 microamperes discharge current. Extension to other discharge currents

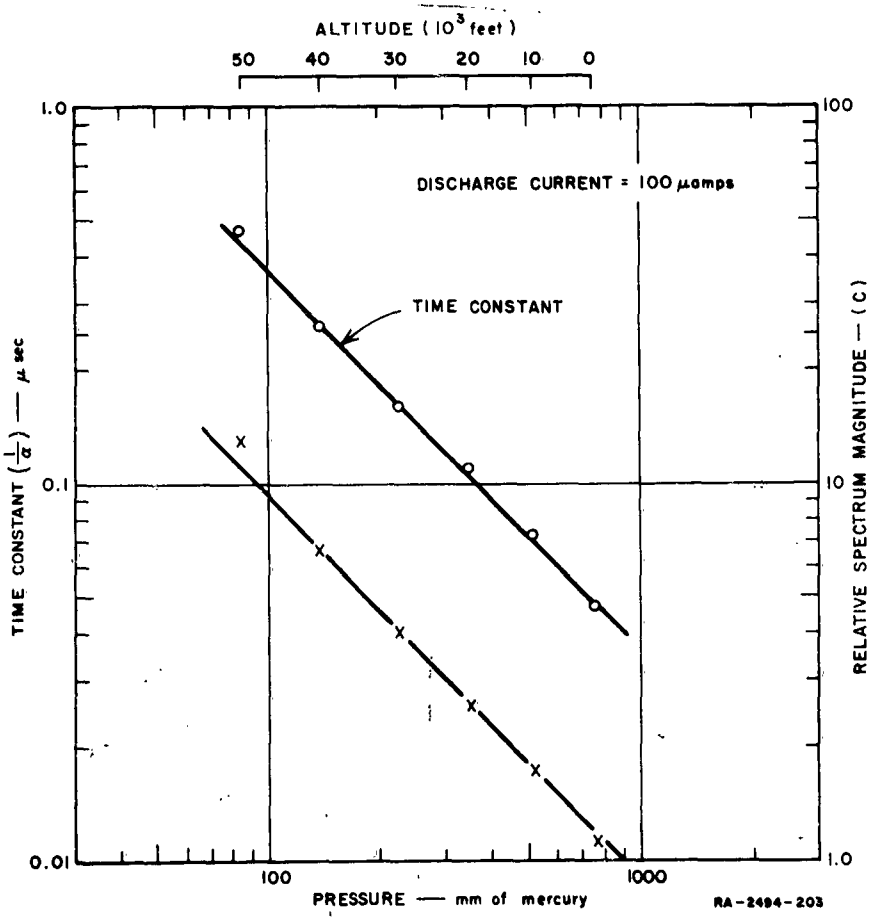

FIG. 6
CORONA SPECTRUM CHARACTERISTICS VS. PRESSURE

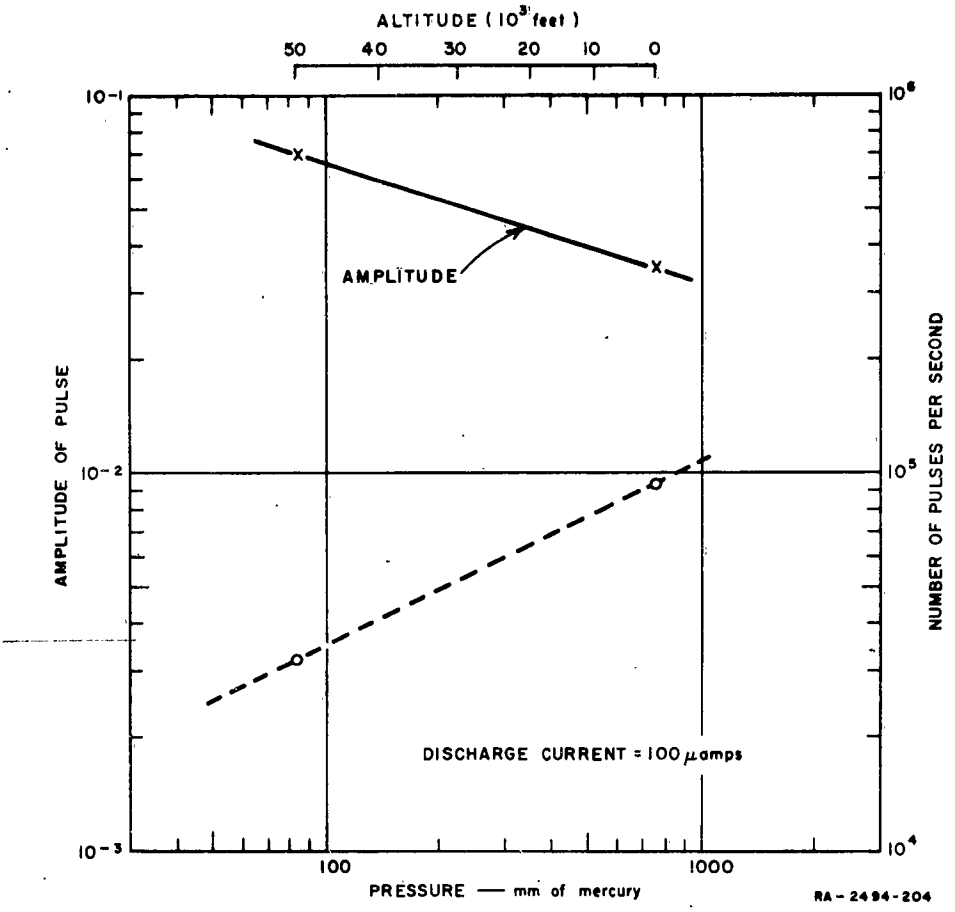

FIG. 7

CORONA PULSE AMPLITUDE VS. PRESSURE

can be made either by using Fig. 4 or by simply recalling that ν is proportional to the discharge current.

C. DISCHARGE FROM TIPS

The measurements of corona discharges presented in the last section hold good for an edge such as the trailing edge of a wing. A point of great interest, however, is the tip of the trailing edge—for example the wing tip, which is the point that first breaks into corona on a typical aircraft. Other points of interest are the tip of the horizontal stabilizer and the tip of the rudder. For these regions further measurements must be made.

In the small region of the discharge from the vicinity of the tip it is assumed that the conditions are such that the frequency spectrum shape will remain the same. Thus, the only difference will be in the magnitude of the coupling due to the change in geometry. A model of the wing tip of the Boeing 707 was made and the triangular section was placed in the elliptic geometry used previously with the tip situated at the focus. Although this geometry does not provide a completely true replica of the actual field, it simulates these fields very closely in the immediate vicinity of the tip. This is because the geometry of the field very close to the tip is determined almost entirely by the conducting boundary surface provided by the tip, itself. Using the procedure outlined in the previous section, measurements of short circuit current as a function of discharge current were obtained. The results are shown in Fig. 8. Comparison with Fig. 4 indicates good agreement in shape; however, as expected, the magnitude has increased. The change in noise level, from the edge to the tip, in the region where the half-power relation is established, is approximately 2.8. Thus, the amplitude of a noise pulse from the tip will be 2.8 times the pulse amplitudes from an edge as given in Fig. 7.

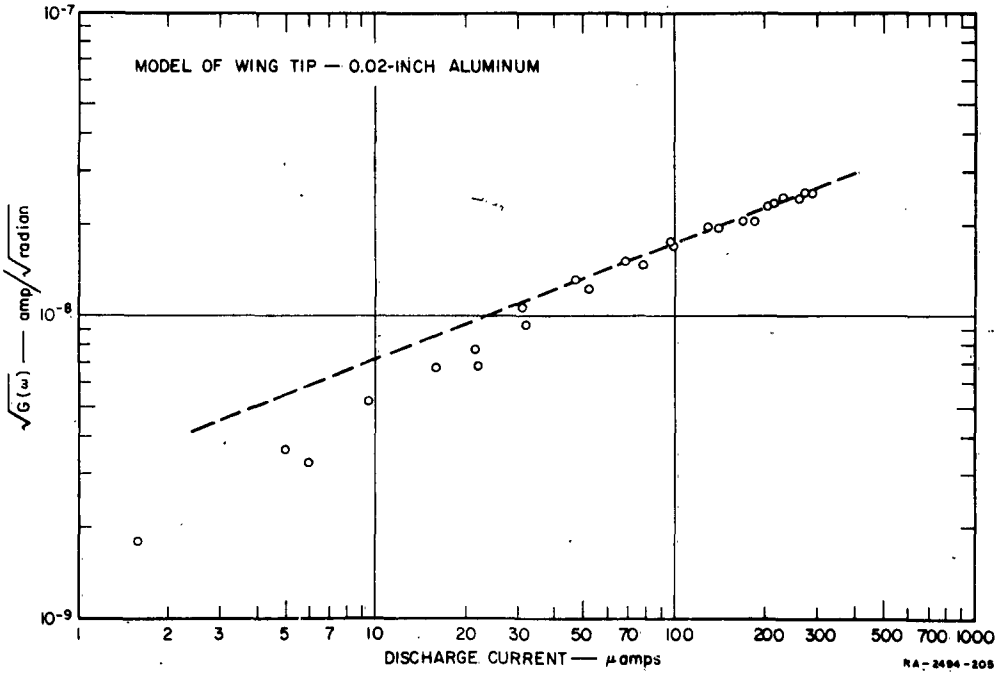

FIG. 8

NOISE AMPLITUDE FROM WING TIP

IV COUPLING FUNCTIONS

A. GENERAL CONSIDERATIONS

As outlined in Sec. II, the short-circuit current at the antenna terminals is determined by two functions of frequency. The function $D(\omega)$ which describes the character of the noise source was determined in the previous section. It remains to evaluate the coupling function $\psi(\omega)$ which is due to the aircraft and the antenna. Since the form of the coupling function will depend not only on the shape of the aircraft, but also on the location of the antenna and the location of the point where the discharge takes place, it becomes necessary to select a particular aircraft and a specific antenna on that aircraft. The aircraft selected for study is the Boeing 707; the antenna is a tail cap.

The complexity of the coupling functions makes a theoretical ca calculation virtually impossible. Thus, the coupling functions must be determined experimentally. The procedure outlined below provides a way of measuring the absolute magnitude of the coupling functions between the tail-cap antenna and the various points of interest.

B. EXPERIMENTAL TECHNIQUE

The method employed to measure the coupling functions uses the small discharge probe which was mentioned in Sec. III B-1.

The measurements are made on a scale model of the aircraft with the antenna properly scaled. Since the model must be completely isolated, it must be large enough to accommodate a meter, a receiver, attenuators, and associated equipment. A tenth scale model of the Boeing 707 was used for the measurements. The trailing edges and tips do not have to be modeled with extreme accuracy since we are not interested with the fields in the very close proximity of the edge. The discharge probe is then placed so that the small discharge is located at a distance ξ_0 from the edge at the point where the coupling is to be measured (see Fig. 9). This distance properly scaled, must correspond to the one used in the previous chapter for the measurements of $D(\omega)$.

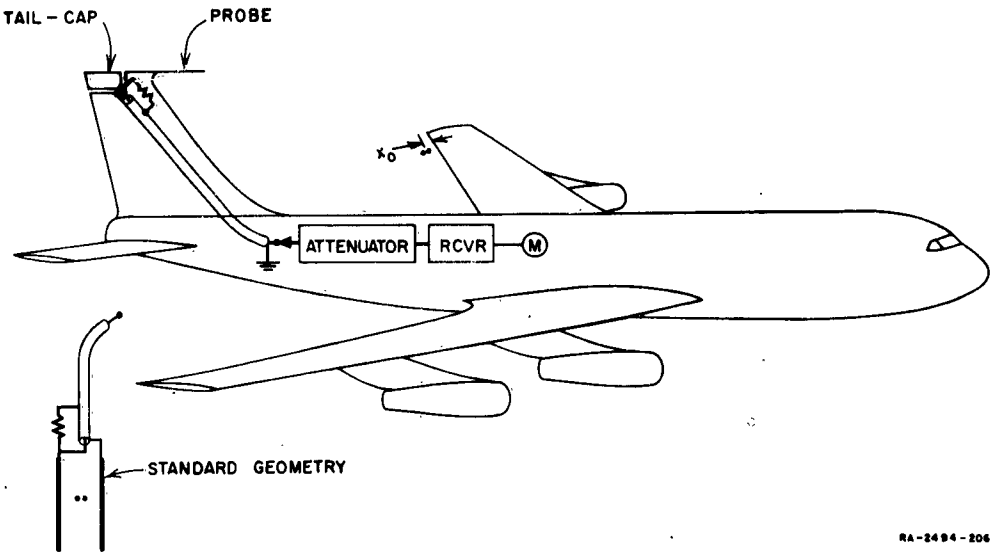

FIG. 9
COUPLING FUNCTION MEASURING SET-UP

The fields at this distance are not changing very rapidly and are not altered appreciably by the fact that the thin trailing edges are not scaled exactly. At the same time the distance ξ_0 is much smaller than the shortest wavelength of interest; thus, the short-circuit current at the antenna terminals, as measured by the instrument within the model, will be proportional to the field at the point ξ_0 and therefore will provide a measure of $\psi(\xi,\omega)$. The discharge probe is then placed in a standard parallel plate geometry. The short-circuit current measured in this case will again be proportional to the reciprocal field, which is known. Thus the coupling function can be obtained as a ratio of the two currents and the coupling function of the simple parallel plate electrodes.

Thus, the procedure for the measurement of the coupling functions is straightforward. With the receiver tuned to a properly scaled frequency, the probe is held at the point of interest on the aircraft (see Fig. 10) and the reading on the meter is noted. The probe is then placed in the standard field and attenuation is inserted so as to make the meter readings identical. This eliminates the unknown constant of the measuring instrument and gives the ratio of the currents directly.

A complete description of the techniques used in these measurements will be found in the report by Tanner and Nanevicz.[14]

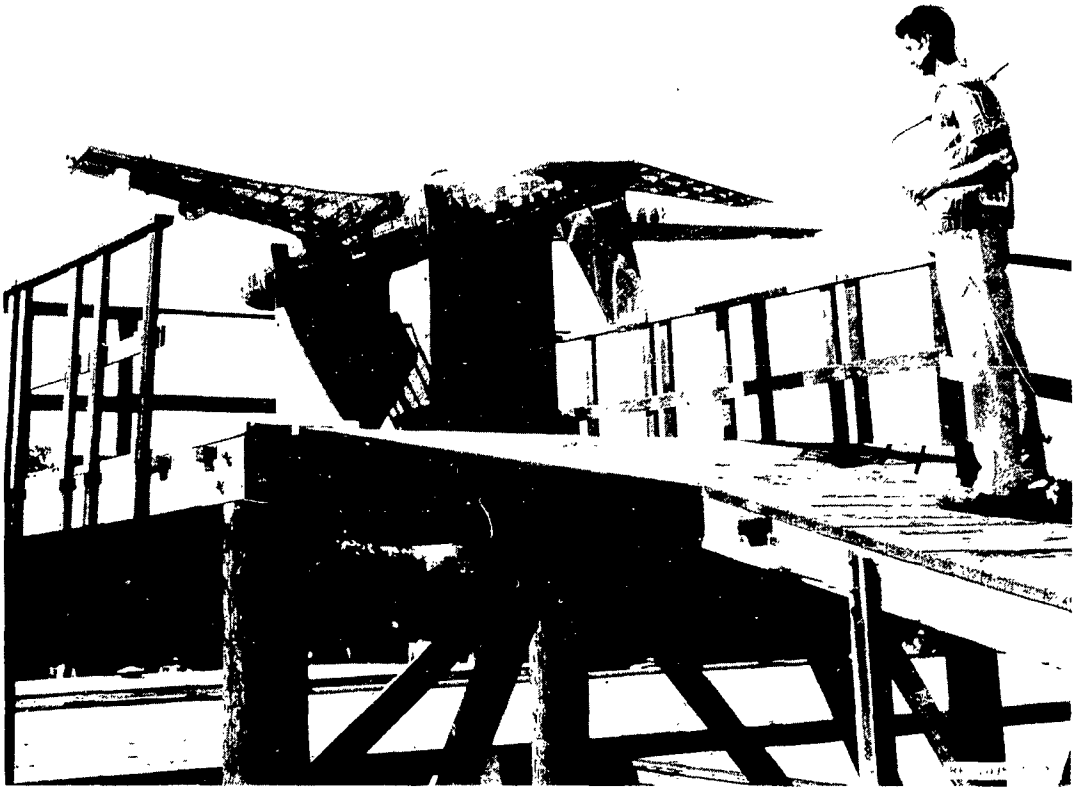

FIG. 10
MEASUREMENT OF COUPLING FACTOR ON 707 MODEL

C RESULTS

Consider an aircraft which is in a charging condition. As the potential of the aircraft increases, the wing tips will be the first to reach threshold and go into corona. As the potential continues to increase, the discharge will spread inward on the wing trailing edge. Before too long however, both the tail and the elevator tips will also break into corona. Even under relatively severe charging conditions no more than the outer 10% of the wing is discharging current. Thus, the three points of particular interest are the wing tip the elevator tip, and the tip of the rudder.

The procedure outlined in the previous section was used to measure the coupling functions between the tail-cap antenna and these points. For each location measurements were taken for a large number of

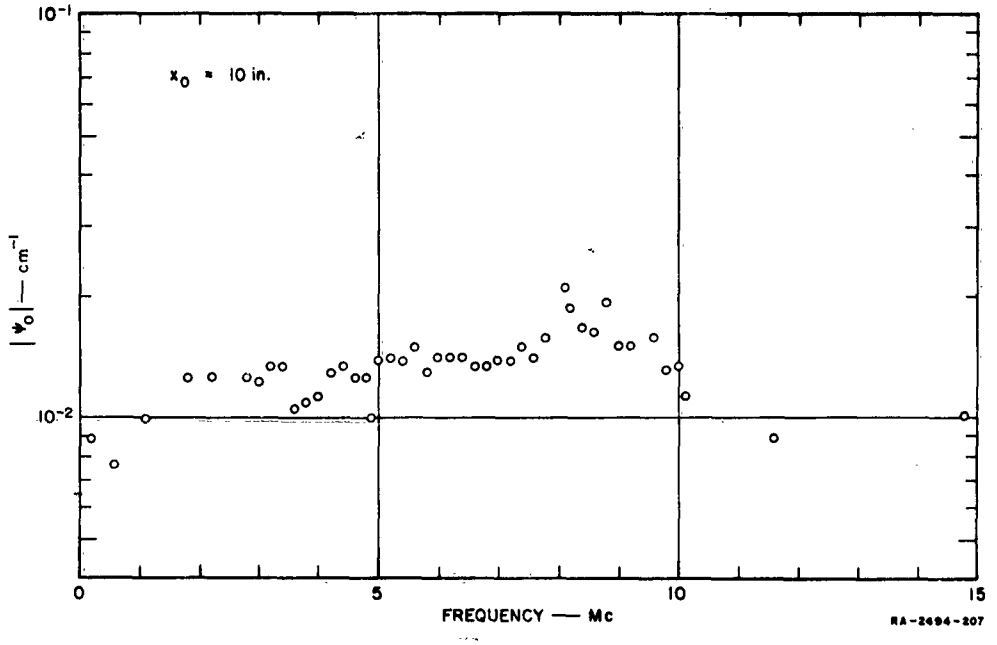

FIG. 11

COUPLING FROM RUDDER TIP TO TAIL-CAP ANTENNA

frequencies so as to obtain a reliable frequency variation for the coupling functions. The measured coupling functions are shown in Figs. 11, 12, and 13, properly scaled for the full sized aircraft.

The frequency variations which are observed, in the absolute value of the coupling functions, are due to the rather complex combination of the electromagnetic resonances of the various sections of the aircraft. Consider for example a frequency of approximately 1.8 Mc where the coupling to the elevator tip, Fig. 12, is observed to have a minimum. At this frequency the wings and fuselage add up to a length of $\lambda/4$ at the base of the horizontal stabilizers. Thus, since the horizontal stabilizers are still well below resonance, the low impedance presented by the front part of the aircraft will cause a minimum in the coupling function to the elevator tip.

At 3 Mc a maximum is observed in all the coupling functions. This is attributed to the $\lambda/2$ resonance of the aircraft, and represents a point of strong electromagnetic coupling to the airframe. Thus, a maximum is observed in the coupling function to the elevator tip even though it is still below resonance. The coupling to the wing tip, Fig. 13, is enhanced

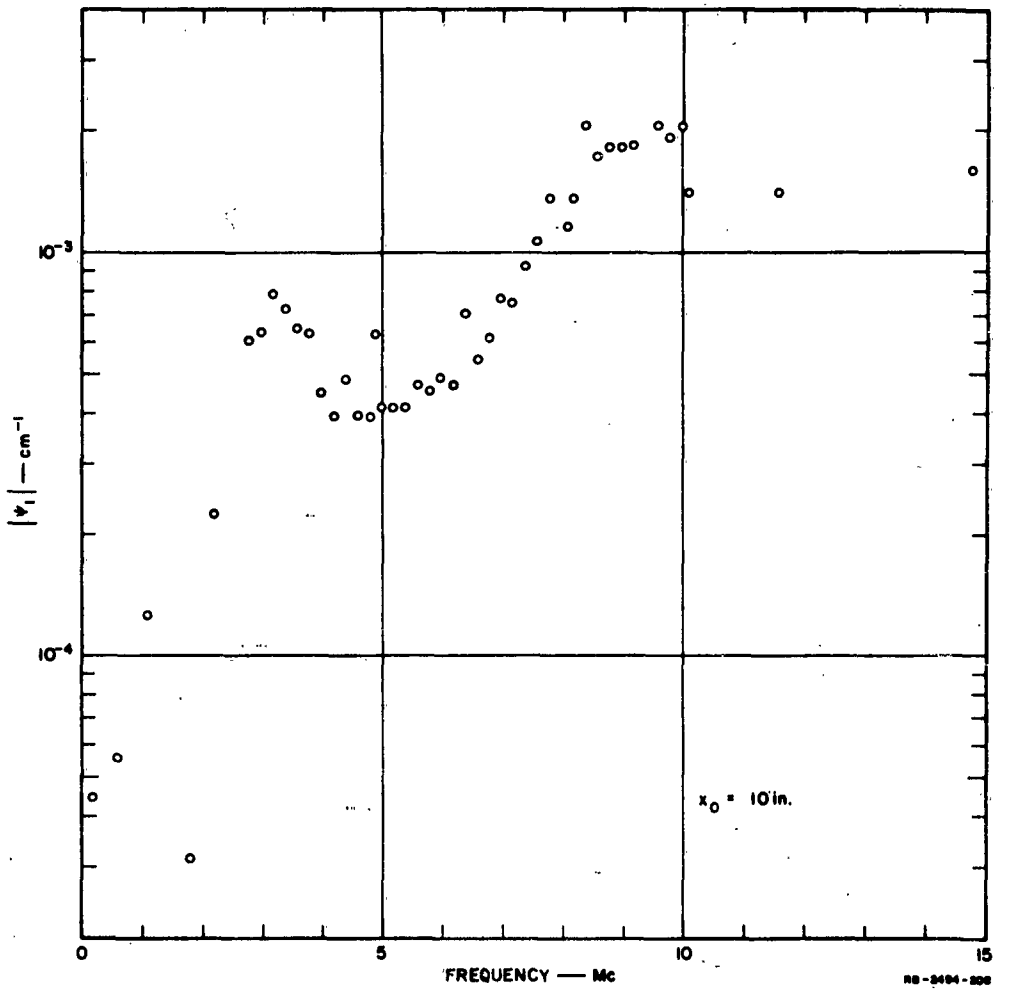

FIG. 12

COUPLING FROM ELEVATOR TIP TO TAIL-CAP ANTENNA

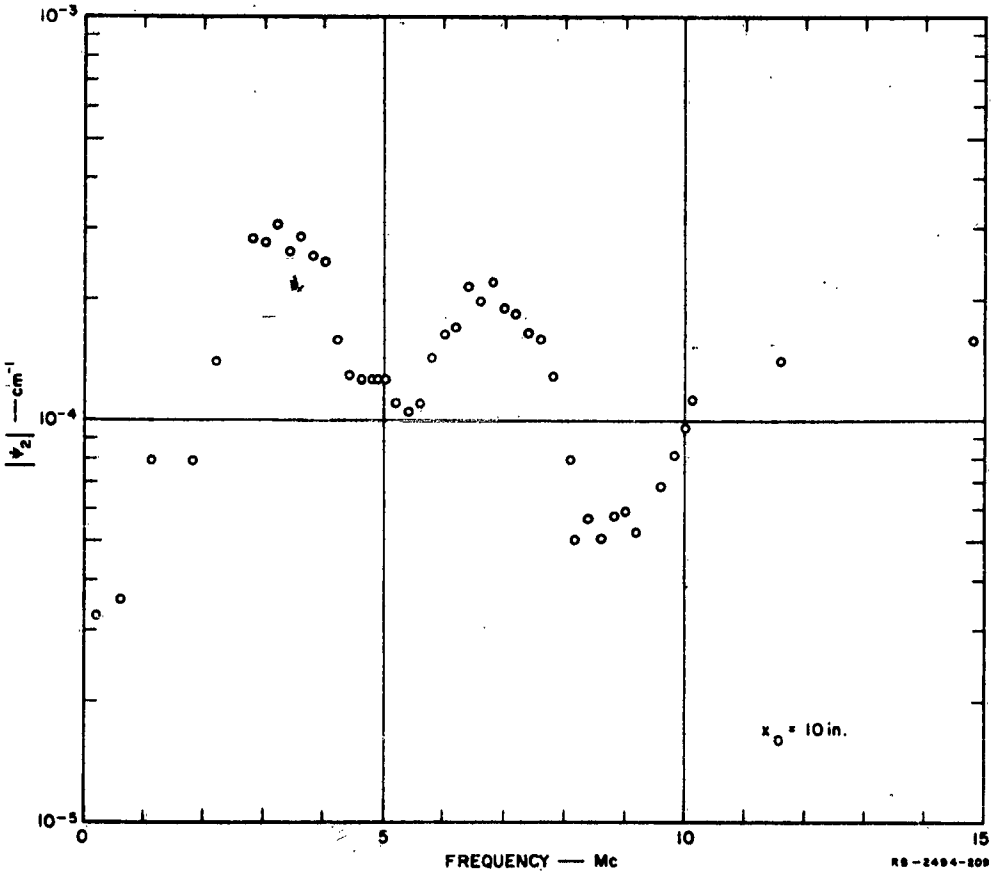

FIG. 13

COUPLING FROM WING TIP TO TAIL-CAP ANTENNA

by the fact that the wing is approximately $\lambda/4$ at this frequency. At 5 Mc, the fuselage ahead of the wing is $\lambda/4$ long and thus a minimum in the coupling to the wing tip results. At the same time, the fuselage, with the slight influence of the wings, presents a $3\lambda/4$ resonance at the junction with the horizontal stabilizer, thus causing the minimum at the elevator tip. At approximately 6.5 Mc a maximum occurs in the coupling to the wing tip. This is probably explained by a $3\lambda/4$ resonance of the wings at this frequency. Finally, at approximately 9 Mc the horizontal stabilizer has reached a $\lambda/4$ resonance. This explains the high maximum which occurs in the coupling to the elevator tip. For the same reason, the coupling to the wing tip will go through a minimum. The coupling to the wing is further reduced at this frequency because it is approximately one wavelength long.

V RATIONAL FUNCTION APPROXIMATION FOR COUPLING FUNCTIONS

A. GENERAL CONSIDERATIONS

By the experimental techniques described in the previous chapter the magnitude of the coupling functions to the tail-cap antenna have been obtained. For a complete description of the coupling functions, however, a means of establishing their phases must be developed. This will enable us to calculate the shape of the corona noise pulses at the antenna terminals, to estimate the response of the receiver, and to evaluate electronic means of noise reduction.

The relation of the coupling function to the antenna impedance provides a means by which a complete description of the coupling function can be obtained.

B. RELATION BETWEEN COUPLING FUNCTIONS AND ANTENNA IMPEDANCE

In Section IIB it was suggested that the coupling function may be considered as the transfer function of a network. Indeed the coupling function may be expressed in terms of four-terminal network parameters. Following Tanner's[10] argument, let us assume that the corona from some point on the aircraft takes place between that point and a small electrode located a distance d away. Let the point of discharge and the small electrode represent terminal pair 2 of the four-terminal network. The antenna terminals are terminal pair 1. If a voltage V_1 is now applied at Terminals 1 then the open circuit voltage at Terminals 2 will be

$$V_2 = z_{12} I_1 = z_{12} \frac{V_1}{z_{11}} \quad . \tag{13}$$

However the voltage V_2 is proportional to the field between the point of discharge and the small electrode, thus

$$V_2 = E_1 d \quad . \tag{14}$$

Combining Eqs. (14) and (13) we find

$$\psi = \frac{E_1}{V_1} = \frac{1}{d}\,\frac{z_{12}}{z_{11}} \quad . \tag{15}$$

If in a general four-terminal network, terminal pair 1 is short-circuited and a current I_2 applied at Terminal pair 2 we obtain

$$I_1 = \frac{z_{12}}{z_{11}}\, I_2 \quad .$$

This can be compared to the result of Eq. (4) and Eq. (15) which gives:

$$I_1 = I_s = \left[\frac{1}{d}\,\frac{z_{12}}{z_{11}}\right] D \quad . \tag{16}$$

Thus the coupling function has the form of a transfer function with dimensions of reciprocal distance (m^{-1}) since the input is not a current but a current moment (amp-meters).

The importance of Eq. (15) lies in the fact that it gives us the functional form of the coupling function. The impedance z_{11} is the input impedance of the antenna and it can be measured experimentally, and z_{12}, as defined above, cannot be measured. However, by using the known properties of network parameters, the measured z_{11} and $|\psi|$, rational function approximations for the coupling functions will be obtained.

C. PROPERTIES OF THE COUPLING FUNCTIONS

It has been shown, Eq. (15), that a coupling function is related to the open-circuit parameters of a four-terminal network. Using this equation some properties of the coupling function may be determined.

If they represent a physical network, the impedances z_{11} and z_{12} can be shown to have a number of properties,[15] some of which are stated below. In the complex frequency plane representation, the impedances must be either rational algebraic functions or meromorphic functions. The poles of the functions are restricted to the left half of the p-plane (where p is the complex frequency variable $p = \sigma + j\omega$) and on the $j\omega$-axis.

The zeros of z_{11} have a similar restriction while the zeros of z_{12} may occur anywhere in the plane. If z_{12} has poles on the $j\omega$-axis, these poles must also appear in z_{11}.

Since the aircraft and the antenna are distributed structures, the impedances z_{11} and z_{12} will be represented by meromorphic functions. Within any limited range of frequency, however, rational algebraic functions may be used to approximate the impedances.

Before discussing the tail-cap antenna, let us consider the case of a simple symmetric dipole. At very low frequencies the dipole becomes a static capacitor, so that the impedance z_{11} must have a pole at the origin of the p-plane. Thus z_{11} may be represented as

$$z_{11} = k_1 \frac{A(p)}{pB(p)} \tag{17}$$

where $B(p)$ represents the conjugate poles of z_{11} and is a polynomial with its roots in the left-half plane and $A(p)$ represents the zeros of z_{11} and has again all roots in the left-half plane.

Let us consider the physical implications of a unit input current at the antenna terminals at a complex frequency which coincides with a pole of z_{11}. Under these conditions an infinite voltage would result, so that infinite fields would be produced. In particular, infinite fields would also exist in the region of the discharge, which implies infinite voltage at Terminals 2. Thus all the poles of z_{11} will appear in z_{12}.

Next, let us consider the implication of a finite zero of transfer impedance z_{12}. A finite zero would require that, at a particular complex frequency, the output voltage be zero for a unit input current. For the simple geometric structure under consideration this will not be possible since the field in the region T_2 will not be zero. Thus, all the zeros of z_{12} must occur at infinity, and z_{12} will have the form

$$z_{12} = \frac{K'}{pB(p)} \tag{18}$$

where K' is a constant. Substituting Eq. (17) and (18) into (15) we find the coupling function depends only on the zeros of the input impedance of the dipole, *i.e.*,

$$\psi = \frac{K''}{A(p)} \quad . \tag{19}$$

Let us now turn to the tail-cap antenna on an aircraft. The tail-cap antenna may be likened to an asymmetric dipole where the aircraft plays the role of a rather complex long element. For the purposes of this discussion, the input impedance of the asymmetric dipole will be taken as the mean between the impedances of the two symmetric dipoles represented by the two elements of the asymmetric dipole. This approximation of the input impedance, discussed by King,[16] Tai,[17] and others, although not accurate quantitatively, is good enough for our qualitative discussion.

Thus the input impedance of the tail-cap antenna may be represented by

$$z_{11} = \frac{1}{2}(z_1 + z_2) \quad , \tag{20}$$

where z_1 represents the impedance of the aircraft and z_2 the impedance of the cap. Since we are interested in a rational function approximation which will be good from very low frequencies up to approximately 15 Mc, z_1 will have the form of Eq. (17). The polynomials $A(p)$ and $B(p)$ will contain the two or three conjugate pairs of poles and zeros, which represent the lowest two or three aircraft resonances. The impedance z_2, however, will have the form

$$z_2 = \frac{k_2}{p} \tag{21}$$

since in the frequency range of interest the cap is well below the first resonance. Thus, the over-all impedance will be

$$z_{11} = \frac{1}{2}\left[\frac{k_2}{p} + \frac{k_1}{p}\frac{A(p)}{B(p)}\right]$$

$$= K_{11}\frac{C(p)}{pB(p)} \quad . \tag{22}$$

It is important to note that since we have defined the impedance as a sum of two impedances arising from the two halves of the antenna, care must be taken in the assignment of poles to the transfer impedances. Thus, the transfer impedance to some location on one of the elements of the asymmetric dipole will be required to have only the poles contained by the input impedance of that half. In other words, the transfer impedance to the tip of the short element will contain only a pole at the origin which is due to z_2, while the transfer impedance to any part of the long element will contain all the poles of z_1.

It follows that the transfer impedance to the tail-cap tip, *i.e.* the rudder tip, contains only one pole located at the origin. From previous considerations, there will be no finite zeros of transmission since the cap has a simple geometric form. Thus the coupling function to the rudder tip ψ_0, will be

$$\psi_0(p) = K_0 \frac{B(p)}{C(p)} \tag{23}$$

The transfer impedance to the other two points of interest, *i.e.*, the elevator tip and the wing tip, will be more complex. The poles of these transfer impedances will consist of all the poles of z_1. Furthermore, there will be the presence of finite zeros of transmission due to branching which occurs in the aircraft. Consider for example, the possibility of zeros of transfer function to the elevator. There are two ways by which zeros can come about:

(1) At frequencies where the fuselage and wings present a short at the junction with the horizontal stabilizer

(2) At frequencies where the horizontal stabilizer presents an open circuit at its junction to the fuselage.

Similarly the zeros to the wing tip arise due to the separate resonances of the horizontal stabilizer, the wing, and the fuselage section forward of the wings. The transfer impedance to these points will then have the form

$$z_{1i} = K_i' \frac{D_i(p)}{pB(p)} \tag{24}$$

Substituting Eq. (24) with Eq. (22) into Eq. (15) we obtain for the coupling function to the elevator tip

$$\psi_1(p) = K_1 \frac{D_1(p)}{C(p)} \quad , \tag{25}$$

and for the coupling function to the wing tip

$$\psi_2(p) = K_2 \frac{D_2(p)}{C(p)} \quad . \tag{26}$$

Note that even if a root of $D_i(p)$ coincides with a root of $B(p)$, the coupling function will still have the form shown.

It is evident that all the roots of the polynomials $D_1(p)$ and $D_2(p)$ will be in the left-half plane since they represent either poles or zeros of input impedances. Therefore, all the coupling functions have their zeros and poles in the left-half plane, so that as transfer functions they represent minimum phase networks. This means that we can determine $\psi(p)$ uniquely from a knowledge of $|\psi|^2$ on the $j\omega$ axis.

D. RATIONAL APPROXIMATION OF TAIL-CAP ANTENNA IMPEDANCE

1. Impedance Measurement

Impedance measurements of the tail-cap antenna were not available. The impedance was determined from the knowledge of the tail-tip probe antenna impedance and the measurement of the static capacitance of the model antenna.

The probe antenna, which projects forward from the top of the tail of the Boeing 707 (See Fig. 9), is located near the tail-cap antenna. For this reason, the same aircraft resonances will influence the impedance of both antennas for frequencies corresponding to wavelengths large compared to the antenna sizes and the distance between the antennas. From Eq. 20 we note that the impedance of either of the two antennas will be a sum of two terms. At sufficiently low frequencies the contribution from the airframe will be identical to both antennas, while the second term in each case will be simply a capacitance. Finally, to complete the equivalent circuits a capacitance must be included across the antenna terminals. This is the base capacitance which is due to the feed configuration.

It can be shown that, if the real part of the impedance due to the airframe is much smaller than the imaginary, the two antennas will contain similar real parts except for a difference in the constant multiplier.

Thus, at low frequencies, the real part of the impedance of the probe antenna and the tail-cap antenna will differ only by a constant multiplier. This factor, which essentially relates the difference in coupling strength, was determined by model measurements made in the electrostatic cage.[18] From these measurements it was found that the real part of the tail-cap impedance is approximately twice that of the probe antenna. The normalized resistive part of the probe input impedance is shown in Fig. 14. The lower two resonances are the pertinent aircraft resonances, while the sharp increase at the higher frequencies is due to the self resonance of the probe and therefore does not apply to the tail-cap antenna impedance.

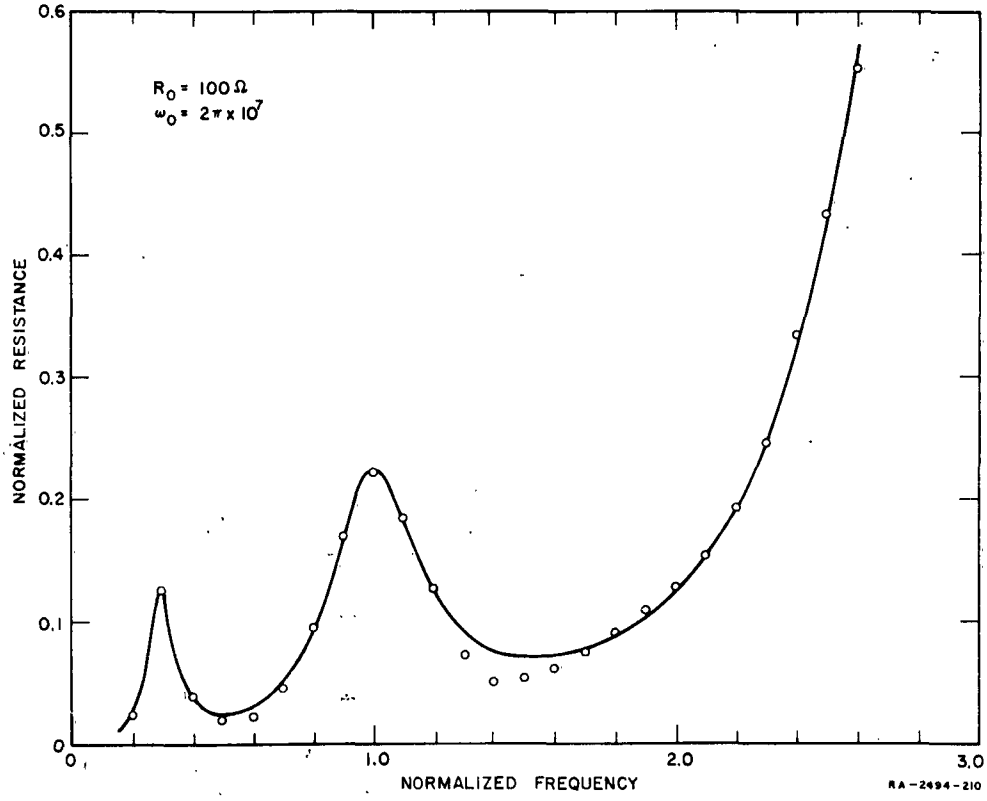

FIG. 14

NORMALIZED REAL PART OF PROBE ANTENNA IMPEDANCE

As far as the imaginary part of the impedance is concerned, at very low frequencies it will be determined purely by the static capacitance. This capacitance was measured on the model which was used for the coupling function measurements. It was found to be 100$\mu\mu$f scaled to the full size aircraft.

2. Normalization

It is convenient to normalize the impedances with respect to frequency and resistance. This normalization provides a means of scaling the frequency and the element values to small numbers.

The frequency scale is normalized to some frequency ω_0, so that

$$\omega = \frac{\omega'}{\omega_0} \tag{27}$$

where

ω' = actual frequency

ω = normalized frequency.

Similarly the impedance is normalized to some resistance R_0, thus

$$Z(\omega) = \frac{Z'(\omega)}{R_0} \tag{28}$$

where

$Z'(\omega)$ = actual impedance

$Z(\omega)$ = normalized impedance.

When this is done, the actual element values (primed) are related to the corresponding normalized element values (unprimed) as follows:

$$\begin{aligned} L' &= \frac{LR_0}{\omega_0} \\ R' &= RR_0 \\ C' &= \frac{C}{\omega_0 R_0} \end{aligned} \tag{29}$$

3. Rational Function Approximation

The behavior about a resonance of the impedance may be described approximately by the equation

$$Z(j\omega) = \frac{1}{\frac{1}{R} + j\left(\omega C - \frac{1}{\omega L}\right)} \tag{30}$$

and the real part is given by

$$R(\omega) = \frac{\frac{1}{R}}{\left(\frac{1}{R}\right)^2 + \left(\omega C - \frac{1}{\omega L}\right)^2} \tag{31}$$

The resonance of this function occurs at $\omega = 1/\sqrt{LC}$ and the peak value is R. Let the measured real part of the impedance be $R^*(\omega)$. Then we want to find the values of R, C, and L which would best fit the measured resistance $R^*(\omega)$. An attempt to set up a mean-square error approximation of the conductances directly would require the solution of complex non-linear equations for R, L, and C. However, Eq. (31) may be rewritten as

$$\left(\frac{1}{\omega L} - \omega C\right) = \pm\sqrt{\frac{1}{RR^*(\omega)} - \frac{1}{R^2}}$$

where the plus or minus is taken depending on whether the frequency is below or above resonance respectively. Thus by treating R as a parameter or by assigning to it the peak value if it is known, we can form a residual

$$\xi = \sum_{i=1}^{N} \left[\left(\frac{1}{\omega_i L} - \omega_i C\right) - K(\omega_i)\right]^2 \tag{32}$$

where

$$K(\omega_i) = \pm\sqrt{\frac{1}{RR^*(\omega)} - \frac{1}{R^2}}$$

and using the extremum conditions $\partial\xi/\partial L = \partial\xi/\partial C = 0$ we obtain the following equations which may easily be solved for L and C.

$$\left.\begin{aligned} \frac{1}{L}\sum_{i=1}^{N}\frac{1}{\omega_i^2} - NC &= \sum_{i=1}^{N}\frac{K_i}{\omega_i} \\ N\frac{1}{L} - C\sum_{i=1}^{N}\omega_i^2 &= \sum_{i=1}^{N}K_i\omega_i \end{aligned}\right\} \qquad (33)$$

The rational function approximation for $R(\omega)$ shown in Fig. 14 was obtained by the use of Eqs. (32) and (33). The equations were applied to the points below the self resonance of the probe ($2 < \omega < 2.5$) by assuming a number of R's and computing the corresponding residuals. The R giving the minimum residual is found and the optimum L and C are then calculated. The resonance curve may then be computed and subtracted from the over-all impedance. The two remaining resonances are easily approximated without resorting to Eqs. (32) and (33) since the peaks and the resonant frequencies are known.

In this way the two lowest resonances of the tail-cap antenna were obtained as

$$R_T(\omega) = \frac{4.14}{(4.14)^2 + \left(\frac{3.22}{\omega} - 35.8\omega\right)^2} + \frac{2.45}{(2.45)^2 + \left(\frac{6.8}{\omega} - 6.8\omega\right)^2} \qquad (34)$$

The tail-cap impedance is obtained from Eq. (34) by substituting the complex frequency variable p for $j\omega$ and recalling Eqs. (30) and (31), in addition, the antenna capacitance which was measured on the model must be included. Thus, the tail-cap input impedance is found to be

$$z_{11}(p) = \frac{1.59}{p} + \frac{0.0279p}{p^2 + 0.1154p + 0.09} + \frac{0.147p}{p^2 + 0.36p + 1} \qquad (35)$$

where p is a normalized complex frequency related to the actual frequency by $p = p'/\omega_0$.

E. COUPLING FUNCTION APPROXIMATIONS

1. Coupling to Rudder Tip

The coupling function to the tip of the rudder is easily obtained directly from the poles and zeros of the tail-cap input impedance.

Thus, using Eq. (35), the coupling to the rudder tip is obtained from Eq. (23) in the form

$$\psi_0(p) = K_0 \frac{11.11p^4 + 5.282p^3 + 12.57p^2 + 1.642p + 1}{12.33p^4 + 5.471p^3 + 12.86p^2 + 1.642p + 1} \quad (36)$$

The constant K_0 is evaluated by visually fitting the absolute magnitude of ψ_0 calculated from Eq. (36) to the experimental points. The calculated coupling function $|\psi_0|$ is shown in Fig. 15 where K_0 is found to be 1.3×10^{-2}. The calculated curve has very small variations from a constant value. Thus, although it exhibits the proper frequency variations, comparison with the measured points indicates larger variations should have been obtained. The most feasible explanation is that the measured antenna capacitance was low compared to the actual capacitance.

An increase in the static capacitance in Eq. (35) would result in a calculated coupling function $|\psi_0|$ which would have greater excursions from a constant value and the fit to the measured points would be better.

2. Coupling to Elevator Tip

The coupling function to the elevator tip, as indicated by Eq. (25), will contain the zeros of the antenna impedance in the denominator. The numerator of the coupling function, however, is unknown. The numerator was determined by a trial and error procedure to provide a good fit to the experimental points. The calculated coupling function to the elevator tip is found to be approximated by the equation

$$\psi_1(p) = K_1 \frac{122.5p^4 + 59.78p^3 + 53.74p^2 + 3.118p + 1}{12.33p^4 + 5.471p^3 + 12.86p^2 + 1.642p + 1} \quad (37)$$

where K_1 is again determined from the fit of the calculated $|\psi_1|$ to the measured data. The calculated function $|\psi_1|$ is shown in Fig. 16 where K_1 is found to be 0.8×10^{-4}.

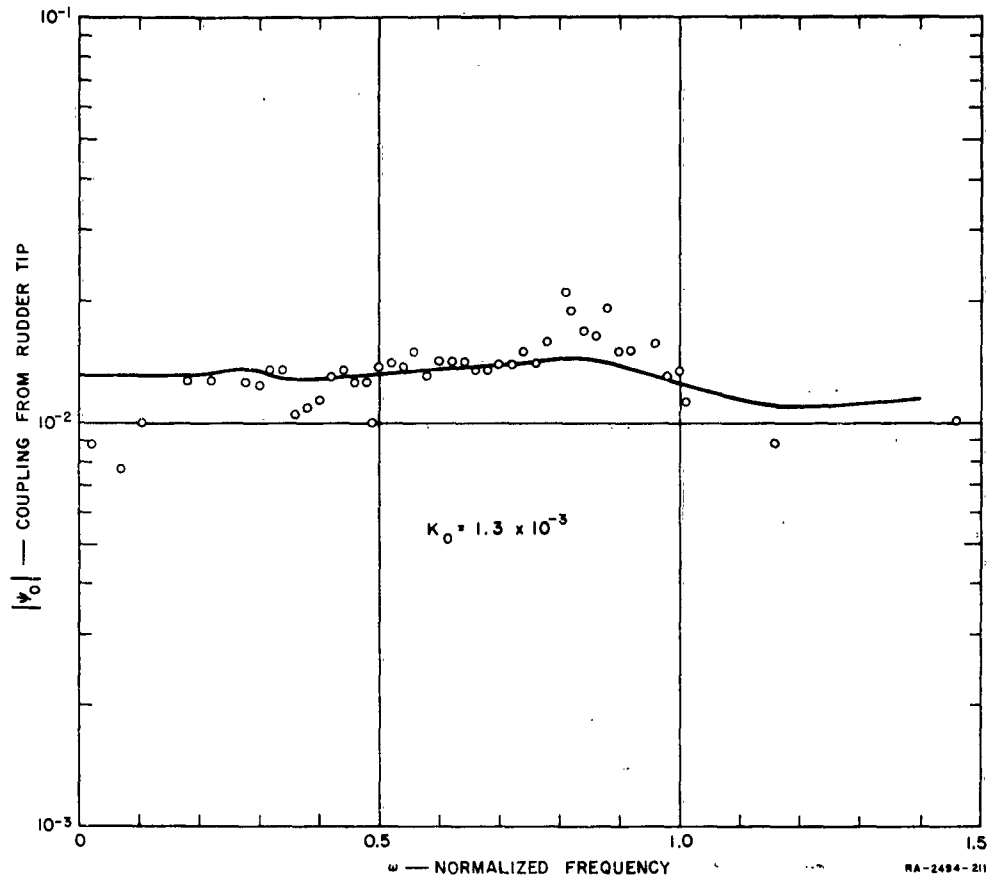

FIG. 15

CALCULATED COUPLING FUNCTION FROM RUDDER TIP

3. Coupling to the Wing Tip

The coupling function from the wing tip has a form similar to that from the elevator tip. Thus, in this case again the trial and error method must be used in order to determine the numerator. The coupling function to the wing tip was found to be approximated best by the expression

$$\psi_2(p) = K_2 \frac{50.77p^4 + 17.05p^3 + 44.02p^2 + 9.252p + 1}{12.33p^4 + 5.471p^3 + 12.86p^2 + 1.642p + 1} \quad . \quad (38)$$

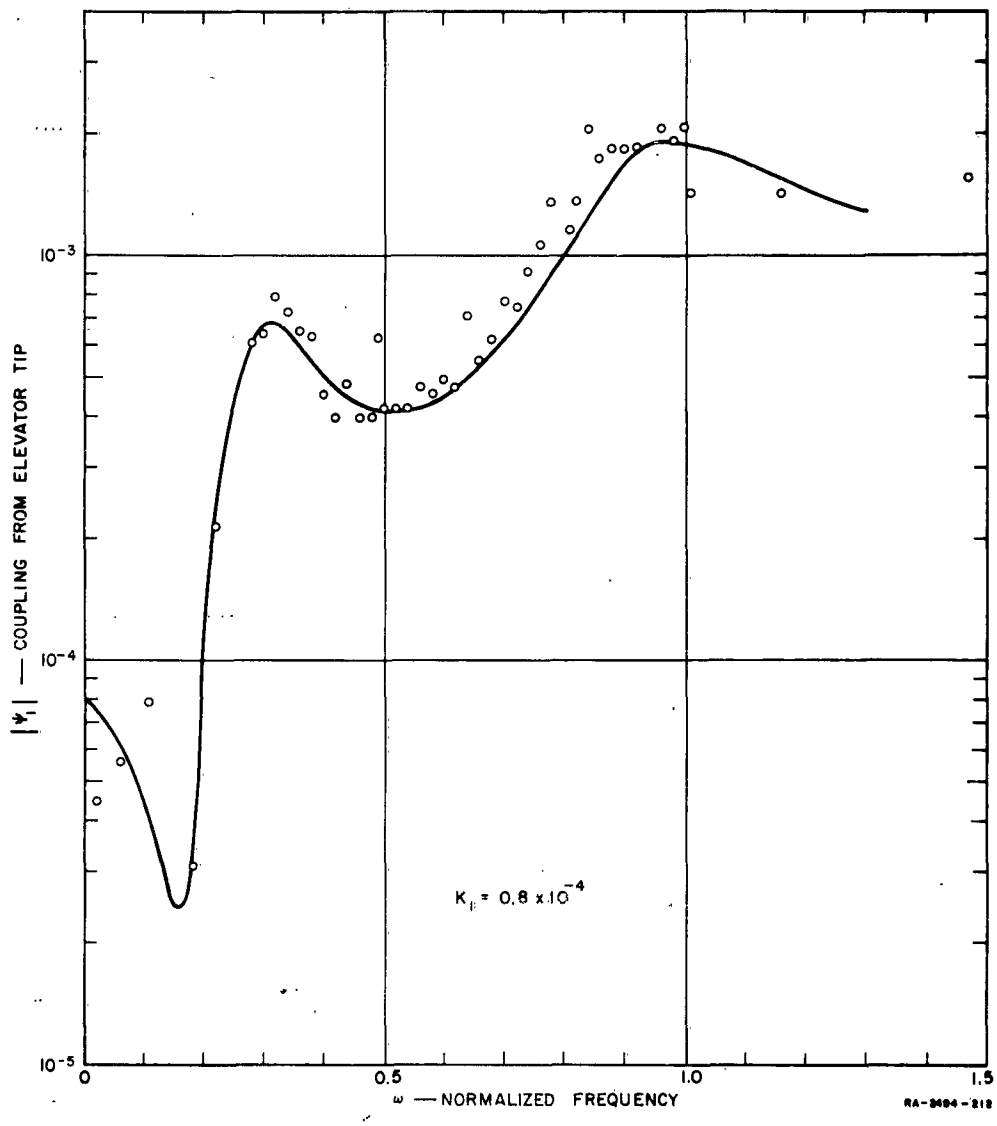

FIG. 16

CALCULATED COUPLING FUNCTION FROM ELEVATOR TIP

The absolute value $|\psi_2|$ was calculated from Eq. (38) and is plotted in Fig. 17 for a comparison with the measured points, and K_2 found to be 0.32×10^{-4}. The approximating function ψ_2 of Eq. (38) does not reproduce the resonance of the measured function at around 7 Mc. Naturally a function as simple as $\psi_2(p)$ of Eq. (38) could not be expected to reproduce the number of maxima and minima displayed by the measured data. A better approximation would require at least another pair of conjugate poles at around 7 Mc. This would require that the antenna impedance contain a weak resonance at a frequency slightly higher than 7 Mc which was not apparent from the measured data of the impedance shown in Fig. 14.

This conclusion is supported by the following observation on the approximation to the impedance shown in Fig. 14. The approximation for the second resonance is poor on the upper side (at around 14 Mc).

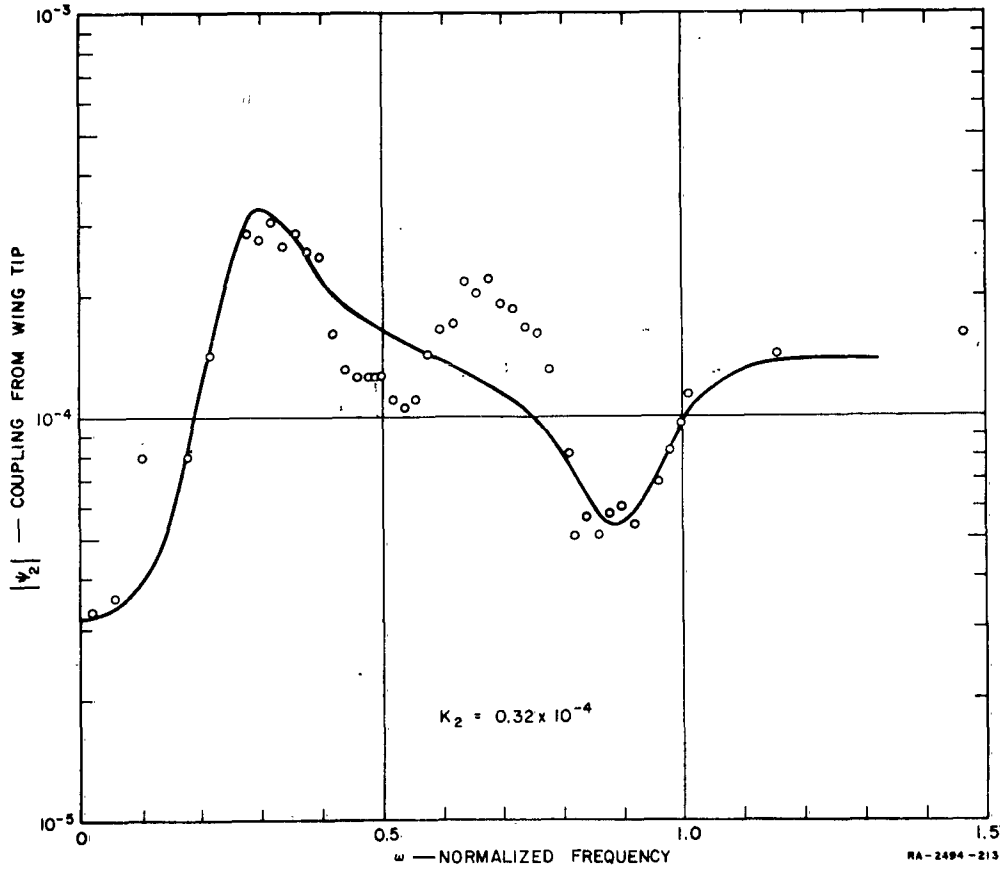

FIG. 17

CALCULATED COUPLING FUNCTION FROM WING TIP

This indicates that a much sharper resonance could be taken perhaps with a resonant frequency slightly higher than 10 Mc. This would in turn require a weaker resonance at around 8 Mc in order to provide a good fit to the low side of the measured resonance curve.

This more complex approximation was not undertaken since it was felt that the added complications would not be justified by the small improvement which would be obtained in the coupling function approximation. Since we are basically interested only in the length of the resulting noise pulses, the low frequency behavior is of major interest. Indeed the location of the lowest frequency pole is sufficient information in determining the largest time constant, and this would not be greatly altered by the addition of another set of poles to the coupling function.

VI CHARACTERISTICS OF NOISE AT ANTENNA TERMINALS

A. SHORT-CIRCUIT CURRENT PULSES

In Sec. II a relation was obtained, Eq. (4), which expressed the short-circuit current at the antenna terminals in terms of two functions. These two functions were determined independently in the previous sections and we are now in a position to calculate the noise pulse at the antenna.

The Laplace transform equivalent of Eq. (4) is

$$I_l(p) = \psi_l(p)D(p)$$

where p is the complex frequency variable. The function $D(p)$ is the Laplace transform of a simple exponential function which we have used to approximate the corona pulse characteristics [Eq. (10)]. For a pulse beginning at time $t = O$, $D(p)$ will have the form

$$D(p) = \frac{\frac{A}{\omega_0}}{p + \gamma} \tag{39}$$

where the frequency is normalized to ω_0 and $\gamma = \alpha/\omega_0$. The quantities A and α are the amplitude and decay constant of the corona pulse. The measured values and variation with pressure of these quantities are obtained from Figs. (6) and (7).

The coupling function $\psi(p)$ depends on the location of the corona discharge on the aircraft as described in the previous chapter. The coupling function from any part of the aircraft, to the tail-cap antenna, will have the same poles. Thus, let us write the coupling function from point l in the form

$$\psi_l(p) = K_l \frac{F_l(p)}{(p^2 + a_1p + b_1)(p^2 + a_2p + b_2)} \tag{40}$$

Then the short-circuit current will be given by

$$I_l(p) = \frac{K_l A}{\omega_0} \frac{F_l(p)}{(p+\gamma)(p^2+a_1p+b_1)(p^2+a_2p+b_2)} \quad (41)$$

The inverse transform will give the current pulse shape at the shortcircuited antenna terminals. Thus,

$$i_l(t) = \frac{K_l A}{2\pi i} \int_{-j\infty+C}^{j\infty+C} \frac{F_l(p)e^{p't}}{(p+\gamma)(p^2+a_1p+b_1)(p^2+a_2p+b_2)} \frac{dp'}{\omega_0}$$

where p' is the actual complex frequency variable and is related to the normalized variable p by the relation $p = p'/\omega_0$. Thus, changing variable of integration we find

$$i_l(t) = \frac{K_l A}{2\pi i} \int_{-j\infty+C\omega_0}^{j\infty+\omega_0 C} \frac{F_l(p)e^{p\omega_0 t}}{(p+\gamma)[(p+\alpha_1)^2+\beta_1^2][(p+\alpha_2)^2+\beta_1^2]} dp \,. \quad (42)$$

This integral is easily evaluated by separating the integrand into partial fractions. The short circuit current pulse shape will have the form

$$i_l(t) = B_{l0}e^{-\gamma\omega_0 t} + B_{l1}e^{+\alpha_1\omega_0 t}\left\{K_{l1}\sin\beta_1\omega_0 t + \cos\beta_1\omega_0 t\right\} + B_{l2}e^{-\alpha_2\omega_0 t}\left\{K_{l2}\sin\beta_2\omega_0 t + \cos\beta_2\omega_0 t\right\} \,. \quad (43)$$

The coefficients, B_l and K_l, were evaluated for the three major points of interest for three different altitudes. These coefficients are tabulated in Table I. Using these values and Eq. (43) the pulse shapes were calculated for noise coupled from the three extremities at sea level and at 40,000 feet. The alteration of the corona pulse by the aircraft resonances is observed in Figs. 18-20. It will be recalled, that the corona pulse is assumed to be a simple exponential whose normalized time constant, γ, is given in Table I. Figure 18 shows the pulses

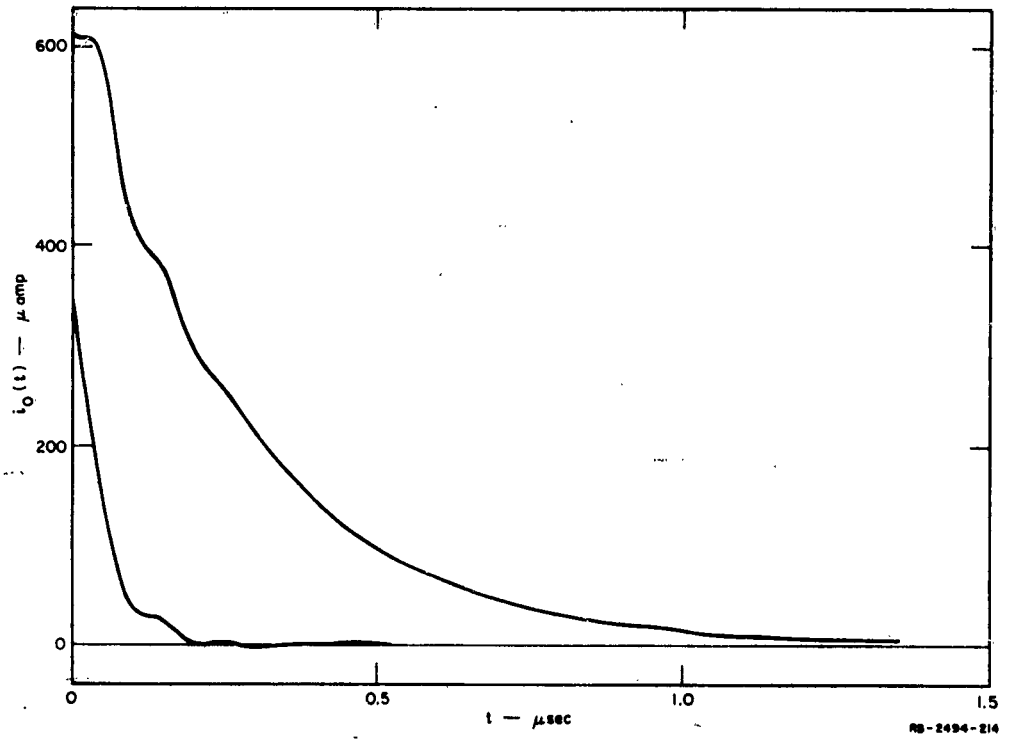

FIG. 18
CURRENT PULSE FROM RUDDER TIP

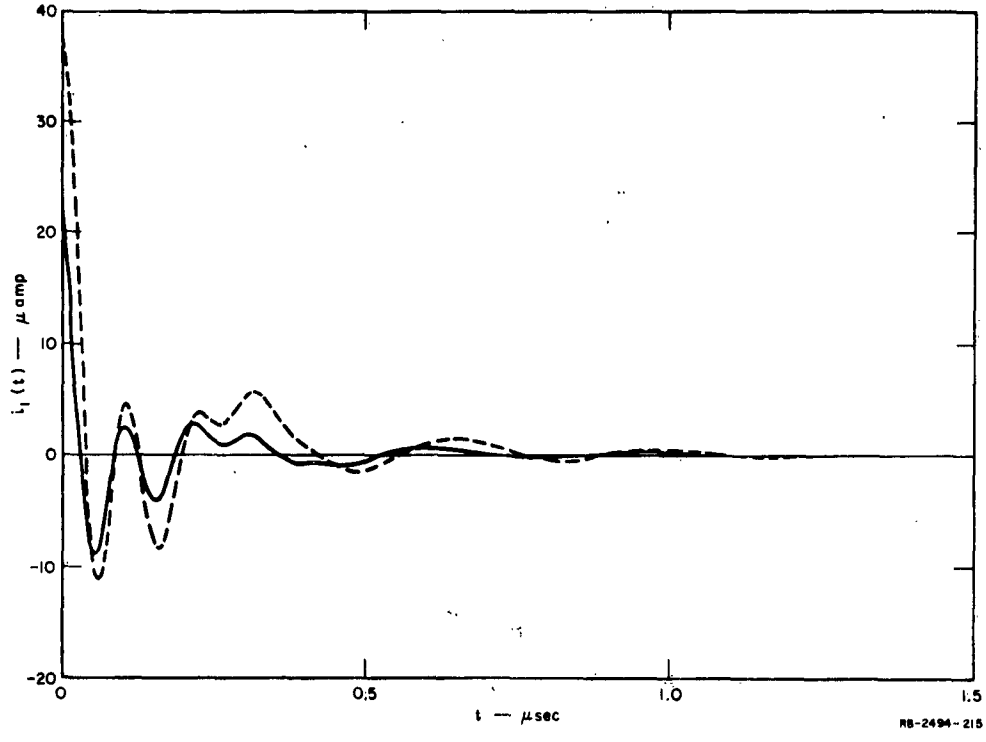

FIG. 19

CURRENT PULSE FROM ELEVATOR TIP

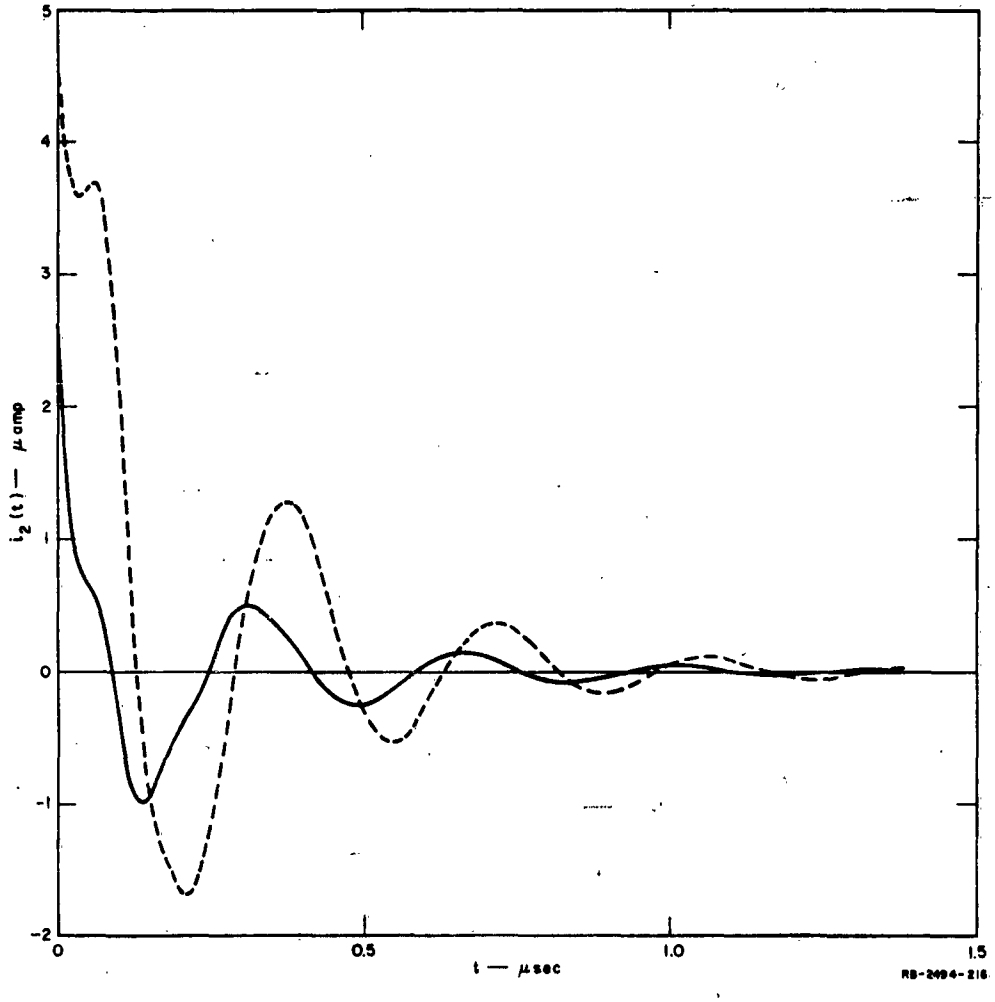

FIG. 20

CURRENT PULSE FROM WING TIP

TABLE I

SHORT-CIRCUIT CURRENT PULSE CHARACTERISTICS

$\omega_0 = 2\pi \times 10^7$		$\alpha_1 = 0.0567$ $\alpha_2 = 0.1651$	$\beta_1 = 0.292$ $\beta_2 = 0.943$	
ALTITUDE		$(\psi_0) \times 10^6$	$(\psi_1) \times 10^7$	$(\psi_2) \times 10^8$
Sea level				
($\gamma = 0.34$)	B_0	9.38	2.04	4.42
	B_1	-0.05	0.35	6.43
	K_1	-2.29	-4.75	-0.383
	B_2	-0.685	4.6	0.744
	K_2	-0.581	-0.0445	-5.06
20,000′				
($\gamma = 0.145$)	B_0	12.1	1.36	1.95
	B_1	-0.165	1.66	11.1
	K_1	-0.812	-1.33	0.267
	B_2	-0.973	5.88	1.68
	K_2	-0.333	0.189	-2.68
40,000′				
($\gamma = 0.061$)	B_0	16.4	1.27	3.04
	B_1	-0.275	3.00	14.1
	K_1	-0.427	-0.748	1.21
	B_2	-1.34	7.74	2.66
	K_2	-0.237	0.298	-2.15

at the antenna terminals due to corona at the rudder tip. As expected the form of the pulse was altered only slightly, and the amplitude of the pulses is very large. The noise pulses due to corona occurring from the elevator tip, shown in Fig. 19, show a considerable reduction in amplitude and a marked change in shape. Finally, the noise pulses due to corona occurring from the wing tip, see Fig. 20, show an extremely modified and expanded form while the amplitude has decreased even more.

B. STATISTICS OF PULSES

The corona discharge from a thin hemi-spherically capped cylinder consists of a pulse sequence which is almost periodic—*i.e.*, the pulses are almost equally spaced in time. This is particularly observed at relatively low levels of discharge. At high discharge rates, however, the pulse sequence loses the periodic quality.

When we consider the discharge from an edge, a similar observation is made just above threshold. The discharge from the edge will be taking

place from one point which, due to local unevenness, has a slightly higher field at the surface. In this case, however, the sequence of pulses is not nearly as periodic as the discharge from the point. The separation in time, of two consecutive pulses might be described as a slowly varying function in time according to some random function.

As the electric field at the edge is increased above threshold, and more current is discharged, it is observed that numerous points on the edge begin to discharge. So that, for high current discharges, which are our main concern, the over-all corona noise current will consist of a large number of these semi-periodic sequences of pulses. Indeed, the discharge from each of these points will lose its periodic quality as the current discharged is increased. Thus, the discharge from each source will be random in nature and incoherent to the other sources; consequently, the quadratic components will add. This was observed in the laboratory measurements where a half power relation was reached as the discharge current was increased (see Fig. 4). Furthermore, it appears from the spectrum shapes of Fig. 5, that the pulses must indeed reach a random sequence since the over-all aggregate may be considered as consisting of one noise source of an average of ν random pulses per second.

Thus we shall assume that the pulses arrive independently and at random in such a way that, for any small interval of time Δt, the probability that a pulse will occur is $\nu\Delta t$. Here ν is the average number of pulses per second and is determined by the magnitude of the discharge current. This assumption is sufficient to determine that the probability of k pulses occurring in an interval x is

$$P(k) = \frac{(\nu x)^k}{k!} e^{-\nu x} \tag{44}$$

which is the Poisson probability distribution.

It follows that the probability for no pulses to occur in a time of length x is

$$P(0) = e^{-\nu x} \quad . \tag{45}$$

The probability that the separation between two successive pulses lies between t and $t + \Delta t$ is given by $\phi(t)\Delta t$. Here $\phi(t)$ is the probability density function for a pulse to occur at time t. The probability density function may be established by differentiating with respect to x the relation

$$P(0) = e^{-\nu x} = \int_x^\infty \phi(\xi)d\xi$$

which states that the probability of finding no pulse from zero to x is equal to the probability of finding a pulse between x and ∞. From this we find

$$\phi(x) = \nu e^{-\nu x} \quad . \tag{46}$$

VII SIGNAL-TO-NOISE RATIOS AT OUTPUT OF IDEAL RECEIVER

A. GENERAL CONSIDERATIONS

Several methods have been proposed for the purpose of reducing the corona noise in aircraft. These methods include decoupled dischargers, blanking, and limiting.

Amplitude limiting has been used as a means of noise reduction by removing the peaks of the noise pulses. However, this scheme requires close control of the signal level to a value just below the limiting level so as to obtain maximum noise reduction with no distortion.

Blanking is an alternate electronic method of noise reduction that has received considerable attention. The principle of operation of the blanker is the following. Whenever a noise pulse arrives, it triggers a gate which then serves to short the input to the receiver for a period of time. This blanking period, during which the signal is blocked from the receiver, must be long enough to eliminate a significant fraction of the noise pulse. Thus, ideally, the blanker is a perfect switch which shorts and opens the input signal as a function of time. This switching of the signal will cause some of the power of the signal to be transferred to other frequencies. The power at these frequencies provides no information at the output and is therefore considered as noise. Thus, although the corona pulses are blocked at the terminals of the receiver, a new noise source is created by the switching of the incoming signal.

In contrast to the above mentioned electronic methods the noise can be reduced very drastically by proper alteration of the discharge region. Application of the coupling theorem indicates that the coupled noise is least when the discharge occurs in a region of low reciprocal field. Furthermore, it has been shown[10] that the discharge from a point of small radius is inherently less noisy than the discharge from a tip of large radius. The decoupled discharger developed by Tanner[19] makes use of these factors to provide a drastic reduction in the noise coupled to the antenna. Noise reduction of at least 45 db has been obtained in the laboratory.

It is of interest, therefore, to evaluate the relative merits of these two methods of noise reduction; decoupled dischargers, and blanking. The signal-to-noise ratio at the output of an ideal receiver will be calculated for both methods.

B. SHORT-CIRCUIT CURRENT DUE TO SIGNAL

The short-circuit current of a receiving antenna will be proportional to the amplitude of the incident wave. This proportionality will depend on the antenna orientation with respect to the direction of propagation and the polarization of the incident wave.

Thus, a comprehensive analysis of signal reception by the tail-cap antenna would require consideration of the probable angle of arrival of the signals and on their polarization. Furthermore such variations as frequency effects on the antenna pattern must also be included. In ofder to avoid these complications we shall make use of the following approximation.

For an antenna which is small compared to a wavelength of the incident wave, the short-circuit current is given by

$$|I_s| = \omega_c \epsilon_0 A |E_c| \tag{47}$$

where E_c is the incident signal field strength, ω_c is the frequency of the signal and A is the effective induction area of the antenna and is essentially a measure of antenna sensitivity. At low frequencies, the tail-cap antenna pattern is very nearly that of a dipole. Consequently, Eq. (47) gives the current that is the maximum for the given field strength in that the signal direction and polarization are assumed as most favorable. Equation (47) thus provides a good estimate up to one to two megacycles where the aircraft length begins to approach a tenth of a wavelength. Above this frequency, the relation will provide a more approximate estimate of antenna performance.

The effective induction area, A, may be determined by electrostatic techniques[18] in the laboratory. For the tail-cap antenna under consideration the area was measured at 33.9 m^2.

C. GENERAL ANTENNA TERMINATION

In a practical situation, the antenna will be terminated in a load impedance, $Z_L(p)$. Thus, the short-circuit current can be considered as a current generator with the parallel combination of $z_{11}(p)$ and $Z_L(p)$, across it, as shown in Fig. 21.

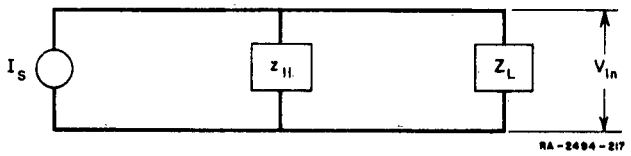

FIG. 21
GENERAL ANTENNA TERMINATION

The input voltage to the receiver will be given by

$$V(p) = I_s(p) \frac{z_{11}(p) Z_L(p)}{z_{11}(p) + Z_L(p)} \quad . \tag{48}$$

A case of special interest occurs when $Z_L(p) = \rho$, a pure resistance which is very small compared to z_{11}. When these conditions are met, then a good approximation is obtained by

$$V(p) = \rho I_s(p) \quad . \tag{49}$$

This special case provides us with a simpler expression for the input voltage and at the same time it consists of an input to the receiver which includes no filtering. This is the required input in the application of a blanker for the purpose of noise reduction. Since we shall be comparing the relative merits of performance with and without blanker, this termination will be used in the analysis which follows.

D. ANALYSIS FOR DECOUPLED DISCHARGERS

1. Ideal Receiver

For our analysis we shall consider the highly idealized receiver shown in Fig. 22.

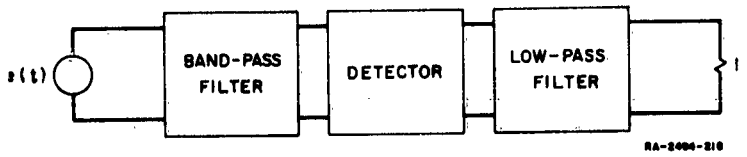

FIG. 22
IDEAL RECEIVER

The received signal is an amplitude-modulated-carrier and the receiver consists of a band-pass filter centered about the carrier frequency, a detector, and a low pass filter. The detector will be assumed to be an ideal frequency translator. The attenuation of the ideal filters is zero in the pass band, and infinite outside this band.

The system may be simplified considerably by combining the two filters into one filter. The pass-band filter may be transposed to the other side of the detector, since the detector is ideal and introduces no distortion or noise. In doing this, the pass band must be properly altered. Suppose the band-pass filter has a pass band of $2f_s$ centered about f_c, the carrier frequency. The detector translates up and down in frequency by a frequency f_c, while the low pass filter has a cutoff at some frequency f_k such that $f_s < f_k < 2f_c - f_s$. When the band-pass filter is moved to the other side of the detector the pass band will divide into two parts. Thus, the filter will consist of a low pass section with a cutoff at f_s and a band pass section of $2f_s$ centered about $2f_c$. When this filter is combined with the low pass filter, the result is a low pass filter with a cutoff at f_s. The system we must analyze is shown in Fig. 23.

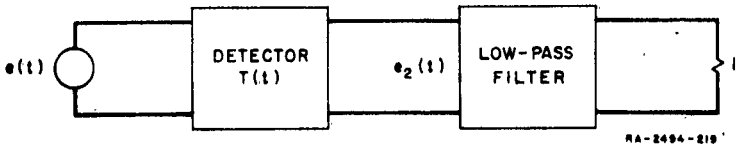

FIG. 23
EQUIVALENT RECEIVER

2. Input Signal

We shall consider an input which consists of a carrier of frequency ω_c amplitude modulated by a single frequency ω_s. In addition, the input will have numerous other carriers of frequencies ω_l and the noise pulses due to the aircraft corona discharges. In the analysis we shall neglect atmospheric noise.

In an interval of time $-T < t < T$, where T is very much larger than the average spacing between the noise pulses, the input will be:

$$e(t) = C_0 \cos \omega_c t + \frac{C_0 m}{2} \cos (\omega_c - \omega_s)t + \frac{C_0 m}{2} \cos (\omega_c + \omega_s)t$$

$$+ \sum_{l=1}^{n} C_l \cos \omega_l t + \sum_{k=-N}^{N} f(t - t_k) \text{ for } -T < t < T \qquad (50)$$

while outside the interval the signal is zero. For the present, it is being assumed that the noise pulses are identical and that the average number per second is ν.

The Fourier transform of the input, $E(\omega)$, is given by the equation

$$E(\omega) = C_0\left[\frac{\sin (\omega - \omega_c)T}{\omega - \omega_c} + \frac{\sin (\omega + \omega_c)T}{\omega + \omega_c}\right] + \frac{C_0 m}{2}\left[\frac{\sin (\omega - \omega_c + \omega_s)T}{\omega - \omega_c + \omega_s}\right.$$

$$\left. + \frac{\sin (\omega + \omega_c - \omega_s)T}{\omega + \omega_c - \omega_s} + \frac{\sin (\omega - \omega_c - \omega_s)T}{\omega - \omega_c - \omega_s} + \frac{\sin (\omega + \omega_c + \omega_s)T}{\omega + \omega_c + \omega_s}\right]$$

$$+ \sum_{l=1}^{n} C_l\left[\frac{\sin (\omega - \omega_l)T}{\omega - \omega_l} + \frac{\sin (\omega + \omega_l)T}{\omega + \omega_l}\right] + F(\omega) \sum_{k=-N}^{N} e^{-j\omega t_k} \qquad (51)$$

3. Ideal Detector

The output of the detector is given by the product of the input $e(t)$ and the detector response $T(t)$, *i.e.*,

$$e_2(t) = T(t)e(t) \qquad (52)$$

The ideal frequency translator has a response of the form

$$T(t) = A \cos(\omega_d t + \theta_d) \tag{53}$$

and it translates the frequency of input signals up and down by ω_d. Since we want the output to contain the modulating frequency ω_s we must make $\omega_d = \omega_c$. Furthermore if the power in the side bands is to add up to a maximum in the output the phase θ_d must be equal to the phase of the carrier. Thus θ_d must be equal to zero, and the detector response must be

$$T(t) = A \cos \omega_c t \tag{54}$$

The Fourier transform is found to be

$$T(\omega) = A\pi [\delta(\omega - \omega_c) + \delta(\omega + \omega_c)] \tag{55}$$

where we use

$$2\pi\delta(x) = \int_{-\infty}^{\infty} e^{-jxt}\, dt$$

It can be shown that the product of two functions in the time domain in Eq. (52), results in a convolution integral in the frequency domain. Thus,

$$E_2(\omega) = \frac{1}{2\pi} \int_{-\infty}^{\infty} T(\Omega) E(\omega - \Omega) d\Omega \tag{56}$$

Substituting Eq. (55) into the above equation we find

$$E_2(\omega) = \frac{A}{2} \left[E(\omega - \omega_c) + E(\omega + \omega_c) \right] \tag{57}$$

for convenience we let $A = 2$ so that

$$E_2(\omega) = E(\omega - \omega_c) + E(\omega + \omega_c) \tag{58}$$

This indicates a power gain through the detector, although no effect on the signal to noise ratio is implied. Applying Eq. (58) to Eq. (51) we obtain

$$E_2(\omega) = C_0\left[\frac{2\omega T}{\omega} + \frac{\sin(\omega - 2\omega_c)T}{\omega - 2\omega_c} + \frac{\sin(\omega + 2\omega_c)T}{\omega + 2\omega_c}\right]$$

$$+ \frac{C_0 m}{2}\left[2\,\frac{\sin(\omega - \omega_s)T}{\omega - \omega_s} + 2\,\frac{\sin(\omega + \omega_s)T}{\omega + \omega_s} + \frac{\sin(\omega - 2\omega_c + \omega_s)T}{\omega - 2\omega_c + \omega_s}\right.$$

$$\left. + \frac{\sin(\omega - 2\omega_c - \omega_s)T}{\omega - 2\omega_c - \omega_s} + \frac{\sin(\omega + 2\omega_c - \omega_s)T}{\omega + 2\omega_c - \omega_s} + \frac{\sin(\omega + 2\omega_c + \omega_s)T}{\omega + 2\omega_c + \omega_s}\right]$$

$$+ \sum_{l=1}^{n} C_l\left[\frac{\sin(\omega - \omega_c - \omega_l)T}{\omega - \omega_c - \omega_l} + \frac{\sin(\omega - \omega_c + \omega_l)T}{\omega - \omega_c + \omega_l}\right.$$

$$\left. + \frac{\sin(\omega + \omega_c - \omega_l)T}{\omega + \omega_c - \omega_l} + \frac{\sin(\omega + \omega_c + \omega_l)T}{\omega + \omega_c + \omega_l}\right]$$

$$+ F(\omega - \omega_c) \sum_{k=-N}^{N} e^{-j(\omega-\omega_c)t_k} + F(\omega + \omega_c) \sum_{k=-N}^{N} e^{-j(\omega+\omega_c)t_k} . \tag{59}$$

The power spectrum $G(\omega)$ is defined by the limit

$$G(\omega) = \lim_{T\to\infty}\left\{\frac{|E_2(\omega)|^2}{2\pi T} + \frac{|E_2(0)|^2}{2T^2}\,\delta(\omega) + \frac{\sum_j |E_2(\omega_j)|^2}{2T^2}\,\delta(\omega - \omega_j)\right\} \tag{60}$$

consisting of a continuous and a discrete spectrum. Substituting Eq. (59) into Eq. (60) and recalling that the times t_k are random we find

$$G(\omega) = \frac{\nu}{\pi}\left[|F(\omega-\omega_c)|^2 + |F(\omega+\omega_c)|^2\right] + 2C_0^2\,\delta(\omega)$$

$$+ \frac{C_0^2}{2}\left[\delta(\omega-2\omega_c) + \delta(\omega+2\omega_c)\right] + \frac{C_0^2 m^2}{8}\left[\delta(\omega-\omega_m) + \delta(\omega+\omega_m)\right]$$

$$+ \sum_{l=1}^{n} \frac{C_l^2}{2}\left[\delta(\omega-\omega_c+\omega_l) + \delta(\omega-\omega_c-\omega_l) + \delta(\omega+\omega_c-\omega_l)\right.$$

$$\left. + \delta(\omega+\omega_c+\omega_l)\right] \quad .$$

4. OUTPUT

The power in a band of frequencies ω_1 to ω_2 is found from the power spectrum by the integration

$$P = \int_{\omega_1}^{\omega_2} G(\omega)\,d\omega \quad .$$

The cutoff of the low pass filter is ω_k which must be greater than the modulating frequency ω_s. Then the power in the unit resistance at the output will consist of the signal power S given by

$$S = \frac{C_0^2 m^2}{8} \quad , \tag{61}$$

and the noise power N given by

$$N = \frac{\nu}{\pi}\int_0^{\omega_k}\left[|F(\omega-\omega_c)|^2 + |(\omega+\omega_c)|^2\right]d\omega \quad .$$

The range of integration is very small compared to the range in which $F(\omega)$ changes appreciably, so that we may evaluate the integral to a good approximation by

$$N = \frac{2\nu\omega_k}{\pi}|F(\omega_c)|^2 \quad . \tag{62}$$

Equation (61) may be related to the incident signal field by Eq. (47). Thus we have

$$S = K \frac{(\rho\omega\xi\epsilon_0 A)^2 |E_c|^2 m^2}{8} \quad . \tag{63}$$

In a similar way Eq. (62) may be rewritten, using Eq. (4),,

$$N = K \frac{2\nu\omega_k}{\pi} \rho^2 |\psi(\omega_c)|^2 |D(\omega_c)|^2 \quad . \tag{64}$$

Thus the signal to noise ratio is given by

$$\frac{S}{N} = \frac{(\omega_c \epsilon_0 A m)^2 |E_c|^2}{16 \frac{\nu\omega_k}{\pi} |\psi(\omega_c)|^2 |D(\omega_c)|^2} \quad . \tag{65}$$

5. Signal-to-Noise Ratio for Aircraft With no Decoupling

In the above analysis, which led to the noise power given by Eq. (64), it was assumed that all the noise pulses were identical. In the case of an aircraft in a relatively severe charging condition, corona discharges result from the wings, the elevators, and the rudder.

Let us now consider only the corona discharges taking place on the wing. There will be corona occurring at numerous points from the wing tip along the trailing edge to some inboard point on the wing. The coupling function from these points, as we move inboard from the tip, will slowly change in its frequency characteristics but more important, its magnitude will drop off with distance from the tip. This is illustrated in Fig. 24.

Thus the noise pulses at the antenna, due to corona from the wing, will consist of pulses of varying amplitudes and slight differences in shape. Due to the method we have used to compute the pulse characteristics, the following approximation will provide an adequate compensation.

The coupling function which we measured, *i.e.* $|\psi_2|$ was taken at the tip of the wing. This then represents a high value of coupling for the wing discharges as a whole. On the other hand, if we use the $|D|$ as

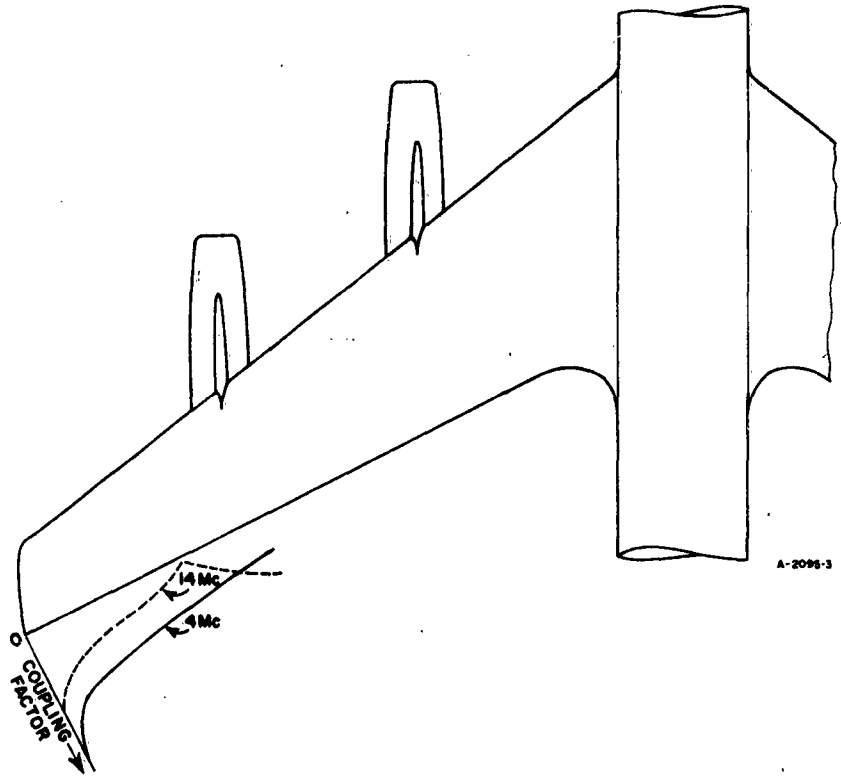

FIG. 24

VARIATION OF COUPLING NEAR WING TIP OF BOEING 707

measured from an edge rather than the one from the tip, a satisfactory compensation will be made. Thus we shall assume that all the pulses from the wing are identical and have an amplitude given by the product of $|\psi_2|$ and $|D|$ of Fig. 7.

By similar argument for the elevator and rudder discharges, we will assume that the noise in the antenna will consist of three sets of identical pulses of the type shown in Figs. 18, 19, and 20. The number of pulses of each type will depend on the proportion of current discharging from the wing tips, the elevator tips, and the rudder tip. This division of current depends upon the rate of charging; and also, upon other factors subject to variations with altitude, airspeed, and the particular aircraft under consideration, and cannot be determined exactly.

Estimates of the proportions have been obtained, however, from instrumented flight tests carried out on a Boeing 707. It has been found

that in sufficiently high charging situations, the following proportions are appropriate:

Current from wings = $4/7$ of total

Current from elevators = $2/7$ of total

Current from rudder = $1/7$ of total

Since the receiver is linear, it is apparent that if the input, Eq. (50), contains three sums, each containing identical pulses, the output noise power will consist of three terms similar to Eq. (64). Thus, if the total discharge required ν pulses per second, the noise power in the output will be

$$N = K \frac{2\omega_k \rho^2 \nu}{\pi} |D(\omega_c)|^2 \left\{ \frac{1}{7} |\psi_0(\omega_c)|^2 + \frac{2}{7} |\psi_1(\omega_c)|^2 + \frac{4}{7} |\psi_2(\omega_c)|^2 \right\}$$

and the signal to noise ratio

$$\frac{S}{N} = \frac{|\epsilon_0 A m \omega_c E_c|^2}{\frac{16}{7} \frac{\nu \omega_k}{\pi} |D(\omega_c)|^2 \left[|\psi_0(\omega_c)|^2 + 2|\psi_1(\omega_c)|^2 + 4|\psi_2(\omega_c)|^2 \right]} \quad (66)$$

For a specific modulation index and receiver bandwidth the signal to noise ratio is

$$\frac{S}{N} = K_N \frac{|\omega_c E_c|^2}{\frac{\nu |D|^2}{7} \left[|\psi_0|^2 + 2|\psi_1|^2 + 4|\psi_2|^2 \right]} \quad (67)$$

where

$$K_N = \frac{(\epsilon_0 A m)^2}{32 f_k}$$

The signal to noise ratio is affected by the magnitude of the discharge current, the signal frequency, the altitude, and of course, the incident field strength of the signal. Note that if an antenna of different

sensitivity was placed in the same location, the signal-to-noise ratio would remain unaffected, since both the signal and the noise would change in the same proportion.

6. Signal-to-Noise Ratio With Decoupling

We shall assume the following situation:

(1) Receiver bandwidth f_k = 3 kc

(2) Modulation index $m = 0.5$

(3) Decoupling of 50 db provided by the dischargers.

As we have mentioned previously, the use of Tanner's[19] decoupled dischargers result in a reduction in noise of at least 45 db.

Thus the signal-to-noise ratio with decouplers located at all the significant discharge regions will be

$$\left(\frac{S}{N}\right)_D = K_N \frac{\omega_c^2 E_c^2}{\frac{\nu|D|^2}{7}\left[|\psi_0|^2 + 2|\psi_1|^2 + 4|\psi_2|^2\right]} \times 10^5 = \chi_D e_c^2 \qquad (68)$$

where

e_c-is in μ volts/m

and

$$\chi_D = \frac{K_N \omega_c^2 \times 10^{-8}}{\frac{\nu|D|^2}{7}\left[|\psi_0|^2 + 2|\psi_1|^2 + 4|\psi_2|^2\right]}$$

The function χ_D is plotted in Fig. 25. The plot is for a discharge of one milliamp at two altitudes.

A considerable improvement can be obtained for this antenna by allowing no discharges to occur from the rudder tip. This can be accomplished by covering the rudder tip and trailing edge with a dielectric coating of high electrical strength. When this is done, assuming the discharge current to divide in a two to one proportion between the wing and elevator,

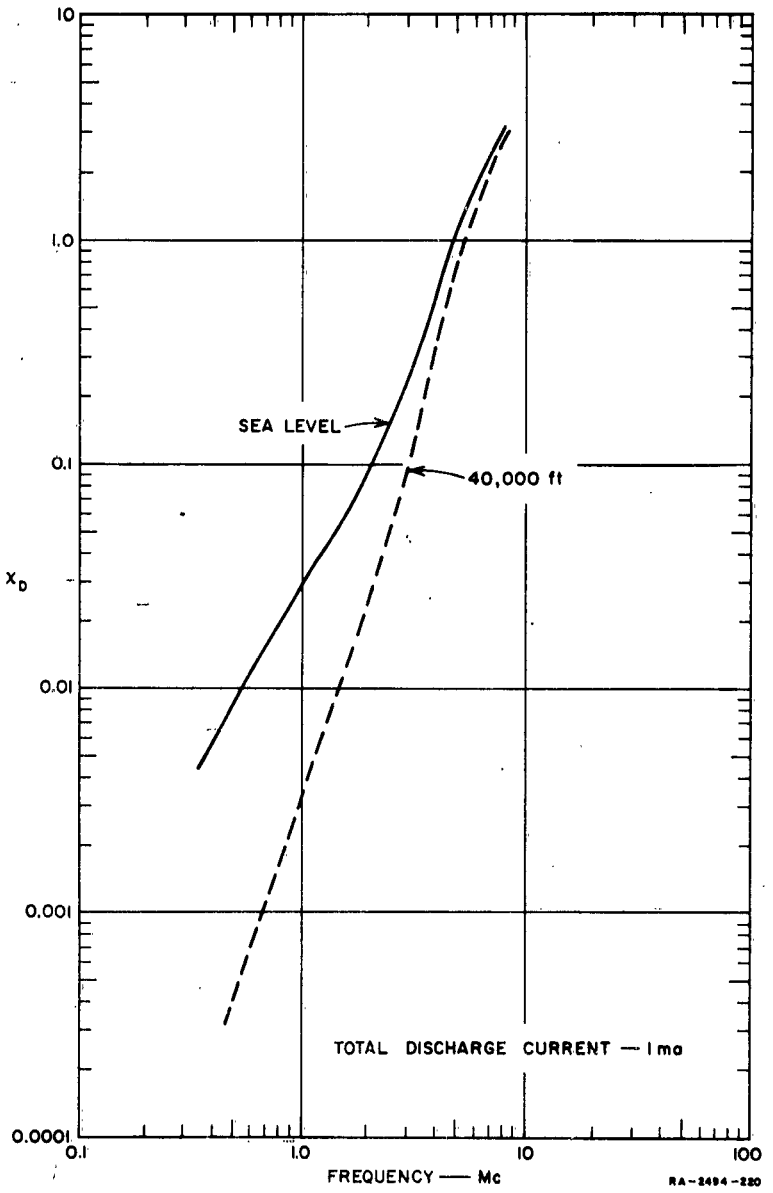

FIG. 25

SIGNAL-TO-NOISE RATIO WITH DECOUPLING FOR UNIT INCIDENT FIELD STRENGTH

we obtain

$$\left(\frac{S}{N}\right)_{D'} = \chi_{D'} e_c^2 \tag{69}$$

where

e_c-is in μ volts/m

and

$$\chi_{D'} = \frac{K_N \omega_c^2 \times 10^{-8}}{\frac{\nu |D|^2}{3} \{|\psi_1|^2 + 2|\psi_2|^2\}}$$

This function $\chi_{D'}$ is plotted on Fig. 26 for a discharge current of one milliamp at sea level and at 40,000 ft altitude.

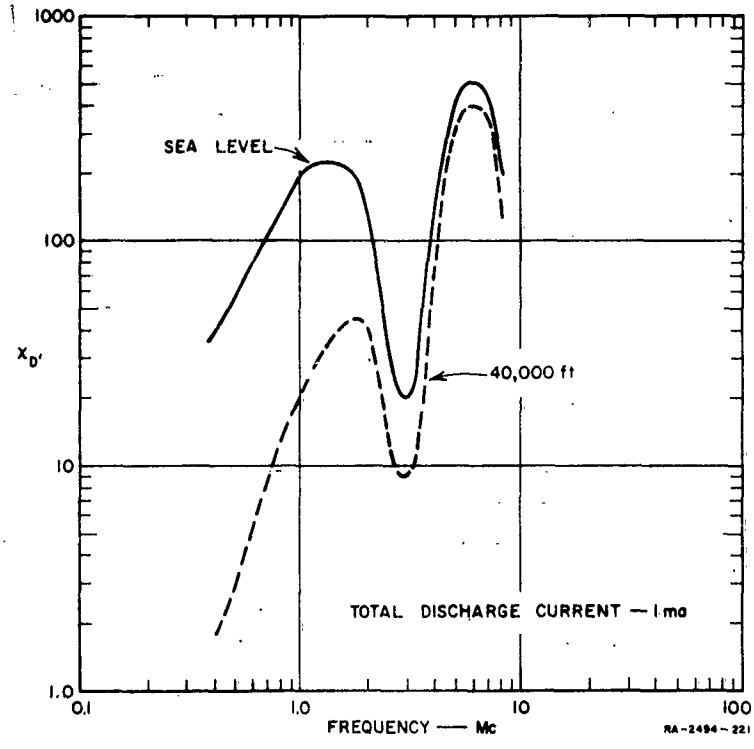

FIG. 26

SIGNAL-TO-NOISE RATIO WITH DECOUPLING FOR UNIT INCIDENT FIELD STRENGTH WITH RUDDER CORONA DISALLOWED

A current of 1 ma represents a condition of relatively high charging on the Boeing 707, though discharge currents of 6 ma have been observed for short periods of time.

E. ANALYSIS FOR BLANKER

1. Ideal Blanker

The ideal blanker is a perfect switch which shorts the input to the receiver whenever a noise pulse is present in the input. Thus, when a noise pulse arrives, it triggers a gate which in turn shorts the input to the receiver for a period of time. This blanking period, during which the signal is blocked from the receiver, must be long enough to suppress a significant portion of the noise pulse.

It appears evident, that as the length of the blanking period increases, the signal to noise ratio in the output will decrease. Indeed, as will be shown presently, the signal power decreases and at the same time the noise power increases as the blanking period is increased. Because of this, blanking will have the greatest chance of succeeding, if it is accomplished before any filtering is applied to the incoming signals. Otherwise, the impulses produced by the corona discharges will be stretched out in time (as slowly damped oscillations) by the narrow band filters, necessitating longer blanking periods.

At the same time, unwanted carriers which will be present in the input will contribute noise in the output, due to the switching action of the blanker. Thus, some filtering of low Q could be introduced ahead of the blanker with beneficial results. The Q of the filter should be sufficiently small so that the oscillations produced in the tuned circuits will be negligible by the end of a blanking period that is based on the original length of the pulses.

Consider, for example, that a simple tuned circuit, resonant at the carrier frequency, is placed ahead of the blanker. It is known that the response of the circuit to an impulse will be a damped sinusoid with a decay constant $\alpha = \omega_c/2Q$ where ω_c is the resonant frequency and Q the quality factor of the circuit (assuming $Q > 1/2$). Also, it is known that the bandwidth B, of the circuit—as measured between half power points—is given by $B = \omega_0/Q$. Combining these two equations we find that $B = 2\alpha$. Now, α must be made equal to the smallest decay constant involved in the

incoming pulses, Eq. (43), *i.e.*, $\alpha \equiv \alpha_1\omega_0$ (From Table I). In this way, we find that the bandwidth must be slightly over a megacycle, independent of the carrier frequency ω_c.

In our analysis we will assume that there is no filter ahead of the blanker while the blanker is placed ahead of the receiver shown in Fig. 22. As before, the filters in the receiver may be combined and the resulting system with blanker is shown in Fig. 27, where the cutoff of the low pass filter occurs at a frequency ω_k.

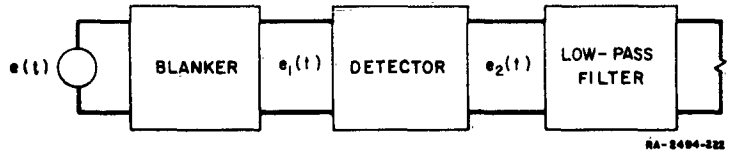

FIG. 27
BLANKER AND IDEAL RECEIVER

The blanking function $b(t)$ will be a random function which is determined by statistics of the noise pulses and the exact mode of operation of the blanker. Lucke and Weaver,[20] who made an extensive study of blanking, considered several forms of blanking functions such as periodic, fixed blanking length with random occurrence, random length with fixed occurrence, etc. In our analysis, which differs from theirs, we shall consider a blanking function which represents the type of operation a blanker should ideally perform.

2. Blanking Function

A blanker that has a fixed blanking period is the simplest form which might be applied for noise reduction. Thus, when a noise pulse arrives, if the receiver is unblocked, a blanking period of length τ is initiated. On the other hand, if the receiver is blocked, the pulse has no effect. This blanker would block a large number of noise pulses and the output signal to noise ratio would improve. Note that there may be appreciable noise in the output due to the tails of the pulses which are not fully blanked out.

If we assume noise pulses having the form of simple exponentials, the analysis of Appendix B allows us to estimate the noise in the output due

to the remainders of the pulses which are unblanked. We find that for $\nu = 10^6$ and $\tau = 10^{-5}$ for pulses with $\alpha = 4 \times 10^6$ the noise in the output due to the unblanked pulses is 0.026 of the noise with no blanking. This would result in less than a 16-db improvement in the signal to noise ratio since the blanker switching would also introduce additional noise in the output.

It appears that a more practical blanker would be one which provides a means of extending the blanking period whenever it is necessary. We shall assume that once a blanking period is triggered by a noise pulse, it will last for a period of time τ, provided no other pulses arrive during this time. Otherwise the blanking period will be extended and it will continue until the separation between two consecutive pulses is greater than τ. In other words, every pulse that arrives creates a gate which lasts for a time τ after its arrival. In this way all the tails of pulses will be eliminated and the noise in the output will be due only to the switching action of the blanker.

It is necessary to determine the probability density function $W(x)$ of the length of the blanking periods. Naturally, it is the statistical properties of the noise pulses, Sec. VI-B, which will govern this distribution. We can immediately write down the probability of occurrence of the minimum blanking period of length τ as

$$P(\tau) = e^{-\nu\tau} \tag{70}$$

which is the probability of no pulses occurring during a time τ. Thus, $W(x)$ will contain a delta function at $x = \tau$ whose area is given by Eq. (70).

For a blanking period of length x, we have postulated that there are no pulses for a time τ from the end. Thus, we can write that the probability density for a blanking period of length x is equal to the probability density for a pulse to occur at $(x - \tau)$, times the probability for no pulses to occur for a time τ, *i.e.*,

$$W(x) = e^{-\nu\tau} X(\xi) \tag{71}$$

where

$$\xi = x - \tau$$

Thus let us consider the range of x restricted to $\tau < x < 2\tau$. Then using Eq. (46) we can write $X(\xi)$ as the sum of the probability distribution for zero or more pulses to occur between zero and ξ, *i.e.*

$$X_1(\xi) = \nu e^{-\nu\xi} + \nu^2 \int_0^{\xi} e^{-\nu(\xi-\xi_1)}\, e^{-\nu\xi_1}\, d\xi_1$$

$$+ \nu^3 \int_0^{\xi} \int_0^{\xi_2} e^{-\nu(\xi-\xi_2)}\, e^{-\nu(\xi_2-\xi_1)}\, e^{-\nu\xi_1}\, d\xi_1 d\xi_2 + \ldots$$

$$= \nu e^{-\nu\xi} \left\{ 1 + \nu\xi + \frac{(\nu\xi)^2}{2!} + \frac{(\nu\xi)^3}{3!} \ldots \right\}$$

thus

$$X_1(\xi) = \nu \tag{72}$$

and using Eq. (71)

$$W_1(x) = \nu e^{-\nu\tau} \qquad \text{for} \qquad \tau < x < 2\tau \quad . \tag{73}$$

The result for $X_1(\xi)$ in Eq. (72) is in agreement with our assumptions of Section VI-C and we could have written this down directly from the assumption that the probability that a pulse occurs between ξ and $d\xi + \xi$ is given by $\nu d\xi$.

For the range $2\tau < x < 3\tau$, we must begin taking into account that the separation between pulses must be τ or less. Thus for this range we can write:

$$X_2(x) = \int_{\xi-\tau}^{\tau} \nu e^{-(\xi-\xi_1)} X_1(\xi_1) d\xi_1$$

$$+ \int_{\tau}^{\xi} \int_{\xi_2-\tau}^{\tau} \nu e^{-\nu(\xi-\xi_2)} \nu e^{-\nu(\xi_2-\xi_1)} Y_1(\xi_1) d\xi_1 d\xi_2$$

$$+ \int_{\tau}^{\xi} \int_{\tau}^{\xi_3} \int_{\xi_2-\tau}^{\tau} \nu e^{-\nu(\xi-\xi_3)} \nu e^{-\nu(\xi_3-\xi_2)} \nu e^{-\nu(\xi_2-\xi_1)} X_1(\xi_1) d\xi_1 d\xi_2 d\xi_3$$

summing the results of integrations we find

$$X_2(\xi) = \nu e^{-\nu\tau} [e^{\nu\tau} - \nu(\xi - \tau) - 1] \quad . \tag{74}$$

It follows that

$$W_2(x) = \nu e^{-2\nu\tau}[e^{\nu\tau} - \nu(x - 2\tau) - 1].$$

$$= \nu e^{-\nu\tau} - \nu e^{-2\nu\tau}\,[1 + \nu(x - 2\tau)] \qquad (75)$$

which holds for the range $2\tau < x < 3\tau$.

In a similar way we can find the probability density in the next range of length τ

$$W_3(x) = \nu e^{-\nu\tau} - \nu e^{-2\nu\tau}[1 + \nu(x - 2\tau)] \qquad (76)$$

$$+ \nu e^{-3\nu\tau}\left[\nu(x - 3\tau) + \nu^2\,\frac{(x - 3\tau)^2}{2!}\right]$$

in the range $3\tau < x < 4\tau$.

In this way we obtain the over-all distribution which can be written in the following form

$$W(x) = e^{-\nu\tau}\,\delta(x - \tau) + \nu e^{-\nu\tau}\,U(x - \tau)$$

$$- \nu e^{-2\nu\tau}[1 + \nu(x - 2\tau)]U(x - 2\tau)$$

$$+ \nu e^{-3\nu\tau}\left[\nu(x - 3\tau) + \nu^2\frac{(x - 3\tau)^2}{2}\right]U(x - 3\tau) + \ldots \qquad (77)$$

where

$U(x)$ is the unit step function.

It can be shown that the distribution function $W(x)$ of Eq. (77) satisfies the condition

$$\int_0^\infty W(x)dx = 1$$

and the average value of the pulse length $\bar{x}$ is found

$$\bar{x} = \int_0^\infty x W(x)\,dx$$

$$= \frac{e^{\nu\tau} - 1}{\nu} \qquad (78)$$

Another quantity which is of interest is the number of blanking periods that would result if we started with ν noise pulses per second.

The average number of blanking periods per second, μ, is related to the average number of noise pulses by the relation

$$\mu[P_1 + 2P_2 + 3P_3 + \ldots] = \nu \qquad (79)$$

where

P_i is the probability that a blanking period covered i pulses.

If a blanking period covers only one noise pulse then it must be of minimum length and the probability is equal to the probability of finding no pulses in the period τ.

That is

$$P_1 = e^{-\nu\tau}$$

Similarly, if a blanking period covers only two noise pulses, then the maximum length is 2τ and the probability is given by

$$P_2 = e^{-\nu\tau} P(\text{one pulse in } \tau)$$

$$= e^{-\nu\tau}(1 - e^{-\nu\tau})$$

It follows that the general term is given by

$$P_n = e^{-\nu\tau}(1 - e^{-\nu\tau})^{n-1} \qquad (80)$$

Substituting Equation (80) into Eq. (79) it can be shown that

$$\mu = \nu e^{-\nu\tau} \qquad (81)$$

3. Blanker Response

The output of the blanker may be defined in terms of some function of time, $b(t)$, which describes the ideal switching action. This function, $b(t)$, will, in most applications, be a random function of time. Thus we can write the output of the blanker in terms of the input as (See Fig. 27):

$$e_1(t) = b(t)e(t) \quad . \tag{82}$$

If we combine this with the response of the detector, Eq. (52), we find

$$e_2(t) = b(t)T(t)e(t) \quad .$$

It is evident that the sequence of blanking and ideal frequency translation is unimportant since, if their order is changed, the over-all output remains unchanged. Thus the order of detection and blanking can be interchanged so that the input of the blanker may be taken as the output of the detector as given in Eq. (59).

Since the system is linear, we consider an input to the blanker which consists of a single term. The total output can then be calculated as the sum of the individual responses. Thus, for the analysis, we assume that the input to the blanker is

$$e(t) = A \cos \phi t \tag{83}$$

and wish to find the power spectrum of the output. The output power spectrum will be governed by the blanking function $b(t)$ which depends on the statistics of the noise pulses. It is important to note that although the times of occurrence are random there is a minimum distance between blank periods, since by definition there can be no overlapping of the blank periods. For this reason, direct calculation of the power spectrum of the output becomes awkward.

For this reason we use the alternative method, which is found to be very convenient for the particular blanker of our analysis. This method requires the computation of the output autocorrelation function, from which the power spectrum can be obtained easily.

The blanker response, $b(t)$, has a number of interesting properties. The probabilities of the events involved are certainly independent of

the origin of time; and furthermore, these system probabilities are independent of time. Some reflection will show that the "intersymbol influence" of the signal is finite in extent. In other words, the function can be predicted only for a finite extent of time. Thus, the function is stationary and it may also be considered as a member of an ergotic ensemble. This in turn allows us to calculate the ensemble average instead of the time average, since they are equal.

The autocorrelation function is defined as the time average of two measurements of the same signal taken a time l apart; that is,

$$R(l) = \overline{y(t)y(t+l)} = \lim_{T\to\infty} \frac{1}{2T} \int_{-T}^{T} y(t)y(t+l)dt$$

$$= \overline{y_1 y_2}$$

However, since in an ergotic ensemble the time average equals the ensemble average, we make use of the following integral for the autocorrelation function

$$R(l) = \int\int y_1 y_2 \, W(y_1, y_2; l) dy_1 dy_2 \qquad (84)$$

where y_1 and y_2 are the amplitudes at the times t_1 and t_2 which are l seconds apart, and $W(y_1, y_2; l)$ is the probability density function of measuring y_1 and y_2 at a separation of l seconds.

For the assumed input of a cosine wave, Eq. (83), the output of the blanker will consist of a cosine wave which is interrupted at random times for random lengths. The output is illustrated in Fig. 28. It is apparent that the times t_1 and $t_1 + l = t_2$ where y_1 and y_2 are measured must both occur during a time when the signal is not blanked, otherwise the contribution to the autocorrelation integral, Eq. (84) will be zero. Since both y_1 and y_2 mustobe measured at unblanked regions, y_2 will always be

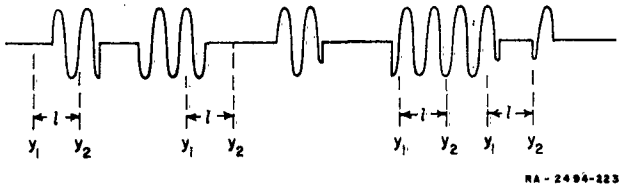

FIG. 28
SAMPLE OF BLANKER OUTPUT

an exact function of y_1 since the input signal is known for all times. Thus we can easily show that

$$y_2 = y_1 \cos \phi l \pm \sqrt{A^2 - y_1^2} \sin \phi l \tag{85}$$

in the functional relation between y_2 and y_1 whenever a non-zero contribution is made to the autocorrelation.

The probability density function $W(y_1, y_2; l)$ in the integrand of Eq. (84) may be rewritten as a product of two functions, *i.e.*,

$$W(y_1, y_2; l) = W_1(y_1) W(y_2 | y_1; l) \tag{86}$$

Here, $W_1(y_1)$ is the amplitude probability density of the signal while $W(y_2 | y_1; l)$ is the conditional probability density of measuring y_2 on the second reading, given that y_1 was measured l seconds earlier.

Let us first determine the amplitude probability density $W(y_1)$ of the signal. If a measurement is taken at a random time we know the probability of finding the signal blanked or unblanked, *i.e.*, whether the signal is present or not present. The only time we obtain a contribution to the autocorrelation integral is when the signal is present. Thus, $W_1(y_1)$ will be given by the product of the probability of finding the signal unblanked and the amplitude probability density for a signal of the form of the input. The amplitude probability density for a sine wave of amplitude A may be shown to be

$$Y(y_1) = \frac{1}{\pi} \frac{1}{\sqrt{A^2 - y_1^2}} \quad -A < y < A$$

$$= 0 \qquad |y| > A$$

Thus the function $W_1(y_1)$ is given by

$$W_1(y_1) = (1 - \mu\bar{x}) \frac{1}{\pi} \frac{1}{\sqrt{A^2 - y_1^2}} \quad -A < y_1 < A \tag{87}$$

$$= 0 \qquad |y| > A$$

where $(1 - \mu\bar{x})$ is the probability of the signal to be in unblanked condition. Using Eqs. (78) and (81) for μ and $\bar{x}$ we find for the blanker under consideration,

$$(1 - \mu\bar{x}) = e^{-\nu\tau}$$

where, it is recalled, τ is the minimum blanking period.

We turn now to the conditional probability density function $W(y_2|y_1;l)$ which appears in Eq. (86). We stated earlier that the only contribution we obtain to the autocorrelation is when neither y_2 nor y_1 occur in blanked regions. At the same time if this condition is satisfied then y_2 can be exactly expressed in terms of y_1. Thus, it is apparent that the conditional density function is given by the delta function.

$$W(y_2|y_1;l) = P(l)\delta[y_2 - (y_1 \cos \phi l \pm \sqrt{A^2 - y_1^2} \sin \phi l)] \qquad (88)$$

where we have used Eq. (85). Here, $P(l)$ is the probability that y_2 will be in an unblanked region, and it will be a function of, l, the spacing between the sampling points.

Substituting Eqs. (87), (88) and (86) into Eq. (84) we find

$$R(l) = P(l)e^{-\nu\tau} \int_{-A}^{A} \frac{1}{\pi}\left[\frac{y_1^2}{\sqrt{A_1^2 - y_1^2}} \cos \phi l \pm y_1 \sin \phi l\right] dy_1$$

since the delta function made the evaluation of the integration with respect to y_2 very simple. In turn the above is a simple integral and we obtain

$$R(l) = P(l)e^{-\nu\tau} \frac{A^2}{2} \cos \phi l \qquad (89)$$

In this expression, it remains to establish the probability function $P(l)$. This function will consist of two parts which are found by the following arguments.

First, let us consider the range of $l < \tau$. Since the minimum blanking period is τ, it follows that if $l < \tau$ then the only time y_2 will be in an

unblanked region will be if no noise pulse arrives in this interval of length l. Thus, the probability $P(l)$ must be equal to the probability of no pulses in a time l, *i.e.*,

$$P(l) = e^{-\nu l} \qquad \text{for} \qquad 0 < l < \tau \quad .$$

It remains to investigate the range $l > \tau$. When the spacing between the sampling points l is greater than τ, blanking periods of limited extent may be allowed in this period of time. Note, however, that due to the way we have defined the blanker operation, it does not matter how the noise pulses arrive during the time l, as long as there are no pulses occurring for a time τ before y_2 is sampled. Thus we find

$$P(l) = e^{-\nu\tau} \qquad \text{for} \qquad l \geq \tau \quad .$$

The autocorrelation function, then, is given by

$$\left.\begin{aligned} R(l) &= \frac{A^2}{2} e^{-\nu(\tau+l)} \cos \phi l \qquad 0 < l < \tau \\ &= \frac{A^2}{2} e^{-2\nu\tau} \cos \phi l \qquad l > \tau \end{aligned}\right\} , \tag{90}$$

The relation between the power spectrum and the autocorrelation function is well known. We have then,

$$G(\omega) = \frac{2}{\pi} \int_0^\infty R(l) \cos \omega l dl \quad . \tag{91}$$

Substituting Eq. (90) into the above and performing the integration, we obtain*

* It has been brought to the author's attention that a similar result was obtained by E. M. Glaser. See D. P. Coffin, "Integration of Interference Blanker Techniques into Low-Frequency Receivers," WADC TR-59-525, (September 1959).

$$G(\omega) = e^{-2\nu\tau}\frac{A^2}{2}[\delta(\omega-\phi)+\delta(\omega+\phi)] + e^{-\nu\tau}\frac{A^2}{2\pi}\left[\frac{\nu}{\nu^2+(\omega-\phi)^2}+\frac{\nu}{\nu^2+(\omega+\phi)^2}\right]$$

$$- e^{-2\nu\tau}\frac{A^2}{2\pi}\left[\frac{\nu\cos(\omega-\phi)\tau-(\omega-\phi)\sin(\omega-\phi)\tau}{\nu^2+(\omega-\phi)^2}+\frac{\sin(\omega-\phi)\tau}{\omega-\phi}\right]$$

$$- e^{-2\nu\tau}\frac{A^2}{2\pi}\left[\frac{\nu\cos(\omega+\phi)\tau-(\omega+\phi)\sin(\omega+\phi)\tau}{\nu^2+(\omega+\phi)^2}+\frac{\sin(\omega+\phi)\tau}{\omega+\phi}\right] \quad (92)$$

The power spectrum of the output, as given by Eq. (92) clearly shows the effects of the switching of the blanker. The signal at the output contains power, not only at the signal frequency [$\delta(\omega \pm \phi)$ term] but we note a continuous spectrum which represents lost power. We recall that the average fraction of time during which the input signal is blanked is $(\overline{\mu x}) = e^{-\nu\tau}$, and we expect that the total power in the output should decrease to this fraction of the power with no blanking. The spectrum $G(\omega)$ of Eq. (92) integrated from 0 to ∞ gives us the following result:

$$P = \int_0^\infty G(\omega)\,d\omega$$

$$= \frac{A^2}{2}e^{-2\nu\tau} + \frac{A^2}{2}e^{-\nu\tau}(1-e^{-\nu\tau})$$

$$= \frac{A^2}{2}e^{-\nu\tau} .$$

This agrees with the expected total power in the output. Note that the first term $(A^2/2)e^{-2\nu\tau}$, which represents the signal power in the output, decreases very rapidly with an increase in ν or τ. The second term, $(A^2/2)e^{-\nu\tau}(1-e^{-\nu\tau})$ represents the total power in the continuous spectrum and is considered as noise.

For convenience we make the following substitutions. We let

$$x = \omega\tau$$

$$x_0 = \nu\tau$$

$$x_i = \phi_i\tau$$

Then we can write, for the power spectrum,

$$G(x) = \frac{A^2}{2} e^{-2x_0}[\delta(x - x_1) + \delta(x + x_1)]$$

$$+ \frac{A^2\tau}{2\pi} [g(x - x_1) + g(x + x_1)] \qquad (93)$$

where

$$g(x) = \frac{x_0 e^{-2x_0}}{x_0^2 + x^2} \left[e^{x_0} - \cos x - x_0 \frac{\sin x}{x}\right] . \qquad (94)$$

The effects of the blanker switching are clearly established. The actual signal frequency term decreases in power by the square of the average blanking duration, *i.e.* $(\mu\bar{x})^2$. At the same time power appears in a continuous spectrum and represents lost signal power and must be considered as noise.

The function $g(x)$, as given by Eq. (94), which essentially determines the noise spectra in the output is not a very simple function. This function is plotted in Fig. 29 for parametric values of x_0.

4. OUTPUT

The solution which we have just obtained was for an input consisting of a single sinusoid. We are interested in a more general input and in fact recalling that the input to the blanker may be taken as the output of the detector we have for the input

$$e(t) = C_0 + C_0 m \cos \omega_s t + C_0 \cos 2\omega_c t + \frac{C_0 m}{2} [\cos (2\omega_c + \omega_s)t + \cos (2\omega_c - \omega_s)t]$$

$$+ \sum_{j=1}^{n} C_j [\cos(\omega_c - \omega_j)t + \cos (\omega_c + \omega_j)t] . \qquad (95)$$

This is equivalent to the expression for the output of the detector given by Eq. (59) with the exception of the corona noise pulses which we

omit since the blanker will always be shorted when these noise pulses appear. We are, therefore, assuming again that the only noise is corona noise and that each pulse will initiate a blank period as previously described.

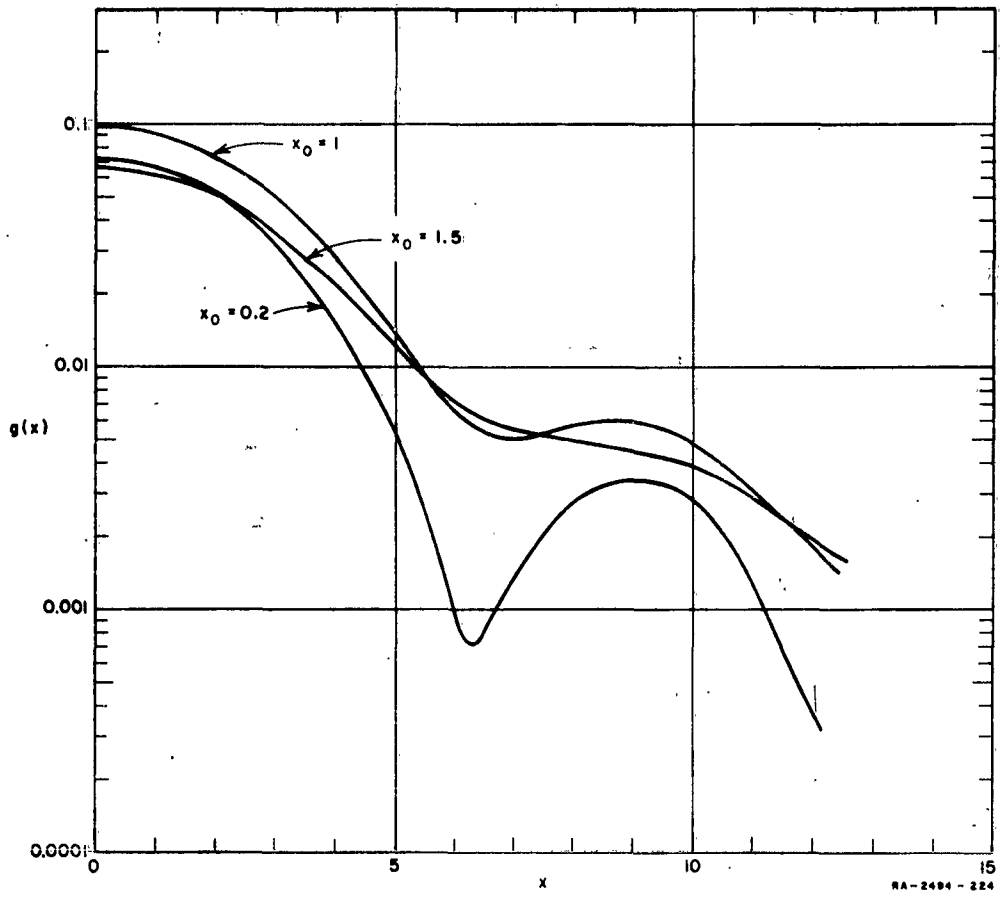

FIG. 29

FUNCTION g(x) VS $\underline{x}$

The analysis of the previous section was carried out for a cosine input of Eq. (83) By following the analysis through for an input of constant value equal to A, it becomes apparent that the power spectrum will be given by

$$G(x) = e^{-2x_0}\, 2A^2\delta(x) + \frac{2A^2}{\pi}\,\tau g(x) \qquad (96)$$

We are now prepared to find the power at the output resistance. The power will be given by

$$P = \int_0^{\omega_k} G(\omega)\,d\omega$$

where ω_k is the upper cutoff of the ideal low pass filter. In this way we find that the output power for an input given by Eq. (95) is

$$P = S + N$$

where the signal power is

$$S = \frac{C_0^2 m^2}{2} e^{-2x_0} \tag{97}$$

and the noise power consists of

$$N = \frac{2C_0^2}{\pi}\int_0^{x_k} g(x)dx + \frac{C_0^2}{2\pi}\int_0^{x_k} [g(x - 2x_c) + g(x + 2x_c)]dx$$

$$+ \frac{C_0^2 m^2}{2\pi}\int_0^{x_k} [g(x - x_s) + g(x + x_s)]dx$$

$$+ \frac{C_0^2 m^2}{8\pi}\int_0^{x_k} [g(x + x_s + 2x_c) + g(x - x_s - 2x_c) + g(x + 2x_c - x_s) + g(x - 2x_c + x_s)]dx$$

$$+ \sum \frac{C_j^2}{2\pi}\int_0^{x_k} g(x + x_c + x_j) + g(x - x_c - x_j) + g(x + x_c - x_j) + g(x - x_c + x_j)]dx$$

where

$$x_k = \omega_k \tau \qquad x_c = \omega_c \tau$$

$$x_s = \omega_s \tau \qquad x_j = \omega_j \tau$$

The numerous integrations which are involved above may be approximately evaluated again since the bandwidths we shall be interested in—*i.e.*, f_k = 3 kc—makes the range of integration extremely small. Thus, we can write

$$N = 2x_k \left\{ \frac{2C_0^2}{\pi} g(0) + \frac{C_0^2}{\pi} g(2x_c) + \frac{C_0^2 m^2}{\pi} \left\{ g(0) + \frac{g(2x_c)}{2} \right\} + \sum \frac{C_j^2}{\pi} [g(x_c - x_j) + g(x_c + x_j)] \right\} \quad (98)$$

The case where there are no outside carriers present is of particular interest, since this represents the blanker operation in the most favorable light possible. For this case then, *i.e.* $C_j = 0$, we find

$$N = 4C_0^2(f_k\tau)\left[g(0) + \frac{1}{2} g(2x_c)\right] + 2C_0^2(f_k\tau)m^2\left[g(0) + \frac{1}{2} g(2x_c)\right]$$

or

$$N = 2C_0^2(f_k\tau)(2 + m^2)\left[g(0) + \frac{1}{2} g(2x_c)\right]. \quad (99)$$

The dominant terms in the above expressions are the ones involving $g(0)$. Indeed, for carrier frequencies above one megacycle the second terms are completely negligible if τ is about 10^{-6} or smaller. The variation of $g(0)$ with x_0 is shown in Fig. 30. This shows that the noise in the output will increase as x_0 increases. A point is reached, however, where the noise begins to decrease sharply. This indicates that a saturation of blanking has been reached. That is, the pulses are so numerous (or τ so long) that blanking is almost continuous, and so that very little signal comes through. Thus, although the noise power is apparently decreasing very rapidly, the signal power is decreasing even more rapidly.

5. Signal-to-Noise Ratio with Blanking

We assume there are no outside carriers so that the noise is the least we might expect from an ideal blanker system.

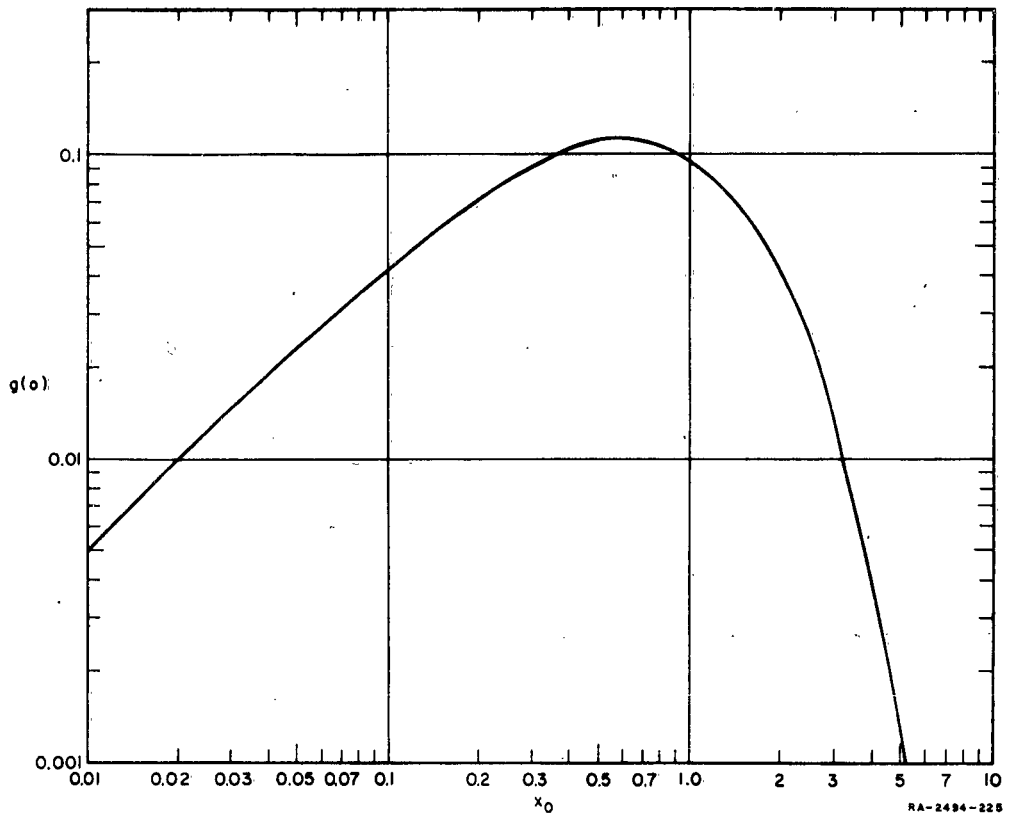

FIG. 30

FUNCTION g(o) VS $\underline{x}$

The signal power is given by Eq. (97) and the noise power by Eq. (99). We shall consider the approximation that the second order term $[g(2\omega_c\tau)]$ is negligible. Thus the signal-to-noise ratio becomes

$$\sigma_0 = \frac{S}{N} = \frac{m^2}{4(2 + m^2)(f_k\tau)} \quad \frac{x_0}{[e^{x_0} - (1 + x_0)]} \qquad (100)$$

The S/N will of course be slightly higher than it should be so that this result is optimistic.

Considering Table I it seems that a reasonable value for the minimum blanking period is $\tau \sim 10^{-6}$. Let us also consider the case of $m = 0.5$ and $f_k = 3$ kc.

$$\frac{S}{N} = 9.26 \frac{x_0}{e^{x_0} - (1 + x_0)} .$$

This is plotted in Fig. 31 *vs.* x_0.

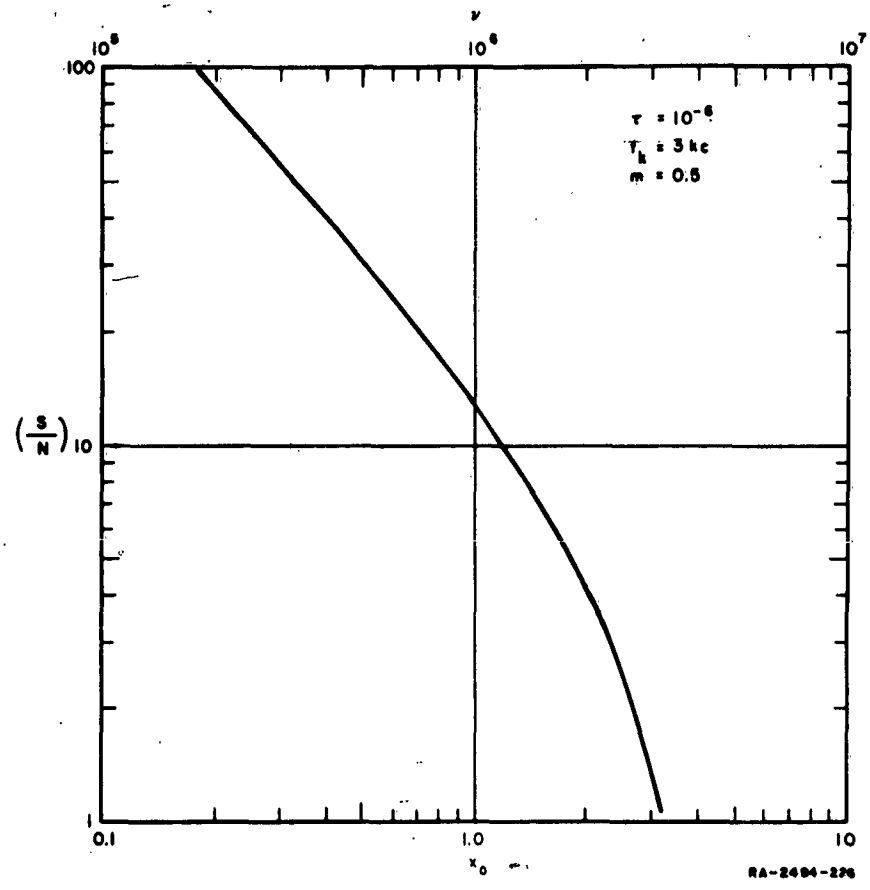

FIG. 31
SIGNAL-TO-NOISE RATIO WITH BLANKER

A comparison of the variable blanking period and the fixed period blanking, as computed by Lucke and Weaver,[20] is shown in Fig. 32. As is expected, the signal-to-noise ratios of the two methods agree for low x_0. The fixed period blanking apparently is superior. However, it is important to keep in mind that considerable noise is carried through to the output as the unblanked sections of the pulses. (Appendix B)

For the above calculations we have assumed that the minimum blanking duration was a fixed value which we selected as $\tau = 10^{-6}$ secs. For very small incoming signals, however, this may not be long enough to reduce

the unblanked tails of the pulses to a sufficiently small amplitude. On the other hand, for extremely high amplitude input signals it would not be necessary to blank for quite as long a period of time. Thus, we will now assume that the length of the blanking period τ, will be determined by the input signal amplitude.

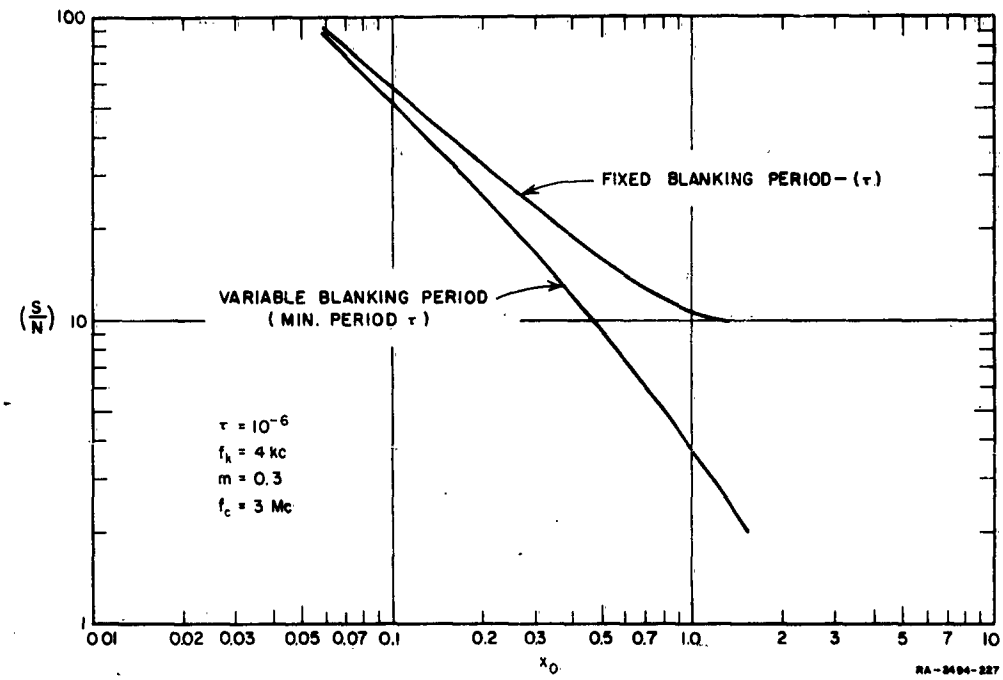

FIG. 32

COMPARISON BETWEEN FIXED BLANKING AND VARIABLE BLANKING PERIOD

Let us assume that the value to which the amplitude of the noise pulses must be blanked will be equal to the amplitude of the input signal. Thus if we assume exponential noise pulses of amplitude I_0 and decay constant α, then τ will be obtained from

$$y_0 = I_0 e^{-\alpha\tau}$$

where y_0 is the signal amplitude. From this equation we find

$$x_0 = \nu\tau = \frac{\nu}{\alpha} \ln \frac{I_0}{y_0} \quad . \tag{101}$$

Note that the situation of a signal with exponential noise pulses of equal amplitude leads to a signal-to-noise ratio which is extremely high even for high pulse rates, *i.e.*, $\nu = 10^6$ and greater. Thus, if the pulse tails are of the same magnitude as the signal, negligible noise will result from them.

For our application we take I_0 of Eq. (101) equal to the average amplitude of the term containing the longest time constant--*i.e.*, the term containing α_1 in Table I. The signal amplitude is given by

$$y_0 = \epsilon_0 \omega E_0 A$$

so that, substituting into Eq. (101) we get

$$x_0 = \frac{\nu}{\alpha_1} \ln \frac{I_{(0)}}{\omega \epsilon_0 A E_0} \tag{102}$$

Let us consider the same specific situation as in previous discussion, *i.e.*,

$$m = 0.5$$

$$f_k = 3 \text{ KC}$$

and a discharge current of 1 ma. Then at sea level we find

$$\sigma_1 = \frac{S}{N} = 9.26 \frac{1}{e^{x_0} - (1 + x_0)}$$

where x_0 is now given by Eq. (102) in terms of incident signal field.

$$i.e. \qquad x_0 = 2.3 - 0.28 \ln e_c$$

where

e_c is in μ volts/m.

Similarly for an altitude of 40,000 feet, assuming again a discharge of 1 ma

we find

$$\sigma_2 = \frac{3.8}{e^{x_0} - (1 + x_0)}$$

where

$$x_0 = 2.54 - 0.28 \ln e_c \quad .$$

It is noted that the signal-to-noise ratio computed in this way, which requires blanking of long duration for weak signals and shorter duration for strong signals, does not deteriorate extremely fast as the signal level goes down. This is due to the fact that the noise pulses are exponentials so that lengthening of blanking periods is not increasing very fast.

6. Effect of Outside Carriers

The effect of outside carriers, which we have thus far neglected, can be serious. An estimate of their effect can be obtained in the following manner. Combining Eqs. (97) and (98) we find that the signal-to-noise ratio is given by

$$\sigma_c = \frac{S}{N} = \frac{\frac{C_0^2 m^2}{2} e^{-2x_0}}{2C_0^2(2 + m^2)(f_k\tau)g(0) + 2\Sigma A_i^2 g(x_i)(f_k\tau)} \quad .$$

If we assume that the outside carriers can occur at random frequencies within an assumed bandwidth centered on the carrier of interest we can write

$$\sigma_c = \frac{\frac{C_0^2 m^2}{2} e^{-2x_0}}{2C_0^2(2 + m^2)(f_k\tau)g(0) + 2n\overline{A_i^2}\,\overline{g(x)}(f_k\tau)}$$

where $g(x)$ is averaged over the arbitrarily selected frequency range about the carrier. The above expression can be rewritten as

$$\sigma_c = \sigma_0 \frac{1}{1 + \dfrac{\overline{A^2 n}}{C_0^2(2 + m^2)} \dfrac{\overline{g(x)}}{g(0)}} \qquad (103)$$

Let us first consider, for example, the case of a discharge current of one milliamp at sea level. With the conditions

$$m = 0.5 \quad \text{and} \quad \tau = 10^{-6}$$

and the required $\nu = 10^6$, we find by rough graphical integration

$$\frac{\overline{g(x)}}{g(0)} = 0.45$$

where x is taken over a range 0 to 2π. Now if $\overline{A_i^2} = C_0^2$ we obtain

$$\sigma_c = \frac{\sigma_0}{1 + 0.2n}$$

For example, if we have 20 stations within a two megacycle bandwidth, centered about the carrier of interest, the signal-to-noise ratio would decrease by a factor of five. Here we have arbitrarily assumed that the carrier of interest is equal in power to the average of all the incoming carriers.

In general, the ratio $\overline{g(x)}/g(0)$ will change depending on the discharge current. A limiting case can be obtained by assuming that the ratio $\overline{g(x)}/g(0) = 1$. This will tend to give a pessimistic reading for the signal-to-noise ratio. This then assumes that the effect of each carrier is as severe as that due to the carrier signal of interest. In this way we find the following

$$\sigma_c = \frac{\sigma_0}{1 + \dfrac{Kn}{2 + m^2}} \qquad (104)$$

where

n = number of carriers

$K = \overline{A_i^2}/C_0^2$

m = modulation index.

Note that n, the number of carriers, will be large. There are two ways, however, by which the carriers that are distant in frequency from the carrier of interest became negligible. One is due to the fact that $g(x)$ decreases rapidly with x while the second is that some filtering accomplished before the input will decrease their influence.

F. COMPARISON OF DECOUPLED DISCHARGER AND BLANKING

1. Direct Comparison

The comparison between noise reduction methods which follows is simply a presentation of the bare numbers obtained from calculations in the previous sections. Thus, it is important to remember some of the assumptions which are included in the calculations.

In the case of the decoupled dischargers for the calculations of the signal-to-noise ratio we have assumed a decoupling of 50 db. Actually, the decoupling is extremely difficult to measure because it is so large. Indeed, the laboratory measurements indicate that the decoupling obtained is greatly in excess of this figure. Furthermore, theoretical calculations which have been carried out by Tanner and Nanevicz,[14] indicate decouplings of the order of 80 db. Thus, the calculations involving the decoupled dischargers represent a situation which is pessimistic and it is emphasized that the actual performance is much better.

The calculations presented for the blanker, however, are absolutely the extreme limit of possible accomplishment, and the best possible blanker operation results when no outside carriers are present. Thus, for the decoupled dischargers we use data of nominal actual performance while the blanker in practice may fall far short of the assumed ideal operation involved in the calculations.

The signal-to-noise ratio of the blanker as shown in Fig. 31 for $\tau = 10^{-6}$ is independent of input signal strength. Then in order to

compare the performance of the decoupled dischargers we shall calculate the signal strength e_c above which performance of the decoupled dischargers will be superior.

Thus e_c is calculated for the condition

$$\left(\frac{S}{N}\right)_{\text{No Blank}} = \chi_D e_c^2 = \left(\frac{S}{N}\right)_{\text{With Blank}}$$

This is done for a discharge current of 1 ma and the results shown in Fig. 33. Under the assumptions of the analysis, this figure indicates that the ideal blanker performance can, be superior to the decoupled

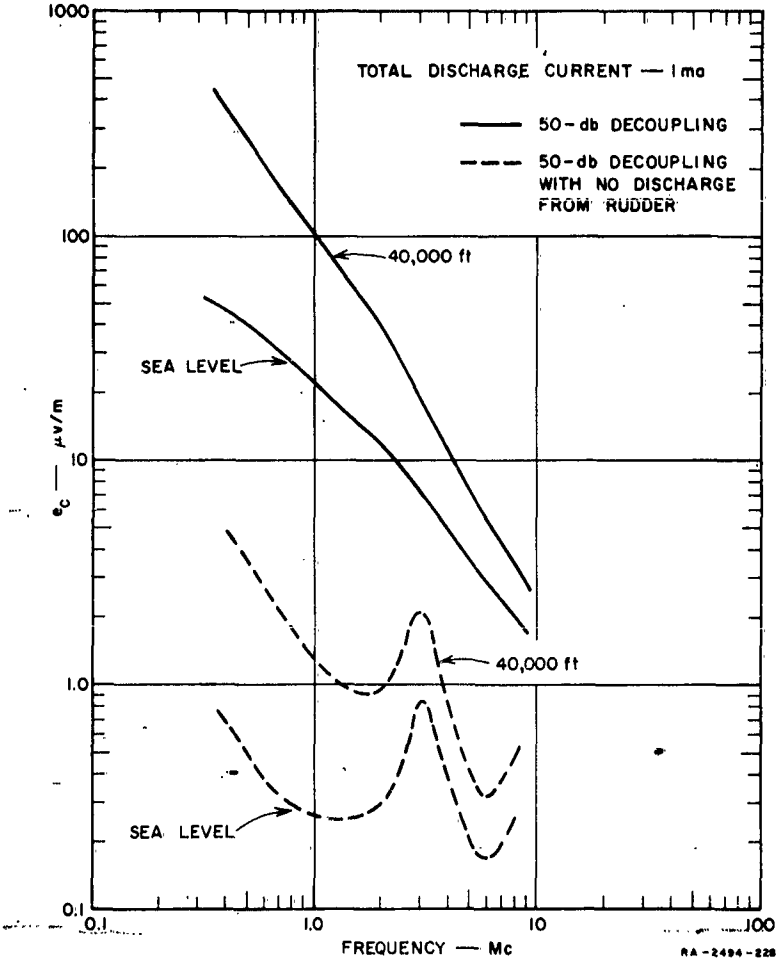

FIG. 33
BOUNDARY INCIDENT SIGNAL FIELD STRENGTH

dischargers at the lower signal levels. As will be pointed out presently, this region of signals provides a signal-to-noise ratio that is too low. A more realistic presentation is made by the analysis which assumes that the minimum blanking period is governed by signal amplitude, as shown in Fig. 34. These curves are calculated using Eqs. (102) and (100).

The presence of outside carriers, on the signal-to-noise ratio with a blanker, is also illustrated on Fig. 34. Using the equations of the previous section, we see that even one station with an average amplitude

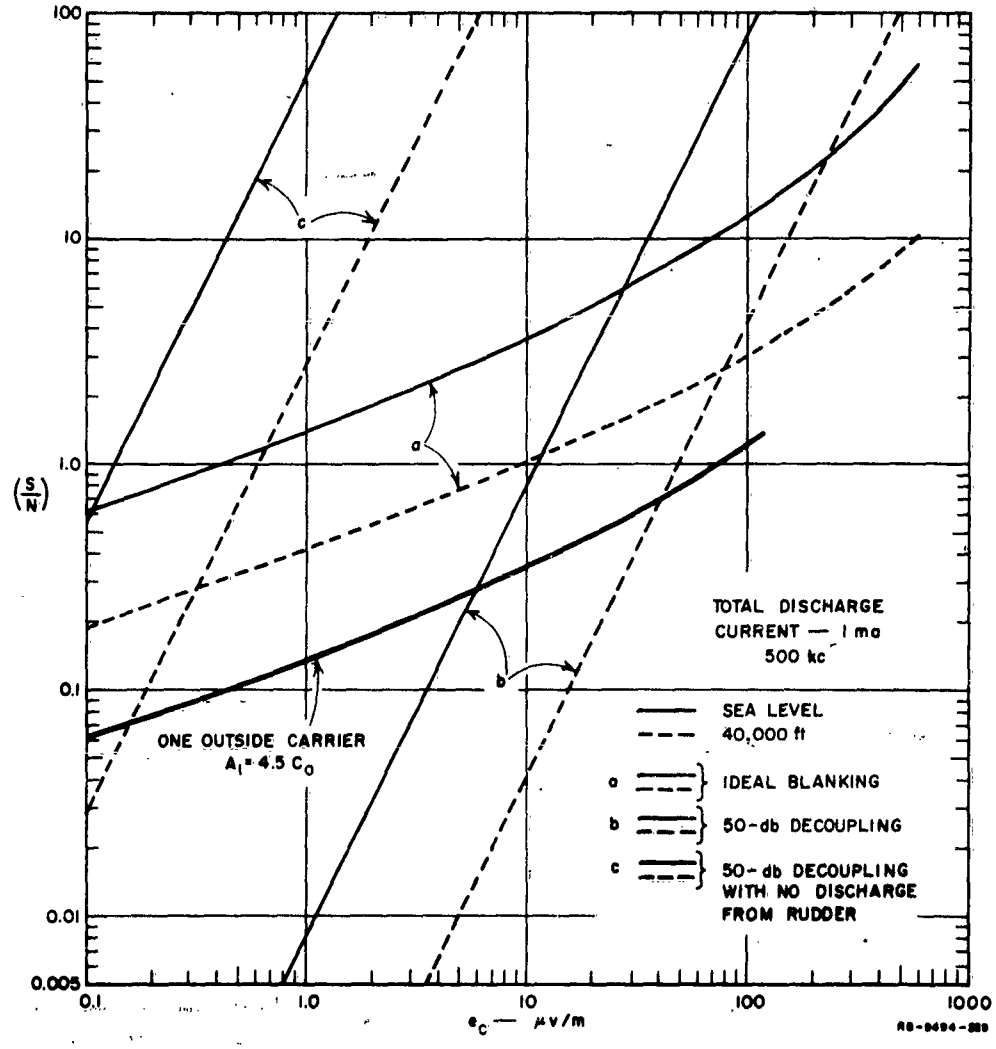

FIG. 34

SIGNAL-TO-NOISE RATIOS FOR BLANKER AND DISCHARGERS

of only 4.5 times the carrier of interest reduces the signal-to-noise ratio by a factor of ten.

From Fig. 34 it appears that at low signal levels, the blanker method might be superior (this is assuming ideal blanker with no outside carriers). However this is a false conclusion since the signal-to-noise ratio is unsatisfactory by the time the blanker method indicates a better capability of noise suppression.

Thus it must be emphasized that for a completely comprehensive evaluation, a signal-to-noise threshold must be included. In other words there must be established the minimum signal-to-noise ratio that is acceptable for a given quality of communication. This threshold will vary with the type of communication channel, type of output display, human perceptive interpretation, etc. If we assume a signal-to-noise of 10 is necessary for adequately reliable communication, then from Fig. 34 it is evident that the decoupled dischargers provide better noise suppression than the ideal blanker operation for the 1 ma discharge situation.

This is definitely a conclusive result since the practical blanker will actually perform at a level considerably lower than the ideal blanker. Not only will outside carriers seriously decrease the signal-to-noise ratio but the sensitivity of the system is considerably decreased due to the lack of tuning at the antenna terminals.

A rough estimate of the sensitivity loss may be obtained as follows.

Let the antenna, represented by a voltage generator V_a and an impedance $Z_a = R_a + jX_a$ be connected directly across a resistor R at the receiver input. The voltage, V_0, at the receiver input would be given by

$$V_0 = V_a \frac{R}{|R + Z_a|} ,$$

If, as in the case of the blanker application, $R \ll |Z_a|$ then to a good approximation

$$V_0 = V_a \frac{R}{|Z_a|}$$

Next, we assume an ideal coupler designed for maximum power transfer is placed between the antenna and the resistance. For this case, it can be shown that

$$V_0' = \frac{V_a}{2}\sqrt{\frac{R}{R_a}}$$

Thus, the ratio of the sensitivities is given by

$$\frac{V_0'}{V_0} = \frac{1}{2}\frac{|Z_a|}{\sqrt{RR_a}}$$

Consider, for example, a frequency of 2 Mc where $X_a >> R_a$. If we let $R = R_a$ and use tail-cap antenna impedance values of Eq. (35) we obtain

$$\frac{V_0'}{V_0} \cong 160$$

At lower frequencies the loss of sensitivity will be even greater than computed in the above example.

Finally, the numerous practical limitations which must be met in a satisfactory blanker are very severe. Thus for example, in the best available blanker designs, at present, a minimum blanking period of 6 μsecs is considered good. With blanking periods of this length it is easy to calculate that only about a 10-db improvement in signal-to-noise is afforded for a 1 ma discharge current.

2. Effects of Atmospheric Noise

In our analysis we have neglected atmospheric noise. This noise which originates in thunderstorm activity can be of considerable magnitude and its influence on system performance and evaluation can be appreciable.

Figure 35 gives an indication of the magnitude of the noise for an average winter day over the U.S.A. The data was obtained from the Ionospheric Radio Propagation[21] The signal field strength shown is computed on the basis of a 3-kc bandwidth and a signal-to-noise ratio

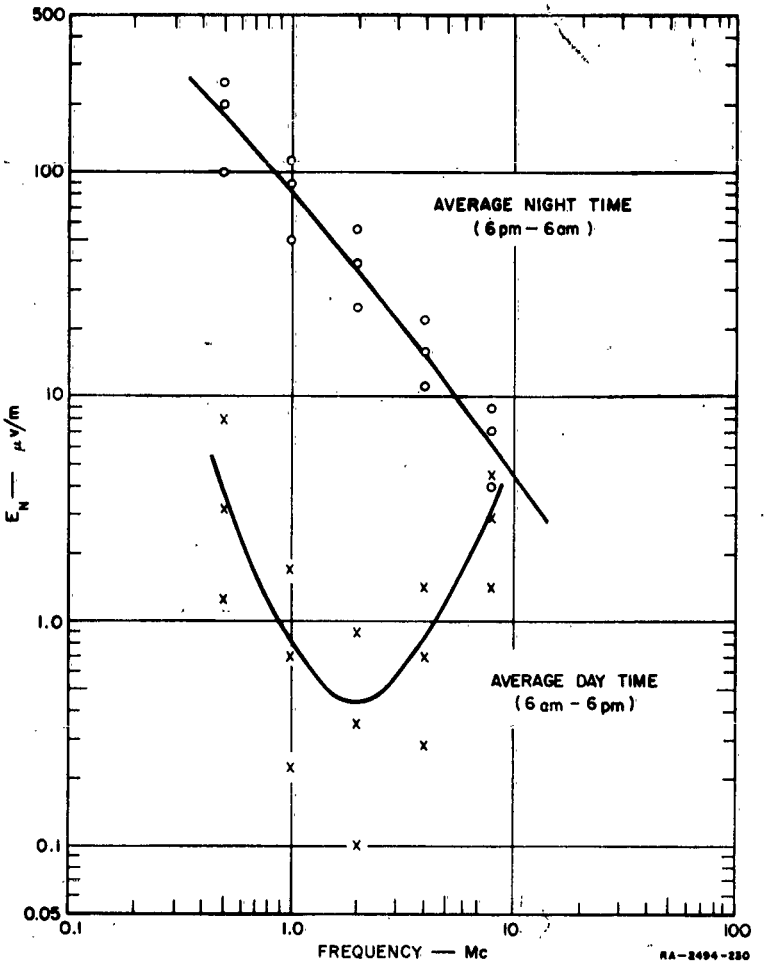

FIG. 35
ATMOSPHERIC NOISE MAGNITUDE

of 15 db at the output. This ratio represents a 90-percent effective communication in this type of amplitude modulated signal input.

Comparison of the above data with Fig. 34 clearly indicates that atmospheric noise will be an equally important factor in operation with decoupled dischargers and that the level at which a blanker would theoretically be superior is considerably lower than the required field strength shown in Fig. 35 necessary to overcome atmospheric noise.

The presence of atmospheric noise would actually make the blanker operation much worse if the noise pulses due to atmospheric noise were large enough in amplitude to trigger the blanker.

3. Effect of Change in Aircraft Size

It is of interest to establish the effect of aircraft size on the signal-to-noise ratios in the two methods of noise reduction we have discussed.

This will be done with the assumption that although the whole aircraft is scaled down in proportion (including the antenna) the thickness of the trailing edges will not be scaled. This assumption will simplify our analysis. It is moreover, a practical assumption. On the Boeing 707, for example, the trailing edge is 20 mils thick, which should definitely be a practical edge dimension for an aircraft even one-fourth the size.

In order to specify the aircraft dimensions we shall introduce a normalized length S such that when $S = 1$ the aircraft corresponds to the full scale Boeing 707. Also, we shall assume that the aircraft will be flying at fixed speeds in a uniform cloud of ice particles. Thus, since the number of noise pulses ν is proportional to the discharge current which in turn is proportional to the intercept area, it follows that

$$\nu \propto S^2$$

Similarly, the scaling of the aircraft and antenna will affect A, the antenna sensitivity. Thus

$$A \propto S^2$$

We have assumed the edge thickness remains unchanged so that if we now choose the reference distance to remain a constant as well, then $|D|$ will remain unchanged. The coupling function, however, will change in proportion to

$$|\psi| \propto \frac{S^{1/2}}{S} = \frac{1}{S^{1/2}}$$

The S in denominator of $|\psi|$ is due to the scaling of the aircraft, since we maintain ξ_0 fixed, however, $S^{1/2}$ appears in the numerator due to the fact that the fields away from the edge fall off as $1/x^{1/2}$.

Finally, as the aircraft is reduced in size the aircraft resonances will increase in frequency so that the time constants will decrease.

Now if we assume that the blanking period τ is proportional to the largest time constant, then at sea level we can say $\tau \propto S$. This relation will hold until that combination of aircraft size and altitude is reached at which the time constant associated with the airframe resonance is less than that associated with the decay of the corona pulse itself. At sea level the approximation will be good for an aircraft larger than about one-sixth that of the Boeing 707. At 40,000 feet, on the other hand, the largest time constant of the 707 is approximately equal to that of the actual corona pulse time constant, so that τ will be relatively independent of S for aircraft smaller than the 707.

If we substitute the above relations into Eq. (66) we find that the signal-to-noise ratio for decoupled dischargers is given by:

$$\left(\frac{S}{N}\right)_{D.D.} = K_D S^3 \tag{105}$$

This indicates that as the aircraft decreases in size the signal-to-noise ratio decreases as the cube of the dimension.

For the case of blanking we shall consider two cases:

(1) At sea level, where we have $\tau \propto S$

$$x_0 = \nu\tau = KS^3$$

and when this is substituted in Eq. (100) we obtain

$$\left(\frac{S}{N}\right)_B = \frac{K_B}{S} \frac{KS^3}{e^{KS^3} - (1 + KS^3)}$$

$$= \frac{K_B}{KS^4} \frac{1}{\left(\frac{1}{2!} + \frac{KS^3}{3!} + \frac{K^2S^6}{4!} \cdots\right)} \tag{106}$$

(2) At a 40,000 foot altitude we have τ = constant so that

$$x_0 = KS^2$$

and

$$\left(\frac{S}{N}\right)'_B = \frac{K'_B}{KS^2} \quad \frac{1}{\left(\frac{1}{2!} + \frac{KS^2}{3!} + \frac{C^2S^4}{4!} \cdots\right)} \tag{107}$$

In Eqs. (106) and (107) it is apparent that blanking will always improve as the size of the aircraft is decreased.

Comparing Eqs. (105) and (106) it also becomes apparent that as the aircraft size is reduced, the blanking signal-to-noise ratio will improve sharply, relative to the signal-to-noise ratio for the decoupled dischargers.

VIII CONCLUSIONS

The two main objectives of this study were to determine the characteristics of corona discharge noise in aircraft antennas and to evaluate noise reduction techniques.

The primary objective was to establish the character of precipitation static noise in aircraft antennas due to corona discharges. Because of the complexity of this problem, it was necessary to restrict the analysis to a particular antenna on a specific aircraft. The combination chosen for analysis was the tail-cap antenna on a Boeing 707 aircraft. The extensive laboratory and model measurements that were required, in order to determine the characteristics of the noise, were very satisfactory.

In the calculation of the coupling functions relatively crude methods of approximation were used. With some additional trouble, considerably better approximations of a higher order could be obtained. In this respect, the accuracy could be greatly improved by obtaining careful antenna impedance measurements. In spite of the resulting shortcomings in the detail of the coupling characteristics, the over-all structure and length of the noise pulses at the antenna are well established. Specifically, the lengthening of the pulses, particularly at sea level, is well illustrated.

The second objective, which is of great interest, is the comparison of the two noise reduction techniques which have received the most attention: decoupled dischargers, and blanking. For this purpose a theoretical analysis was made for a receiver with an ideal blanker at its input. The signal-to-noise ratios for the two methods were calculated and compared. The comparison was made under conditions which would make the relative performance of the blanker most favorable. Thus, for the decoupled dischargers, the decoupling is assumed to be 50 db. Although a good measured figure is not available, theoretical considerations indicate decoupling of 80 db is a more realistic figure. For the blanker operation, however, an ideal performance is assumed. The outcome of the comparison is nevertheless in favor of the decoupled dischargers.

It is further emphasized that the performance of the practical blanker will be considerably inferior to the performance of the ideal blanker. The presence of outside carriers is an important factor, and it is shown that even one carrier with an amplitude 4.5 times the signal amplitude will decrease the signal-to-noise ratio by a factor of ten. The loss in sensitivity which is also inherent in the blanker method of noise suppression is a serious disadvantage, and it may render the system useless. Finally, great practical difficulties are encountered in the construction of an actual blanker, and it is pointed out that only a 10 db improvement is possible with present available blankers for a 1 ma discharge current.

The only area where the blanker may prove useful is in aircraft of much smaller size than the Boeing 707. In this case, it is shown that the blanker performance improves considerably compared to that of decoupled dischargers. Even here, however, there is doubt whether a practical blanker could provide adequate interference noise reduction.

Finally, it is suggested that the most satisfactory solution for the low frequency range we have discussed would be to use decoupled dischargers for the corona noise. A blanker designed for atmospheric noise blanking might then be added to further improve communication success.

APPENDIX A

POWER SPECTRUM FOR SIGNAL OF RANDOM PULSES

APPENDIX A

POWER SPECTRUM FOR SIGNAL OF RANDOM PULSES

Let us assume we have a signal which extends for the interval $-T < t < T$ and is zero outside this range. The signal is assumed to consist of $2N + 1$ pulses occurring at random times at the average rate of ν pulses per second. Thus the signal may be written as

$$I(t) = \sum_{k=-N}^{N} f(t - t_k)$$

where

$$f(t - t_k) = 0 \qquad t < t_k$$

$$= A_k e^{-\alpha_k (t - t_k)} \qquad t > t_k$$

The Fourier transform of the signal is obtained

$$I(\omega) = \int_{-\infty}^{\infty} I(t) e^{-j\omega t} \, dt$$

$$= \sum_{k=-N}^{N} \frac{A_k}{\alpha_k + j\omega} e^{-j\omega t_k}$$

Then, the power spectrum which is defined as

$$G(\omega) = \lim_{T \to \infty} \frac{1}{2\pi T} |I(\omega)|^2$$

is found to be

$$G(\omega) = \lim_{T \to \infty} \frac{1}{2\pi T} \sum_{k=-N}^{N} \frac{A_k^2}{\omega^2 + \alpha_k^2}$$

since the times t_k are assumed random. It follows, that if A_k and α_k are all identical we obtain

$$G(\omega) = \frac{\nu}{\pi} \frac{A^2}{\omega^2 + \alpha^2}$$

Next, let us assume that the amplitudes A_k and the decay constants α_k are independent random variables.

Let

$$\alpha_k = \alpha + \delta_k$$

where α is the average value and δ_k is a random variable such that at maximum it is small compared to α and $\overline{\delta}_k = 0$.

Then the power spectrum is

$$G(\omega) = \frac{1}{\omega^2 + \alpha^2} \lim_{T\to\infty} \frac{1}{2\pi T} \sum_{k=-N}^{N} \frac{A_k^2}{1 + \frac{2\alpha\delta_k + \delta_k^2}{\omega^2 + \alpha^2}}$$

Since $\delta_k << \alpha$ and recalling that A_k and α_k are assumed to be independent, we find

$$G(\omega) = \frac{\overline{A^2}}{\omega^2 + \alpha^2} \lim_{T\to\infty} \frac{1}{2\pi T} \left\{ (2N + 1) - \frac{2\alpha}{\omega^2 + \alpha^2} \sum_{k=-N}^{N} \delta_k - \sum_{k=-N}^{N} \frac{1}{\omega^2 + \alpha^2} \left(1 - \frac{4\alpha^2}{\omega^2 + \alpha^2} \right) \delta_k^2 \right\}$$

and since $\overline{\delta}_k = 0$

$$G(\omega) = \frac{\nu}{\pi} \frac{\overline{A^2}}{\omega^2 + \alpha^2} \left\{ 1 + \frac{3\alpha^2 - \omega^2}{(\omega^2 + \alpha^2)^2} \overline{\delta}_k^2 \right\}$$

Thus a good approximation is obtained by simply keeping the first term, that is,

$$G(\omega) = \frac{\nu}{\pi} \frac{\overline{A^2}}{\omega^2 + \alpha^2}$$

Consider for example that δ_k is equally probable in a 20% range of α, *i.e.* $-\alpha/10 < \delta_k < \alpha/10$. Then at high frequencies $\omega >> \alpha$ there is negligible error using above expression. At mid frequencies, $\omega = \alpha$, the error is approximately ½% while at low frequencies $\omega << \alpha$ the error is worst at approx. 3%.

APPENDIX B

RESIDUAL NOISE IN THE OUTPUT OF A BLANKER OF FIXED BLANKING PERIOD

APPENDIX B

RESIDUAL NOISE IN THE OUTPUT OF A BLANKER OF FIXED BLANKING PERIOD

Let us briefly consider the blanker with a constant blanking period equal to τ. It follows that the number of blank periods will be

$$\mu = \frac{\nu}{1 + \nu\tau}$$

Now let us assume that the incoming noise pulses are simple exponentials arriving at an average rate of ν per second. We also assume that τ is long enough that the pulse which triggers a blank period is completely attenuated. Thus we must consider the noise due to the tails of the remaining pulses which are not completely blanked.

The noise power will be assumed as:

$$N = |H(\omega)|^2 \left(\frac{\nu}{1 + \nu\tau}\right) \bar{a}$$

where

$$\bar{a} = A^2 \int_0^\infty e^{-2\alpha(\tau - x)} \nu e^{-\nu x} dx$$

$$\doteq A^2 \frac{\nu e^{-\nu\tau}}{2\alpha - \nu}$$

where

A = amplitude of pulse

α = decay constant .

For the case

$$\tau = 10^{-6} \qquad \alpha = 4 \times 10^6 \qquad \nu = 10^6$$

$$\bar{a} = 0.052A^2$$

also, the noise before blanking is:

$$N_{NB} = \nu A^2 |H(\omega)|^2$$

Thus the noise after blanking to the noise without blanking is

$$\frac{N}{N_{NB}} = 0.026 \qquad \text{(B-1)}$$

This does not include the noise due to the blanking action. This analysis is approximate since we have not taken into account the fact that the tails of the unblanked pulses are not completely random, *i.e.* they can never be closer than τ. Of course at low frequencies the ratio (Eq. B-1) of noise obtained is exact.

ACKNOWLEDGEMENT

The author wishes to acknowledge the inspiration, encouragement, and suggestions extended by Dr. R. L. Tanner during the course of the study. The author is indebted to Dr. J. E. Nanevicz for the enlightening discussions concerning this work, and to G. R. Hilbers and J. A. Martin for the experimental measurements.

REFERENCES

1. Austin Curtis, "Discussion on 'Radio Range Variations' by R. H. Marriot," *Proc. IRE* **2**, *3*, (March 1914).
2. H. M. Hucke, "Precipitation Static Interference," *Proc. IRE* **27**, *5*, (May 1939).
3. H. W. Morgan, "Rain Static," *Proc. IRE* **24**, *7*, (July 1937).
4. I. Langmuir and H. E. Tanis, "The Electrical Charging of Surfaces Produced by the Impact of High Velocity Solid Particles," Report on Contract No. W-33-106-SC-65, General Electric Co. (May 1945).
5. Ross Gunn, *et al.*, "Army Navy Precipitation Static Project," *Proc. IRE*, **34**, *4* and *5*, (April-May 1946).
6. H. J. Dana, "Block and Squirter for Reduction of Precipitation Static," Second Air Force Operations Analysis Report 15 (February 1945).
7. Philco Corp., "Final Engineering Report on Precipitation Static Reduction," USAF Contract W-33-038 AC 20763, Research Division, (February 1950).
8. Denver Research Institute, "Levelopment of Aircraft Discharge Methods," Final Report, Contract AF 33(616)-157, University of Denver, Denver (April 1956).
9. M. M. Newman and J. R. Stahman, "Radio Interference Rejection at Antenna," Tech. Report 12, Lightning and Transients Research Institute, Minneapolis (1949).
10. R. L. Tanner, "Radio Interference from Corona Discharges," Tech. Report 37, Contract AF 19(604)-266, SRI Project 591, Stanford Research Institute, Menlo Park, California (April 1953).
11. G. W. Trichel, "The Mechanisms of the Negative Point to Plane Corona Near Onset," Physical Review, **54**, p. 107 (1938).
12. R. L. Tanner and J. E. Nanevicz, "Radio Noise Generated on Aircraft Surfaces," Final Report, Contract AF 33(616)-2761, SRI Project-1267, Stanford Research Institute, Menlo Park, California (September 1956).
13. J. E. Nanevicz, "A Study of Precipitation-Static Noise Generation in Aircraft Canopy Antennas," Tech. Report 62, Contract AF 19(604)-1296, SRI Project 1197, Stanford Research Institute, Menlo Park, California (December 1957).
14. R. L. Tanner and J. E. Nanevicz, "A Comprehensive Study of Precipitation Static Radio Interference," Technical Report to be published, Contract AF 19(604)-3458, Stanford Research Institute, Menlo Park, California.
15. D. F. Tuttle, Jr., "Circuit Synthesis," Class Syllabus, Dept. Electromagnetic Engineering, Stanford University (1953).
16. R. King, "Asymmetrically Driven Antennas and the Sleeve Dipole," Technical Report 93, Cruft Laboratory, Harvard University (1949).
17. C. T. Tai, "Asymmetrically Fed Antennas," Technical Report 2, Contract AF 19(122)-78, SRI Project 188, Stanford Research Institute, Menlo Park, California (November 1949).
18. J. T. Bolljahn, "Measurement of Low-Frequency Aircraft Antenna Properties Using Electrostatic Methods," Technical Report 19, Contract AF 19(122)-78, SRI Project 188, Stanford Research Institute, Menlo Park, California (September 1951).
19. R. L. Tanner, "A New Aircraft Static Discharger," IRE Convention Record (1958).
20. W. S. Lucke and D. K. Weaver, Jr., "Theoretical Analysis of Signal Switching Techniques to Reduce Impulse Noise," Final Report, Contract AF 33(038)-23320, SRI Project 441, Stanford Research Institute, Menlo Park, California (August 1951).
21. Ionospheric Radio Propagation, National Bureau of Standards, Circular 462, June 25, 1948.

TECHNICAL REPORTS IN THIS SERIES

Reports Issued on Contract AF 19(122)-78

1. "Electric Dipoles in the Presence of Elliptic and Circular Cylinders," by W. S. Lucke, September 1949.
2. "Asymmetrically Fed Antennas," by C. T. Tai, November 1949.
3. "Double Fed and Coupled Antennas," by C. T. Tai, February 1949.
4. "Equivalent Radii of Thin Cylindrical Antennas with Arbitrary Cross Sections," by Carson Flammer, March 1950.
5. "Use of Complementary Slots in Aircraft Antenna Impedance Measurements," by J. T. Bolljahn, February 1950.
6. "Wing-Cap and Tail-Cap Aircraft Antennas," by J. V. N. Granger, March 1950.
7. "Investigation of Current Distribution on Asymmetrically-Fed Antennas by Means of Complementary Slots," by R. M. Hatch, Jr , February 1950.
8. "Electromagnetic Resonance Phenomena in Aircraft Structures," by A. S. Dunbar, May 1950.
9. "The Effect of a Grounded Slab on the Radiation from a Line Source," by C. T. Tai, June 1950.
10. "A Method for the Calculation of Progressive-Phase Antennas for Shaped Beams," by A. S. Dunbar, June 1950.
11. "Admittance of an Open-Ended Coaxial Line in an Infinite Grounded Plane," by W. S. Lucke, June 1950.
12. "A Variational Solution to the Problem of Cylindrical Antennas," by C. T. Tai, August 1950.
13. "Uniform Progressive-Phase Antennas Having Asymmetrical Amplitude Distributions," by A. S. Dunbar, September 1950.
14. "Small Dipole-Type Antennas," by J. T. Bolljahn, September 1950.
15. "Tables of Modified Cosine Integrals," January 1951.
16. "Prolate Spheroidal Wave Functions," by Carson Flammer, February 1951.
17. "An Antenna Evaluation Method," by W. S. Lucke, April 1951.
18. "Radar Response from Thin Wires," by C. T Tai, March 1951.
19. "The Measurement of Low-Frequency Aircraft Antenna Properties Using Electrostatic Methods," by J. T. Bolljahn, September 1951.

20. (Dropped)

21. "A Method for the Calculation of Progressive-Phase Antennas for Shaped Beams," Part II, by A. S. Dunbar, May 1951.

22. "The Prolate Spheroidal Monopole Antenna," by Carson Flammer, August 1957, issued on Contract AF 19(604)-1296.

23. "Variational Solution for the Problem of the Asymmetric Dipole," by I. Reese, August 1951.

24. "Quasi-Static Solution for Diffraction of a Plane Electromagnetic Wave by a Small-Oblate Spheroid," by C. T. Tai, September 1952 [Issued on Contract AF 19(604)-266].

25. "Transmission Through a Rectangular Aperture in an Infinite Screen," by W. S. Lucke, September 1951.

Reports Issued on Contract AF 19(604)-266

26. "Improvements in Instrumentation for the Investigation of Aircraft Antenna Radiation Patterns by Means of Scale Models," by R. M. Hatch, Jr., August 1952.

27. "The Vector Wave Solution of the Diffraction of Electromagnetic Waves by Circular Disks and Apertures," by Carson Flammer, September 1952.

28. "An Investigation of the Distribution of Current on Collinear Parasitic Antenna Elements," by R. M. Hatch, Jr., August 1952.

29. "On the Theory of Diffraction of Electromagnetic Waves by a Sphere," by C. T. Tai, October 1952.

30. "High-Frequency Airborne Direction Finding," by P. S. Carter, Jr., December 1952.

31. "An Electrolytic Tank Method for Low-Frequency Loop Antennas Studies," by R. F. Reese, July 1953.

32. "Radiation from a Uniform Circular Loop Antenna in the Presence of a Sphere," by C. T. Tai, December 1952.

33. "A Computer for Use with Antenna Model Ranges," by C. E. Fisher, February 1953.

34. "Tail-Cap Antenna Radiation Pattern Studies," by J H. Bryan, January 1953.

35. "U-H-F Tail-Cap Antenna Pattern Characteristics and Their Control," by A. R. Ellis, March 1955 [issued on Contract AF 19(604)-1296].

36. "Mutual Admittance of Slots in Cylinders," by W. S. Lucke, February 1953.

37. "Radio Interference from Corona Discharges," by R. L. Tanner, April 1953.

38. "Effects of Airframe Configuration on Low-Frequency Antenna Characteristics," by C. M. Hoblitzell, April 1953.

39. "The Effects of Thin Resistive Coatings on Low-Frequency Aircraft Antenna Performance," by C. W Steele [issued on Contract AF 19(604)-1296] January 1956.

40. "Analysis of the Overstation Behavior of Airborne ADF Systems," by H. H. Ward, June 1954.

41. "Some Electromagnetic Problems Involving a Sphere," by C. T. Tai, April 1953.

42. "Radiation Pattern Measurements of Stub and Slot Antennas on Spheres and Cylinders," by J. Bain, April 1953.

43. "Current Distribution on Wing-Cap and Tail-Cap Antennas," by Irene C. Carswell, May 1954.

44. "A Study of Radiating Structures for Perpendicularly-Polarized Flush Radar Antennas," by Edward M. T Jones and Seymour B. Cohn, July 1953.

45. "Radiation from Current Elements and Apertures in the Presence of a Perfectly Conducting Half-Plane Sheet," by C. T. Tai, July 1954.

46. "A Glossary of Dyadic Green's Functions," by C. T. Tai, July 1954.

47. "Horizontally Polarized Long-Slot Array," by R. C. Honey, August 1954.

Reports Issued on Contract AF 19(604) 1296

48. "Microwave Radiation from Large Finite Bodies," by Seymour B. Cohn and Tetsu Morita, January 1955.

49. "Radiation from Electric and Magnetic Dipoles in the Presence of a Conducting Circular Disk," by Carson Flammer, February 1955.

50. "A Study of Some Inherent Errors in the Three-Dimensional Raydist System," by Irene Carswell, March 1955.

51. "Operating Characteristics of Flush-Mounted Bombing Antennas," by E. M. T. Jones, November 1955.

52. "Properties of the Asymmetric Dipole," by Irene Carswell, December 1955.

53. "Notch Coupling to the Electromagnetic Resonances of a Delta-Wing Aircraft," by William L. Jones, December 1955.

54. "A Flush-Mounted Horizontally Polarized Directional Antenna," by R. C. Honey, January 1956.

55. "Radiation from a Flush-Mounted Scanning Antenna on the Nose Section of a Supersonic Aircraft," by J. K. Shimizu and T. Morita, December 1955.

56. "An Economical Logarithmic Recording System " by Lloyd A Robinson, June 1956.

57. "Variational Formulae for Domain Functionals in Electromagnetic Theory," by Carson Flammer, March 1957.

58. "Systems Considerations for High Speed Missile Seeker Antennas," by Donald L. Margerum and E. Thomas Brandon, May 1957. Confidential.

59. "High-Strength Dielectric Materials for Very Fast Aircraft," by Henry J. Sang, March 1957.

60. "Impedance Matching Limitations with Application to the Broadband Antenna Problem," by Arthur Vassiliadis, January 1957.

61. "Shunt-Fed and Notch-Fed H-F Aircraft Antennas," by Robert L. Tanner, July 1957.

62. "A Study of Precipitation-Static Noise Generation in Aircraft Canopy Antennas," by Joseph E. Nanevicz, September 1957.

63. "Electromagnetic Wave Propagation in a Medium with Variable Dielectric Constant $1 + kr^{-1}$," by Carson Flammer, January 1958.

Reports Issued on Contract AF 19(604)-3458

64. "The Back-Scattering Cross Sections of Missile Trails," by Carson Flammer, June 1958.

65. "Ray-Tracing and Diffraction in a Medium with Variable Permittivity and Attenuation," by James A Cochran, October 1958.

66. "Feasibility Study of Aircraft Antennas for Forward-Scatter and Meteor-Burst Communication," by J. F. Cline, July 1959.

67. "A Study of Possibilities for Improving Space Utilization and Performance of Rhombic Antennas," by Angel Martin-Caloto, July 1959.

68. "Aerodynamic Characteristics of Trailing-Wire Antennas at Supersonic Speeds," by F. B. Harris, Jr., March 1960.

69. "Voltage Breakdown of Antennas at High Altitudes," by W. E. Scharfman and T. Morita, April 1960.

70. "A Study of Corona Discharge Noise in Aircraft Antennas," by A. Vassiliadis, August 1960.